# Use of Volumetric Heating to Improve Heat Transfer During Vial Freeze-Drying

by

**James P. Dolan, B.S., M.S.**

Dissertation submitted to the Faculty of the
Virginia Polytechnic Institute and State University
in partial fulfillment of the requirements for the degree of

**Doctor of Philosophy**

in

**Mechanical Engineering**

Elaine P. Scott, Chair
Werner E. Kohler
Curtis H. Stern
James R. Thomas
William C. Thomas

September 1998

Blacksburg, Virginia

# Use of Volumetric Heating to Improve Heat Transfer During Vial Freeze-Drying

James P. Dolan, Ph.D.
Virginia Polytechnic Institute and State University, 1998
Advisor: Elaine P. Scott

## Abstract

Freeze-drying (lyophilization) is a drying process which is used to remove water from heat sensitive products, usually for the purpose of preservation. By removing water, the product becomes more stable at room temperature. This is a common process in the pharmaceutical industry because freeze-drying offers the advantage of drying at low temperatures and producing very low residual moisture contents. Often the materials dried in this manner are heat sensitive and require the highest possible quality. However, freeze-drying is a very slow process, often requiring 24 to 48 hours. During the process, vacuum pumps and refrigeration systems run continuously, making freeze-drying a very expensive process.

The goal of this project was to show that volumetric heating can be used in pharmaceutical freeze-drying and that this mode of heating offers some advantages. There were two approaches taken to the work, one experimental and one analytical. The experimental approach was broken into two phases, one focused on comparing microwave and conventional freeze-drying and the other focused on demonstrating the advantages of volumetric heating. In the analytical approach, a mathematical model was used to confirm the trends observed in phase II of the experimental work.

Experiments were conducted in a conventional laboratory freeze-dryer and the drying rate results were compared to the results obtained with an experimental microwave freeze-drying apparatus. Experiments were also conducted with the vaccine strain *A. pleuropneumoniae*. A viability study was conducted, comparing the viability loss caused by

each process. The viability study showed a slightly higher viability loss for the microwave process.

A comparison of drying curves showed that the microwave process resulted in a slight improvement in primary drying time: 2.5 hours for the microwave process compared to 3 hours for the conventional process. There was a significant difference in overall drying times: 4 hours for the microwave process compared to 11 hours for the conventional process. This result was caused by a lower residual moisture content at the start of secondary drying and a higher secondary drying temperature for the microwave process.

Experiments were also conducted to show that using lower chamber pressure results in higher drying rates. This is not the case in a conventional freeze-dryer since heating is dependent on the chamber pressure in the low pressure environment of freeze-drying. Thus, an advantage of volumetric heating was demonstrated. The results show that a modest increase in pressure, from 0.05 to 0.3 Torr, caused a one third reduction in primary drying time.

The mathematical model developed in the analytical work relied on the D'Arcy equation to describe the flow of vapor in the porous dried layer. The results of the model confirm trends seen in the measured temperature and weight profiles. Analyzing the effect of varying the chamber pressures shows that lowering the pressure in the range of 1 to 0.01 Torr results in a significant increase in drying rate giving as much as a two thirds reduction in drying time for the case studied. A model incorporating mass transport equations derived from the dusty gas model was also presented. This model offers the benefit of a more accurate prediction of mass transport through the porous dried layer.

To my parents, Thomas and Sandra and my brothers, Mike and Tom

# Acknowledgments

I would like to thank my parents, Thomas and Sandra Dolan, for all their support over the years. They always stood behind me and encouraged me to reach my goals. Thanks also goes to my two brothers, Mike and Tom, and all the rest of the family for support of one kind or another.

I would like to thank my advisor, Elaine Scott, for all her help and guidance and especially for finding a few good seniors to help out on the experimental work. I would also like to thank the my committee members who were all willing to make time for me.

Also deserving of thanks are Chris Haggerty, Mike Gondalski, and Tony Leung for all their help with the experimental work. These guys did a great job for me. It was a pleasure working with them and getting to know them.

Most of all, I would like to thank Anne-Claire Christiaen and all my friends from the Heat Transfer Lab for all the fun times both in and out of the lab. I couldn't have found a better bunch of people to work with and relax with.

James P. Dolan

*Virginia Polytechnic Institute and State University*

*September 1998*

# Contents

# List of Tables

# List of Figures

# Nomenclature

| | |
|---|---|
| $A_c$ | cross-sectional area ( $m^2$) |
| $c_0$ | relative D'Arcy flow permeability ( $m^2$) |
| $c_1$ | relative Knudsen flow permeability (m) |
| $c_2$ | ratio of bulk diffusivity within the porous material to the free gas bulk diffusivity |
| $D_{va}$ | binary mutual diffusion coefficient for water vapor and air ( $m^2/s$) |
| $c_p$ | specific heat at constant pressure ( $J/kg \cdot K$) |
| $d$ | diameter, characteristic length (m) |
| $\dot{E}_g$ | rate of energy generation (W) |
| $\dot{E}_{\text{in}}$ | rate of energy transfer into a control volume (W) |
| $\dot{E}_{\text{out}}$ | rate of energy transfer out of a control volume (W) |
| $\dot{E}_{\text{st}}$ | rate of increase of energy stored within a control volume (W) |
| $G$ | Gibbs energy (kJ) |
| $G_{\text{sub}}$ | Knudsen's absolute rate of sublimation ( $kg/m^2 \cdot s$) |
| $H$ | enthalpy (kJ) |
| $h$ | height of cylinder of material (m) |
| $K$ | Knudsen diffusion coefficient ( $m^2/s$) |
| $k$ | thermal conductivity ( $W/m \cdot K$) |
| $k_1, k_3$ | bulk diffusivity constants ( $m^2/s$) |
| $k_2, k_4$ | self diffusivity constants ( $m^2/s$) |
| $l$ | characteristic length (m) |
| $M$ | molecular weight ( kg/kmol) |
| $M_1, M_2$ | mass fractions of materials 1 and 2, respectively |
| $N''$ | molar flux ( $kmol/m^2 \cdot s$) |

| | |
|---|---|
| $n''$ | mass flux ( $\mathrm{kg/s \cdot m^2}$) |
| $P$ | pressure ( $\mathrm{N/m^2}$) |
| $P_c'$ | pressure near the condenser surface ( $\mathrm{N/m^2}$) |
| $P_0$ | drying chamber pressure ( $\mathrm{N/m^2}$) |
| $q$ | heat transfer rate (W) |
| $\dot{q}$ | volumetric heating rate ( $\mathrm{W/m^3}$) |
| $q''_{\mathrm{Iout}}$ | heat flux leaving region I ( $\mathrm{W/m^2}$) |
| $R$ | universal gas constant ($8.31441 \times 10^3\,\mathrm{J/kmol \cdot K}$) |
| $R''$ | thermal contact resistance ( $\mathrm{K \cdot m^2/W}$) |
| $R''_{t,c}$ | total thermal contact resistance ( $\mathrm{K \cdot m^2/W}$) |
| $S$ | entropy ( kJ/K) |
| $St$ | Stefan number |
| $s$ | sublimation interface position (m) |
| $T$ | temperature (K) |
| $T^0$ | initial temperature (K) |
| $T_c$ | collapse temperature (K) |
| $T_g$ | glass transition temperature (K) |
| $T_g'$ | glass transition temperature at maximum freeze concentration (K) |
| $t$ | time (s) |
| $W$ | sublimation rate ( $\mathrm{kg/s \cdot m^2}$) |
| $x$ | space coordinate (m) |
| $y$ | mole fraction |
| $\alpha$ | thermal diffusivity ( $\mathrm{m^2/s}$) |
| $\Delta H_{\mathrm{sub}}$ | latent heat of sublimation ( J/kg) |
| $\epsilon$ | porosity |
| $\kappa$ | Knudsen's evaporation coefficient |
| $\lambda$ | mean free path of gas molecules |
| $\rho$ | mass density ( $\mathrm{kg/m^3}$) |
| $\mu$ | viscosity ( $\mathrm{kg/s \cdot m}$) |
| $\xi$ | transformation variable |

*Subscripts and superscripts*

| | |
|---|---|
| $_I$ | dried region |

| | |
|---|---|
| $II$ | frozen region |
| eff | effective value |
| sat | saturation conditions |
| $a$ | air |
| $i$ | ice |
| $s$ | solid |
| $t$ | total value |
| $v$ | water vapor |
| 0 | drying chamber value |

# Chapter 1

# Introduction

Freeze-drying (lyophilization) is a drying process which is used to remove water from heat sensitive products, usually for the purpose of preservation. By removing water, the product becomes more stable at room temperature. The process consists of three stages: freezing, primary drying and secondary drying. The freezing stage consists of freezing the product and bringing the temperature down to the appropriate temperature. During the primary drying stage, frozen water is sublimed. This stage is the most time consuming part of the process. The secondary drying stage consists of desorption of residual moisture contained in the solute phase.

Freeze-drying is a common process in the pharmaceutical, food and biomedical industries. In the pharmaceutical industry, the production of biochemicals involves many processing steps. Extraction, precipitation, fractionation, and purification are some typical processing steps that usually lead to a very dilute aqueous solution. The water is then removed from the solution by freeze-drying, leaving the dried product to be further processed or packaged. In the food industry, freeze-drying is used to dry a wide range of products, including dairy products, meats, coffee and vegetables (Mellor, 1978). The biomedical industry uses freeze-drying to preserve blood products, bone, skin and other labile biomedicals (Adams, 1991).

There are many reasons why the freeze-drying method is used to a great extent in these industries. Probably the single most important reason, common to all three industries, is that the products most often freeze-dried are sensitive to heat and can not be dried with other drying techniques due to the high temperatures associated with these methods.

Also, it is well known that freeze-drying produces the highest product quality of any drying method. Some other advantages of freeze-drying are protection against chemical decomposition, ease of rehydration, minimum loss of activity due to low processing temperatures, and the reduction of the moisture content to very low levels. Generally, the lower the moisture content, the more stable the material. In most cases, the final product can be stored at room temperature, thus eliminating the high energy cost associated with freezer storage. However, the cost of freeze-drying is very high compared to other drying processes because of equipment costs and long drying times (Pikal et al., 1983). Reduction of the overall cost of freeze-drying is the motivation behind much of the freeze-drying research that has been done in the past.

Although the basic concepts of freeze-drying are known, the details are not well understood. Fundamental knowledge in some areas concerning the physical processes of freeze-drying is not complete. Where fundamental knowledge is available, it is not in a form useful to users or manufacturers of freeze-drying equipment. As a result, freeze-drying equipment often can not produce high quality dried products for a wide range of product types. Also, optimum parameter settings are usually found by trial and error, a lengthy and expensive procedure (Snowman, 1993). Some manufacturers will even suggest that a product be stored in a freezer after it has been freeze-dried when the goal is to make products that are stable at room temperature (Franks, 1989).

The pharmaceutical industry in particular can benefit from existing fundamental knowledge of the physical and chemical processes of freeze-drying. However, this knowledge needs to be put into a form that is useful to equipment designers and users. Combining this fundamental knowledge with process development research can result in an improved freeze-drying process for the pharmaceutical industry.

## 1.1 The Freeze-Drying Process

The foundation of the freeze-drying process is sublimation. Sublimation is the process by which a substance, which is usually water in freeze-drying, goes directly from a solid to a vapor without melting. In order for sublimation of water to take place, its temperature is reduced below its freezing point, and when the water has frozen, the surrounding pressure is brought down below the saturated vapor pressure corresponding to the temperature of

the ice.

The result of freeze-drying is that the water is removed while the structure of frozen product is preserved. For aqueous solutions, the remaining structure after drying is the structure that the solute formed as the water froze into pure ice crystals. Since this remaining structure is very porous, it can be reconstituted very quickly, and, provided the drying process has been carried out correctly, the dried product should be shelf-stable. However, achieving these characteristics is not always an easy task.

In any industrial freeze-drying process there are two major concerns: processing cost and final product quality. The processing cost is directly related to the time and energy required to complete the drying stages. The product quality is determined by all stages of freeze-drying, which includes, for pharmaceuticals, formulation. Formulation refers to mixture of various components in an aqueous solution. To optimize the process for the best combination of product quality and drying time, one must have a thorough understanding of formulation and freezing, primary and secondary drying, and product quality issues.

Since freeze-drying is also common in the food industry, a brief discussion of food freeze-drying is included in this section.

### 1.1.1 Food Freeze-Drying

With the great success of freeze-dried coffee, freeze-drying has become an important process for the food industry. Other common applications of freeze-drying in the food industry are onions, soups, fruits, fruit juices, milk, beef, turkey and chicken.

In the food industry, there are two general types of products subjected to freeze-drying: those that have a cellular structure and those that do not. For example, a slice of an apple has it own cellular structure to prevent collapse during the drying process. Collapse of the structure results in a product that has a high residual moisture content and poor rehydration characteristics. On the other hand, apple juice does not have a cellular structure and thus precautions must be taken to avoid collapse. This generally means freeze-drying is carried out at very low temperatures (below -42°C for apple juice versus -13°C for apple), slowing the drying process for the juice.

A particularly important concern in freeze-drying of food is the loss of volatile compounds. For any food product, there are generally hundreds of organic compounds that make up flavor and odor, two very important quality measurements. Loss of certain volatile

compounds may degrade the flavor and aroma of the final product. Other measures of quality in food freeze-drying are relative attractiveness, color, and texture.

### 1.1.2 Pharmaceutical Freeze-Drying

The quality of the final product is the most important factor in pharmaceutical freeze-drying. Shelf life, ease of rehydration and viability of the active component are all important parameters in determining product quality. Probably the most significant parameter is the viability of the active component, because products are often developed simply for the effects of the active components. As a result, other factors such as shelf stability may be compromised.

The viability of an active component is most sensitive to temperature. During the freeze-drying process, the product temperature must be maintained below predetermined limits. If the temperature of the product is raised above the maximum allowed at any time during or after the drying process, isolation of the active component is compromised and loss of activity results.

Shelf life is primarily controlled by the amount of residual moisture in the final product. The maximum allowable temperature for a dried product is usually determined by the glass transition temperature (Hatley and Franks, 1991). Ease of rehydration is affected not only by residual moisture content, but also by structural collapse. Collapse of a product during primary drying results in an increase of the rehydration time as well as in a potential rejection due to its physical appearance (Pikal and Shah, 1990).

The following sections discuss some other important aspects of pharmaceutical freeze-drying.

#### Formulation and Freezing of Aqueous Solutions

The formulation of the solution is a very important step in pharmaceutical freeze-drying. The formulation can affect both the drying characteristics and the quality of the final product. Since this work focuses on pharmaceutical freeze-drying, some discussion is provided on both the formulation and freezing steps of the process.

Freezing is a very important part of the freeze-drying process. The freezing temperature, freezing rate and degree of undercooling are all important factors influencing the overall drying time and product quality for any particular aqueous solution. Based on the

physical and chemical properties of a solution, the freezing protocol can be optimized to produce the most favorable freeze-drying results both in terms of product quality and drying time (Franks, 1989).

Formulation is also an important variable in pharmaceutical freeze-drying. As with the freezing protocol, it can be optimized to produce favorable freeze-drying characteristics and to provide adequate cryogenic protection for the active component. Formulation and freezing are interdependent. A change in formulation can require a change in freezing protocol. Conversely, if a specific freezing protocol is needed, an associated specific formulation may be necessary to yield the most favorable drying characteristics.

Probably the most common type of solution encountered in pharmaceutical freeze-drying is one in which part of the solution crystallizes and part forms an amorphous solid containing a predictable percentage of residual moisture. In the following sections, it will become obvious that nature of the frozen structure has a significant impact on the drying stages and the quality of the dried product. The basics of undercooling, collapse and excipients are explained and the significance of glass transition is also discussed. Knowledge of these concepts is important to fully understand how formulation and freezing can influence drying characteristics and product quality.

**Undercooling**

Undercooling, also called supercooling, is the phenomenon of bringing the temperature of a liquid below its equilibrium freezing point without crystallization. For water, the equilibrium freezing point is 0°C. However, it can remain in the liquid state at temperatures as low as -40°C under specific conditions. The degree of undercooling, $\Delta T$, is the difference between the equilibrium freezing temperature and temperature at which ice crystal nucleation begins.

Below the equilibrium freezing temperature, the solution is thermodynamically unstable. At some point, undercooling is ended by spontaneous nucleation of ice crystals. The morphology and size distribution of these ice crystals is affected by the degree of undercooling. With regards to the dry product, this parameter affects the texture, overall drying time and the rate of rehydration (Franks, 1989).

Increasing the degree of undercooling will produce larger ice crystals, enhancing the permeability of the dried product and thus increasing the drying rate (Dolan, 1994). The

degree of undercooling, however, is primarily dependent on the cooling rate. Slower cooling rates produce a higher degree of undercooling (MacKenzie, 1977).

### Freeze-Concentration

Water is removed from the aqueous system by the formation of ice crystals. As ice crystals of pure water are formed during the freezing process, the concentration of the solute in the remaining liquid phase increases. Therefore, the concentration of the remaining solute increases as the temperature of the aqueous solution decreases. This phenomenon is known as freeze-concentration.

Freeze-concentration can be quite harmful to the active components of a solution, such as proteins and electrolytes. Some of the most harmful effects are significant changes in pH levels and increased concentration of salts (Franks, 1982). However, the use of excipients can help minimize the harmful effects of freeze-concentration.

### Excipients

Excipients are substances used to facilitate freeze-drying of various biological materials, such as proteins and enzymes. They are usually inactive components such as sugars. They are mostly used to protect active components against harmful freeze-concentration effects. Other popular uses for excipients are described in Table 1.1.

## 1.2 Improvement of the Freeze-Drying Process

As previously discussed, freeze-drying is an expensive and lengthy process, but one that can be improved. One way to improve the process is to initially look at the physical mechanisms of drying in the primary and secondary drying stages, then determine the rate limiting mechanisms and subsequently alter the characteristics of the material and/or process which are responsible for the rate limitations.

As an example, consider increasing the drying rate by optimizing the transfer of water from its frozen state within the material to the surface of the condenser. The main driving force for this movement of water is a pressure difference. The high pressure is at the sublimation interface where the water vapor is generated and the low pressure is on the surface of the condenser where the water vapor condenses to form ice again. Most of the

**Table 1.1** Uses of excipients in freeze-drying processes (Snowman, 1993)

| **Type** | **Description** | **Common substances** |
|---|---|---|
| Fillers | bulking agents that provide a matrix for the active ingredients especially if the dose of concentration is small | mannitol |
| Buffers | used to control pH | phosphate |
| Tonicity Modifiers | used to control osmotic pressure | |
| Structure Modifiers | used to enhance the matrix and reduce the effects of collapse and also to overcome the increased resistance to vapor flow due to a surface skin caused by sugars | mannitol |
| Stabilizers | used to protect the active component of the solution from over drying and freeze-concentration effects | glucose, dextran, sucrose |
| Collapse Inhibitors | used to increase the collapse temperature | dextran, maltotriose |

resistance to the water vapor motion is the dried layer that forms as the sublimation front retreats into the material (Pikal et al., 1983, 1984). Vapor transfer through the dried layer can be maximized by increasing the pressure at the sublimation interface to its maximum allowed value while decreasing the chamber pressure.

It is important to note that the pressure at the sublimation interface is determined by the temperature of the interface: a higher temperature results in a higher pressure. The temperature of the sublimation interface is, in turn, limited by characteristics of the material. While there is always an upper limit to the temperature of the sublimation front, there is usually, other than practical concerns such as cost, no lower limit to the chamber pressure associated with very low pressure. Therefore, the lowest practical pressure should be used in the drying chamber to maximize the flow of water vapor through the dried layer.

Despite this logic, the opposite approach has been reported by operators of freeze-drying equipment (Livesey and Rowe, 1987). This is the result of a flaw in the design of freeze-drying equipment. In the pharmaceutical industry, the product is often contained in small vials. These vials are placed on a heated shelf, which maintains an acceptable temperature at the sublimation interface. The gap located between the bottom of the vial and the shelf provides resistance to the flow of heat to the sublimation interface. In

the low pressure range typically encountered in freeze-drying, this resistance is at least partially dependent on pressure: decreasing pressure increases the resistance. Thus, when the chamber pressure is decreased, the heat flow to the sublimation interface decreases and subsequently the drying rate decrease.

A better design for a freeze-dryer would be one in which changes in pressure do not affect the ability to provide heat to the sublimation interface. If heat is supplied volumetrically, as with microwave energy, the working chamber pressure could be lowered and the drying rate increased. Demonstrating this concept and evaluating its significance is the goal for this work.

## 1.3 Summary

Problem: Freeze drying is a long process often requiring 24 to 48 hours. Energy consumption by continuously running condenser refrigeration systems and vacuum pumps result in an expensive process.

Possible Solution: The cost of freeze-drying could be lowered by reducing the operating time. The overall drying time could be reduced by lowering the chamber pressure without reducing heat transfer. Lower operating pressures might be possible with the use of a volumetric heating source to improve heat transfer.

Goal: Investigate the feasibility of the proposed solution.

Objectives:

1. Conduct an experimental comparison between a conventional freeze-drying process and the microwave freeze-drying process.
2. Obtain measurements for the glass transition temperature as a function of moisture content for the material chosen for the experiments of objective 1. (The glass transition temperature is related to product quality and is an important parameter to consider when freeze-drying.)
3. Compare sublimation rates for two different pressures using the existing experimental microwave freeze-drying apparatus.

4. Develop a numerical simulation based on previously published work, but incorporating volumetric heat generation and appropriate boundary conditions.
5. Use the numerical simulation to evaluate the effect of decreasing the chamber pressure on the drying rate.
6. Use the model to verify the experimental data.

Rationale: The freeze-drying process is known to be expensive. Reducing processing times is the most obvious and feasible way to improve process economics. Mere optimization of the conventional process has not resulted in truly significant economic savings. Previous work has shown that volumetric heating by microwave energy has the greatest potential for significantly reducing processing times, and thus, improving process economics (Sunderland, 1982).

Methods: The microwave freeze-drying experiments were conducted using an existing microwave freeze-drying apparatus with a controlled leak for pressure control. The conventional experiments were conducted using a laboratory freeze-dryer owned by the Virginia-Maryland Regional College of Veterinary Medicine. The material utilized was an aqueous solution of brain heart infusion (BHI) and trehalose, a commonly used solution for suspension of a live vaccine, *A. pleuropneumoniae*. The numerical model is based on previously published numerical work by Liapis and Litchfield (1979) on freeze-drying. This model was modified to include volumetric heating and boundary conditions appropriate for experimental microwave freeze-drying and solved using an orthogonal collocation method.

# Chapter 2

# Literature Review

Since the early 20th century there has been much work published on freeze-drying and its applications. This chapter will cover some of the relevant literature concerning freeze-drying in both the food and pharmaceutical industries. The main point here is that there is a lot to learn about the effects of pressure and temperature from the literature. In particular we are interested in experimental investigations into rate limiting mechanisms, modeling of the heat and mass transfer and previous attempts at integrating microwave energy into the freeze-drying process.

## 2.1 The Effect of Chamber Pressure

The effect of chamber pressure is not well understood. Many reports by those operating freeze-drying equipment seem to contradict the theory, but not all (Livesey and Rowe, 1987). In this section, the effect of the chamber pressure on the freeze-drying process, primary drying in particular, is discussed from the point of view of the published literature on freeze-drying.

### 2.1.1 Experimental Studies

Nail (1980) published a detailed study on the effect of chamber pressure. In this work, Nail studied a typical pharmaceutical freeze-drying situation: small glass vials of a frozen product sitting on a metal tray which is placed on a heated shelf in the freeze-dryer. Nail states that in some situations mass transfer may be the rate limiting factor, but that heat transfer from the heat source to the sublimation front is usually the rate limiting process. Nail

states that resistance to heat transfer caused by air gaps between the vial and the tray and between the tray and the heated shelf becomes significant in the low pressure environment of freeze-drying. This is explained by the reduction of the thermal conductivity of a gas at pressures in the range where free molecular heat flow occurs. This theory was examined by measuring drying rates for three pressures (1.3, 0.25 and 0.04 Torr). The results confirm Nail's theory, showing that the drying rate decreases with decreasing pressure.

In a study on the resistance of the dried layer during freeze-drying, Pikal et al. (1983) determined that the resistance of the dried layer decreases with decreasing pressure. Here, the resistance of the dried layer is determined directly from sublimation rate data. Thus, Pikal determined that lower pressure increases the sublimation rate. It is important to note that Pikal's experiments involved a very small sample in a specially designed sample holder and heat was applied radiatively, not through conduction as in Nail's work.

The next work published by Pikal et al. (1984) evaluated heat and mass transfer in a more typical situation. A number of vials were placed on a heated shelf, drying rates were measured and heat fluxes were estimated. The results in this work confirm Nail's earlier findings: lower pressure results in reduced heat fluxes and decreased sublimation rates.

In response to the work of Nail (1980) and Pikal et al. (1984), Jennings (1986) measured the sublimation rate of ice. The results showed that lower pressure increases the sublimation rate. In an effort to explain the results of Pikal and Nail, Jennings stated that increasing the pressure increases heat transfer from the sides of the vial. The result is an increase in the sublimation interface area which offsets the reduction in sublimation rate due to higher pressure.

After publication of the work by Jennings (1986), Livesey and Rowe (1987) tried to make sense of the conflicting reports on the effect of chamber pressure. They considered a situation in which the temperature of the product was at its optimum and pressure was increased. This would result in the decrease of the sublimation rate, because the heat flow to the product had to be reduced to maintain the temperature at its optimum value without overheating. Another situation considered was one in which the shelf temperature was kept at a constant value. In this situation increasing the pressure resulted in an increased heat flow, increased product temperature and an associated increase in sublimation rate. Livesey and Rowe (1987) also considered the thermal capacitance of the shelf and temperature controlled fluids. Here, they noted that the thermal capacitance of the shelf and fluids

prevent rapid changes in shelf temperature. Snowman (1993) stated that the time for equilibrium after a change in shelf temperature is typically 30 minutes to one hour. Thus, pressure, with a rapid response to control, is much more convenient for controlling the temperature of the product during primary drying than changing the shelf temperature.

Finally, Livesey and Rowe (1987) concluded that the observations of Nail (1980) and Pikal et al. (1983) were correct and explained that the sublimation model of Jennings (1986) was not applicable to ice embedded in a porous material. Although the sublimation rate is theoretically expected to decrease with increasing pressure, in a practical application, the increase in heat transfer has a more significant effect on the sublimation rate than an increase in pressure.

In a study that focused on the secondary drying stage, Pikal et al. (1990) determined that pressure variation in the range of 0-0.2 Torr had no effect on drying rate during secondary drying for the materials used. However, it was determined that temperature has a significant effect on the drying rate and that the rate limiting process was either desorption from the solid-vapor interface or diffusion in the solid.

### 2.1.2 Use of Numerical Simulations

Pikal (1985) developed a numerical simulation of vial freeze-drying that included some laboratory data. In this paper, Pikal showed, from experimental data, that with increasing pressure, there is an associated increase in temperature and a decrease in drying times. However, using the numerical simulation, Pikal examined a case with a constant sublimation temperature and found that a decrease in pressure decreases the drying time.

In several papers using similar models (Liapis and Marchello, 1983; Millman et al., 1985; Liapis and Bruttini, 1994; Sadikoglu and Liapis, 1997), it was determined that lower pressures always improve drying rates if the shelf temperatures are properly set. However, even though a contact resistance to heat transfer was included in the model, the pressure dependence of this resistance was not included. Also, in some cases, the sublimation interface was kept at its maximum allowable temperature by adjusting the shelf temperature during the drying process, but the thermal capacitance of the shelf was not included in the model.

### 2.1.3 Cyclic Pressure Freeze-Drying

Mellor (1978) discussed the effect of pressure on heat and mass transfer in freeze-drying. He noted that low pressure increases the driving force for mass transfer, but reduces heat flow in the dried layer because of the dependence of heat transfer coefficients on pressure. In an attempt to overcome this problem, Mellor (1978) developed a cyclic pressure freeze-drying process. In this process, pressure is momentarily increased to increase heat flow and then momentarily decreased to increase vapor flow.

Litchfield et al. (1981) studied a typical vial freeze-drying case using a numerical simulation that includes a resistance to heat transfer between the bottom of the vial and the heated surface. In this study, Litchfield et al. found that even the best of the cyclical pressure policies was not as good as an optimal constant pressure policy previously determined by Liapis and Litchfield (1979).

## 2.2 Rate Limiting Factors in Freeze-Drying

The primary goal of research on freeze-drying is to improve process economics by reducing processing time. An important step in this process is determining the rate limiting factors. Heat transfer and mass transfer are the two processes that are the most likely rate controlling processes.

Determining the rate limiting processes during freeze-drying has proven to be a difficult task. Since a change in heat transfer has an effect on mass transfer and a change in pressure has an effect on heat transfer, the relationship between the two processes is quite complicated. Thus, differentiating between the two processes in order to determine which one is the limiting factor can be difficult.

Understanding the mechanisms of heat and mass transfer and their dependence on temperature and pressure is very important for determining the rate limiting process. There have been many experimental studies of sublimation rates and mechanisms of mass transfer through the dried layer during freeze-drying. Some of the more relevant studies are discussed in this section.

In a study of sublimation rates for aqueous solutions, Pikal et al. (1983) took measurements of weight loss on a cylindrical micro-sample suspended from a vacuum microbalance kept at a constant temperature. The variables in the experiments were freezing

rate, product thickness, temperature, pressure and solute concentration. An important result of this work was the conclusion that at higher temperatures hydrodynamic surface flow is an important flow mechanism in the dried layer.

Livesey and Rowe (1987), in their discussion on the effect of chamber pressure, noted that the rate limiting process in freeze-drying changes as sublimation proceeds. Initially, the process is limited by heat transfer when the dried layer is small and an unrealistic heat flux is required to push the sublimation rate to its maximum. After the dried layer thickens, the process becomes limited by mass transfer since the required heat flux is easily maintained for the decreasing sublimation rate.

Wolff and Gibert (1989) determined the rate limiting factor in vial freeze-drying of milk. By fitting their model to measured data, they were able to determine the three transport parameters in their model. These were the water vapor diffusivity in the dried layer, the external mass transfer coefficient and the resistance to the heat transfer from the heated shelf to the ice. Since the contact resistance between the vial and the shelf is the most significant barrier to heat transfer, it was determined to be the overall rate controlling parameter and thus controlled the dehydration kinetics.

## 2.3 Modeling

Freeze-drying is a complicated process. The correlation between process variables such as chamber pressure, freeze-drying temperature and freezing protocol makes it especially difficult to find an optimum freeze-drying schedule. Currently, the development of optimized freeze-drying schedules is done largely on a trial and error basis (Snowman, 1993), a slow and expensive procedure that often does not yield fully optimized freeze-drying schedules. However, there is increasing interest in reducing cycle development time by using computer simulations of freeze-drying to predict fully optimized freeze-drying schedules.

The basis of any computer simulation is the mathematical model which describes the physics of the problem. A mathematical model can be used to investigate the correlation between process variables and optimize the process as well as to aid in the design of new equipment. This chapter deals with the development of a mathematical model for microwave freeze-drying. Following the discussion of existing models, a model is developed using the method of volume averaging.

Most freeze-drying models have applications in one of two areas: food and pharmaceuticals. Microwave freeze-drying would come under the food applications since all previously published microwave freeze-drying research has focused in this area. Although the earliest mathematical models were developed for food applications, some of these models have been successfully applied to freeze-drying of pharmaceuticals.

The aim of this section is to review previous modeling efforts and determine if any of these models are applicable to microwave freeze-drying of pharmaceuticals. It is also important to take into account the accuracy of the results produced by the model. The goal here is to make use of previous experience and develop a model that is likely to produce results that are more accurate than what has previously been achieved.

The review of previous modeling efforts and their results starts with applications to conventional food freeze-drying. Then the microwave freeze-drying models are discussed. Finally, modeling research for pharmaceutical freeze-drying will be reviewed.

### 2.3.1 Food Freeze-Drying

Zamzow and Marshall (1952) developed one of the first mathematical models of the freeze-drying process. They used a pseudo steady-state assumption as the foundation for their model and investigated cases of radiation and conduction boundary conditions. The pseudo steady-state assumption is a common one that applies to a slow conventional freeze-drying process. It allows for a much simpler solution than that required for a transient sublimation model.

The pseudo steady-state assumption allows one to calculate the heat conduction to the phase interface under steady-state conditions for a fixed interval of time. Then, using this quantity of heat and the known heat of sublimation for water, a new position for the phase interface can be determined. The validity of this model depends on how closely the actual temperature profiles in the product match the assumed steady-state conditions during the fixed interval of time. Since conventional freeze-drying is very slow, the temperature profiles in the product are nearly linear making the steady-state assumption reasonable.

In 1967, the pseudo steady-state model was further developed and named the Uniformly Retreating Ice Front (URIF) model (Sandall et al., 1967). Sandall et al. (1967) used the URIF model to investigate the relationship between transport properties and drying rates for slabs of poultry.

Hill and Sunderland (1970) used a pseudo steady-state model, but considered momentum equations from the free molecular, continuum and transition flow regimes. Equations for the three flow regimes were presented. Because of the steady-state assumption, the flow rate was considered constant throughout the dried layer. Theoretical predictions of the model were compared with published data for beef slabs because of the availability of data and properties. The slight discrepancies between the predictions and experimental data were attributed to experimental error.

In 1980, a model that included both sublimation of the ice and desorption of vapor in the dried region was formulated (Liapis, 1980). Unlike the previously described models, this model uses a transient analysis that allows both sublimation and desorption to occur simultaneously. This type of model is referred to as a sorption-sublimation model. Comparisons of predicted data with experimental data for turkey and non-fat milk showed excellent agreement and an increased accuracy compared to that of a URIF model and a model that includes a transient analysis of sublimation without sorption effects.

The transient sublimation model which predicts the first $60 - 90$ percent of moisture removal is more accurate than the URIF models (Liapis and Bruttini, 1994), but does not predict secondary drying. This can be done with a sorption-sublimation model (Millman et al., 1985). The sorption-sublimation model takes into account moisture transfer between the vapor flow through the dried region and the material being dried. This aspect of the drying process has been overlooked in previous freeze-drying models, giving rise to error in the predicted data (Liapis, 1980; Hill and Sunderland, 1970; Dyer and Sunderland, 1968).

Mass flow through the dried layer in the sorption-sublimation was modeled using a combination of the dusty gas model for diffusive flow and the D'Arcy equation for hydrodynamic flow (Liapis and Bruttini, 1994). The sorption-sublimation model is currently the most comprehensive model of heat and mass transport during freeze-drying. It has also been applied to vial freeze-drying of aqueous solutions (Liapis and Bruttini, 1994, 1995).

### 2.3.2 Microwave Freeze-Drying

Microwave freeze-drying began as another attempt to accelerate the freeze-drying process in the food industry. Thus, the first attempts to model the process were extensions of work that had been done previously with food freeze-drying. Copson, in 1962, modeled the microwave freeze-drying process with the common pseudo steady-state assumption that had

been used in modeling of conventional food freeze-drying. However, it was later determined that this assumption is not valid for the faster case of microwave freeze-drying (Ma and Peltre, 1973). Copson assumed hydrodynamic flow in the dried layer. Calculations of vapor flux were based on the pressure difference between the moving sublimation interface and the outer surface of the dried layer. Significant differences between the predicted data and experimental data were the result of the simplifying assumptions and unknown transport properties.

Ma and Peltre (1973) presented a transient, one-dimensional analysis of freeze-drying with microwave heating. This was the first transient analysis of microwave freeze-drying. Transient mass and energy equations were written for the dried and frozen regions. Conduction was considered in the frozen region while both conduction and convection were considered in the dried region. Based on work previously done by Sandall et al. (1967) and Harper (1962), they assumed the vapor flow to be in the transition region between free molecular and slip flow. However, for simplicity, they opted to use an effective diffusivity, allowing the use of Fick's equation. For the calculations, they used properties found in the literature for lean beef. Here, many assumptions were made. The dielectric properties, which were known to be temperature dependent, were assumed constant. The results seemed to be reasonable. However, there was no comparison to actual experimental measurements. As a means of comparing the microwave process to a conventional radiant heating process, calculations were made using typical surface temperatures for radiant heating.

In 1975, Ma and Peltre presented a more detailed investigation of microwave freeze-drying. This time, essentially the same model was used but with more accurate properties and surface conditions and the dielectric properties were allowed to vary with temperature. Also, this study used a significant amount of experimental results to verify the model and to demonstrate its usefulness in optimization. Good agreement was found between predicted and actual experimental data. However, it was noted that more comprehensive property data was required for effective simulation of the process.

A two-dimensional model, taking into account anisotropy of beef cubes, was presented by Ang et al. (1977). This model was very similar the one-dimensional model of Ma and Peltre (1975a). It also used an effective diffusivity and separate heat transfer equations for the dried and frozen layers of the sample. Using property ratio factors, the ratio of a

transport property in the $y$ direction to that in the $x$ direction, the model could predict drying times when anisotropic characteristics were considered. Experimental results confirmed the theoretical results obtained with the model for beef cubes.

Later, Ma and Arsem (1982) included the effects of solid entrainment in the Ma and Peltre model. Experimental drying rates were typically higher than that predicted by the model. It was found that with rapid sublimation, caused by the use of microwave heating, high velocities were produced in the vapor flow. These velocities were high enough to cause entrainment of solid particles. Since drying rates were calculated based on weight measurements, solid entrainment resulted in drying rates that were consistently higher than the model predictions. Including the effect of solid entrainment enabled Arsem and Ma (1990) to increase the accuracy of their predictions.

### 2.3.3 Pharmaceutical Freeze-Drying

There have been several good papers on the fundamentals of freeze-drying of pharmaceutical aqueous solutions (MacKenzie, 1977, 1985; Franks, 1989). The purpose of these papers is to enhance knowledge on the fundamentals of freeze-drying and encourage further optimization of freeze-drying by application of this knowledge. Efforts to optimize the process have, for the most part, focused on the process variables associated with primary drying. These are shelf temperature, chamber pressure, vial selection (aspect ratio) and enhanced process monitoring (Pikal et al., 1984; Livesey and Rowe, 1987; Pikal, 1985; Connelly and Welch, 1993; Roy and Pikal, 1989).

Pikal et al. (1983) enhanced their model by experimentally measuring sublimation rates. From these data they were able to estimate a normalized dry product resistance to vapor flow. The dry product resistance was later used as essential data in numerically predicting drying rates. The next step was to analyze the resistance associated with various types of partially stoppered vials (Pikal et al., 1984). Mass transfer coefficients were determined through pressure measurements combined with dry product resistances determined in the previously mentioned work. Heat transfer was considered by conduction and radiation. Equations used what were essentially 'effective' heat transfer coefficients based on measured temperature differences.

In 1985, Pikal presented a computer simulation of freeze-drying based on a one-dimensional steady-state model. Dried product resistances and heat and mass transfer

coefficients were determined experimentally. Using these coefficients, Pikal calculated drying times and surface temperatures and compared them to experimental drying data. The coefficients were considered to be constant during sublimation. Adsorption in the dried layer during sublimation was not considered.

The simulation of Pikal (1985) was used to study three aspects of the process. These were: (1) the effect of changes in chamber pressure and shelf temperature on drying time and product temperature; (2) the effect of shelf temperature variability and vial heat transfer coefficient variability on uniformity of drying; and (3) cycle optimization. While it is not recommended that the simulation replace conventional process development studies, it can be helpful in scale-up of optimum processes for freeze-drying of pharmaceuticals Pikal (1985).

The most recent study of vial freeze-drying of pharmaceuticals was presented by Liapis and Bruttini (1995). In this paper, the sorption-sublimation model, previously described in Section 2.3.1, is applied to vial freeze-drying of aqueous solutions. Some qualitative features of vial freeze-drying are derived from the model. However, there are not numerical results, since a numerical solution had not been completed at the time the paper was published.

## 2.4 Use of Microwave Energy in Freeze-Drying

Previous attempts at using microwave energy to accelerate the freeze-drying process have focused on food applications. One of the first studies on the use of microwave energy in freeze-drying was produced by Copson and Decareau (1957). It was found that the use of microwave energy at 2450 MHz enabled the dehydration of beefsteak in much less time than previously possible. They also noted that no detectable loss of quality due to the use of microwave energy was found. However, problems with gas ionization were encountered.

Following papers explored the possibilities of microwave freeze-drying. Studies focused on optimization, material properties related to microwave heating, use of alternative frequencies, equipment development and gas ionization problems (Copson, 1958; Hoover et al., 1966b,a; Gould and Kenyon, 1971). Hoover et al. (1966b) reported drying times for slabs of beef that were 3 to 13 times less than conventional drying times.

In the 1970's, there were two in-depth studies of microwave freeze-drying focusing on

the development of a theoretical model, experimental verification of numerical solutions and optimization (Ma and Peltre, 1975a,b; Ang et al., 1977a,b). In both studies, the models were based on a transient analysis with the assumption that the sample was dry when primary drying was complete. No provisions were made to handle secondary drying. The results of these studies show that the use of microwave energy in the freeze-drying process can significantly reduce drying times to at least a third, and that problems such as gas ionization can be overcome.

Further research on microwave freeze-drying focused on optimization of combined radiant and microwave aided freeze-drying (Chang and Ma, 1985) and solid entrainment (Arsem and Ma, 1985, 1990). There have been no recent attempts to improve the basic approach of the mathematical modeling in microwave freeze-drying and no attempt to develop optimized designs of equipment.

# Chapter 3

# Theoretical Analysis of Vial Freeze-Drying

While the freeze-drying process includes formulation, freezing, sublimation and desorption, it is the last two that are of interest in this work. This chapter focuses on the theory of sublimation and the heat and mass transfer that takes place during primary and secondary drying.

It is important to understand the basic physical processes that take place during freeze-drying. Understanding these processes individually is the first step to understanding their complex interdependencies present in freeze-drying. The important physical processes in freeze-drying are:

- sublimation during the primary drying stage,
- desorption during the secondary drying stage,
- diffusional and viscous flow within the porous material, and
- heat conduction, within both the porous and frozen material.

If heat is supplied volumetrically, as with microwaves, then the mechanisms of dielectric heating and the dielectric properties of the materials involved also are important.

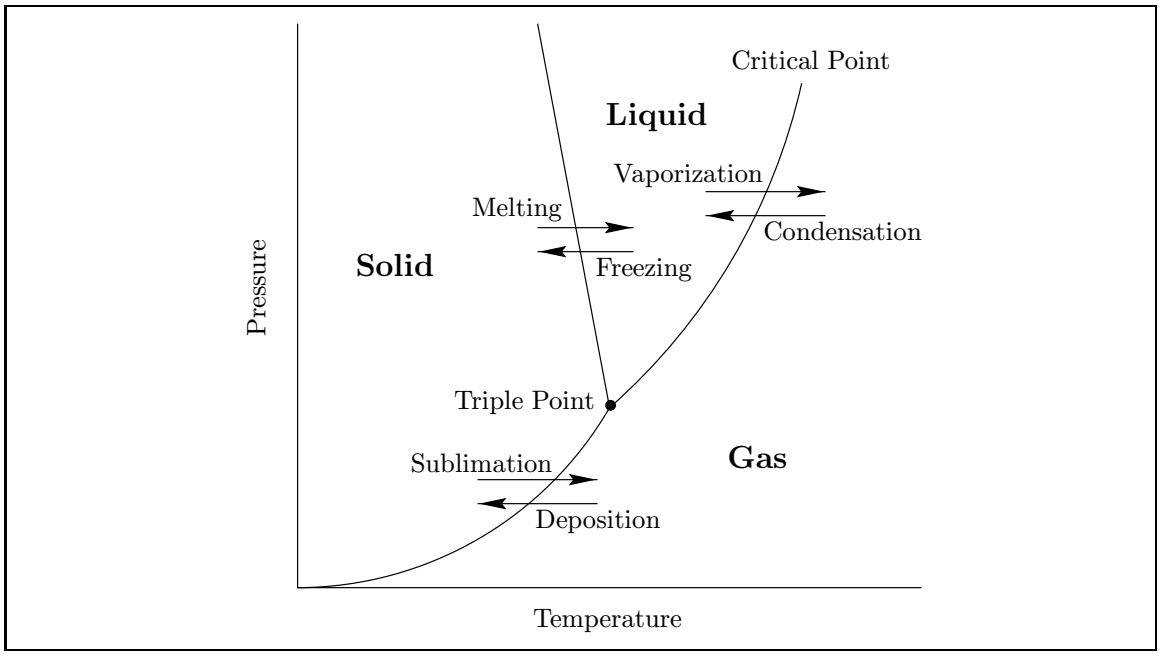


**Figure 3.1** Pressure-temperature diagram for a substance that expands upon freezing.

## 3.1 Theory of Sublimation

The basis of the freeze-drying process is sublimation. Sublimation is the process by which a substance, which is usually water in freeze-drying, goes directly from a solid to a vapor without melting. In order for sublimation of water to take place, the water must first be frozen and then subjected to low total pressure or a very low vapor pressure. This section discusses sublimation in detail, from the point of view of kinetic theory and thermodynamics.

### 3.1.1 Thermodynamics of Sublimation

To determine the conditions for sublimation, it is useful to look at an equilibrium phase diagram for water. An equilibrium phase diagram shows the pressures and temperatures for which different phases of a single component system are in equilibrium. This type of diagram for water can be used to determine the ranges of pressure and temperature required for sublimation.

An example of a pressure-temperature phase diagram for a substance that expands upon freezing, such as water, is shown in Fig. 3.1. Also noted in this figure are the various types of phase changes that can occur. In the present work, only sublimation and deposition are of importance. In Fig. 3.2, the saturation line between the solid phase and the gas phase

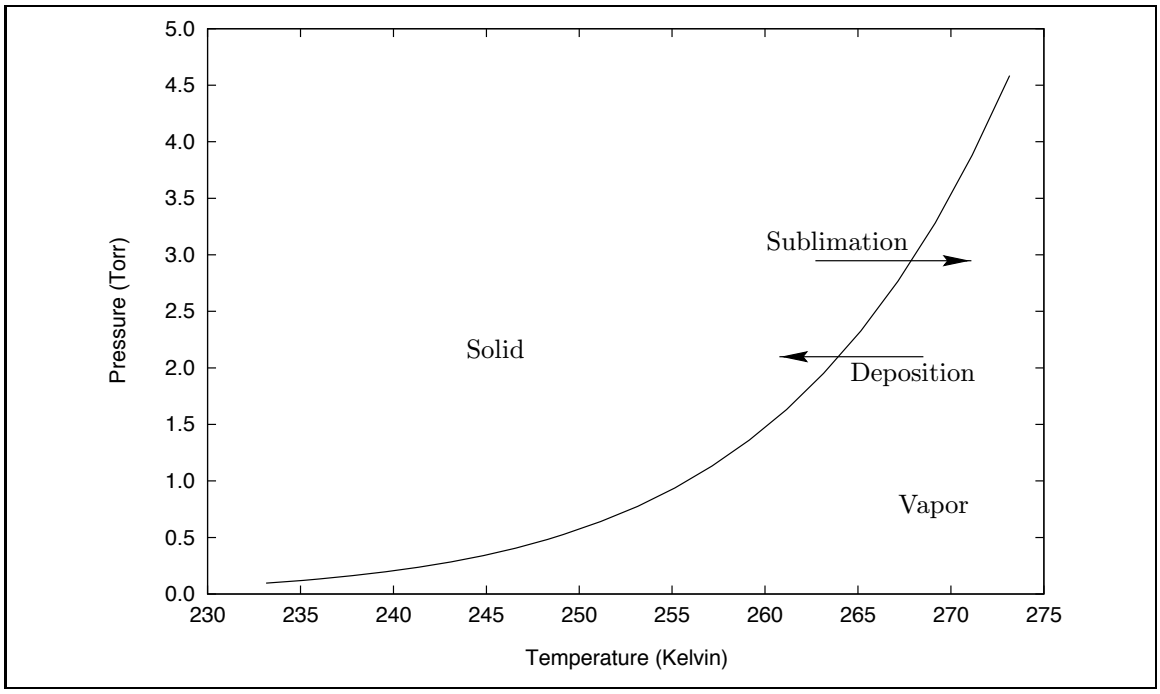


**Figure 3.2** Saturation line between the solid phase and gas phase for water

is plotted for water. It can be seen that to sublimate ice the temperature of the ice should be below the triple point temperature, 273.16 K and the vapor pressure should be below the triple point pressure, 4.58 Torr (0.61 kPa). It is important to note that Fig. 3.2 is an *equilibrium* phase diagram. For the sublimation process to be continuous, the ice and gas at the sublimation interface should not be in an equilibrium state.

In a system that consists of two phases, the phases are in equilibrium for a given temperature and pressure when the Gibbs energy of one phase equals the Gibbs energy of the other phase. The Gibbs energy, $G$, is given by

$$G = H - TS, \tag{3.1}$$

where $H$ is the enthalpy, $T$ is the temperature and $S$ is the entropy. In the case of sublimation, the phase change stops when $G$ of the ice is equal to $G$ of the gas. This equilibrium condition is marked by the line in Fig. 3.2. When the difference between the Gibbs energy of the two phases, $\Delta G$, is not zero, one of the phases will disappear. For sublimation to take place, the Gibbs energy of the ice must be higher than the Gibbs energy of the vapor. This can be achieved by moving away from equilibrium by increasing the temperature of the ice and/or decreasing the pressure of the gas.

When sublimation occurs under equilibrium conditions or very near equilibrium conditions, the relationship between temperature and pressure can be described by the Clausius-Clapeyron equation,

$$\ln \frac{P_2}{P_1} = \frac{\Delta H_{\text{sub}}}{R} \left( \frac{1}{T_1} - \frac{1}{T_2} \right), \tag{3.2}$$

where $P$ is the saturated vapor pressure associated with the temperature $T$ and $\Delta H_{\text{sub}}$ is the latent heat of sublimation. The Clausius-Clapeyron equation also assumes that the latent heat is constant over the interval from state 1 to state 2. This equation can be used to determine vapor pressure at the sublimation interface, given the ice temperature at the interface. However, since the latent heat is a function of temperature, it is usually more convenient to determine a function that represents the line in Fig. 3.2 over the temperature range of interest and use that function in place of the Clausius-Clapeyron equation.

### 3.1.2 Kinetic Theory and the Rate of Sublimation

Thermodynamics provides some insight into the conditions required for sublimation, but it does not provide a way to determine the actual rate of sublimation given non-equilibrium conditions. To obtain this information, one must look to kinetic theory.

In kinetic theory, the state of a substance is described on a molecular level and is determined by intermolecular forces and kinetic energies of the molecules. The molecules of a system all have different kinetic energies and thus, there exists a kinetic energy distribution. A system can be described by its kinetic energy distribution and the resulting average kinetic energy of the molecules.

In a solid, the average kinetic energy of the molecules is less than the energy associated with the intermolecular forces that bind the molecules together. However, on the surface of a subliming solid the kinetic energy distribution shows that some small percentage of molecules have enough energy to overcome those intermolecular forces and break free from the surface. The percentage of molecules that have enough energy to break free from the surface increases with increasing temperature of the solid.

The rate at which molecules in the gas return to the subliming surface of the solid is determined by the pressure of the gas. The pressure of a gas is determined by the number of molecules in the gas, the volume occupied by the gas and the temperature of the gas. At higher pressure, the rate of molecules returning to the solid is greater.

Thus, there are two convenient variables that can be controlled to maximize the sublimation rate of ice: the pressure of the water vapor above the subliming surface of the ice and the temperature of the ice. Increasing the temperature results in a larger number of molecules leaving the surface, while decreasing the pressure removes molecules from the gas above the subliming surface. This situation results in a net flux of molecules away from the sublimation interface.

It can be seen from the kinetic theory that a higher ice temperature combined with a lower pressure increases the rate of sublimation. Knudsen derived an equation for the absolute rate of sublimation of ice, $G_{\text{sub}}$, from kinetic theory (Mellor, 1978),

$$G_{\text{sub}} = \kappa P_{\text{sat}} \left( \frac{M}{2\pi RT} \right)^{\frac{1}{2}}, \quad 0 < \kappa < 1, \tag{3.3}$$

where $\kappa$ is the coefficient of evaporation, $p_s$ is the saturated vapor pressure of ice, $M$ is the molecular weight of water vapor, $R$ is the gas constant, and $T$ is the absolute temperature of the ice. Many researchers have attempted to determine $\kappa$ for ice in various temperature ranges usually arriving at values ranging from .6 to 1 (Mellor, 1978).

A plot of Eqn. 3.3 using data from the sublimation line of a P-T diagram for water (Keenan et al., 1978) shows that higher ice temperatures result in higher sublimation rates. Thus, it is expected that in freeze-drying the ideal temperature is the maximum allowable temperature given the temperature constraints imposed by the product. This is well known among those with experience in freeze-drying (Pikal et al., 1984).

In a real system, there will not only be water molecules leaving the surface of the ice, but also returning to the ice. Thus, the partial pressure of water vapor has an effect on the sublimation rate. A condenser can be used in a vacuum system to keep the vapor pressure low. The effect of a condenser in the vacuum system can be represented as (Mellor, 1978)

$$G_{\text{sub}} = \kappa (P_{\text{sat}} - P_c') \left( \frac{M}{2\pi RT} \right)^{\frac{1}{2}}, \quad l > \lambda, \tag{3.4}$$

where $P_c'$ is the pressure outside the condenser, $l$ is the distance from the sublimation interface to the condenser and $\lambda$ is the mean free path of the vapor molecules.

## 3.2 Freeze-Drying Process

Although sublimation of ice is a fairly straightforward process, when sublimation is considered in the context of freeze-drying, the problem becomes more complex. This section is an

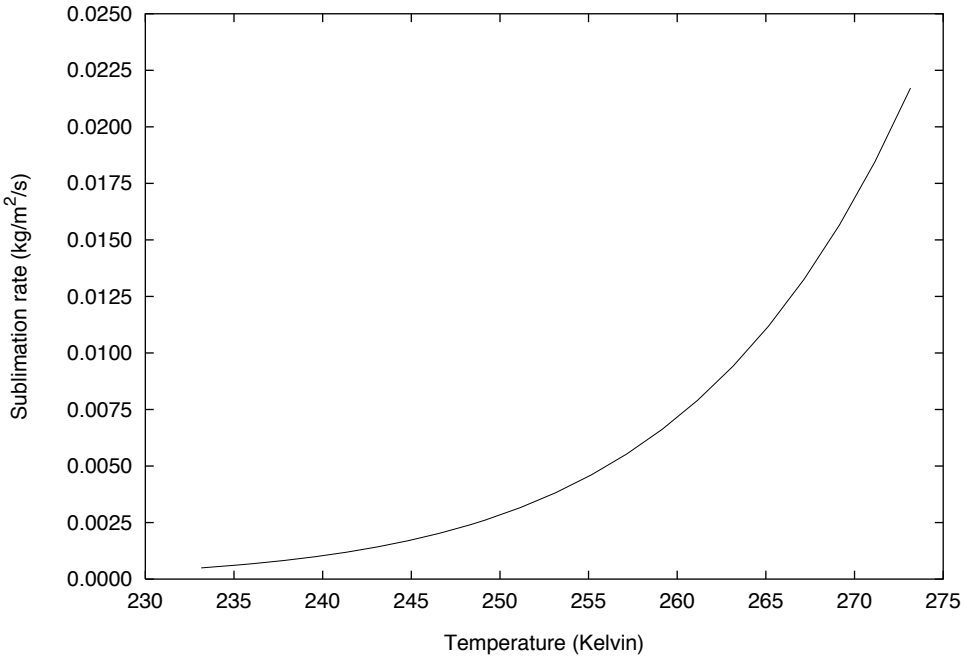


**Figure 3.3** Knudsen's absolute sublimation rate, $G_{\text{sub}}$, versus temperature for ice, using $\kappa = 1$

introduction to sublimation in the context of vial freeze-drying.

### 3.2.1 A Simple Sublimation Process

Now that the theory of the sublimation process for ice has been discussed, it would be helpful to look at the simple case of ice subliming in a low pressure chamber. A low total pressure is not necessary for sublimation, since the low pressure previously mentioned refers to the water vapor pressure. It is possible to achieve sublimation at atmospheric pressure by maintaining a partial pressure of water vapor below the water triple point pressure. However, a low total pressure is often used in freeze-drying to ensure that the ice stays frozen (Mellor, 1978).

Figure 3.4 illustrates a simple sublimation process for water. Initially, the ice and water vapor are assumed in equilibrium. To start the process of sublimation on one side of the chamber and deposition on the other side, one can increase the temperature of the ice at 1 by heating the surface on the left to start the sublimation and decrease the temperature at 2 by cooling the surface on the right. By causing deposition to occur, the effect is a lowering of the chamber pressure below the equilibrium vapor pressure for the

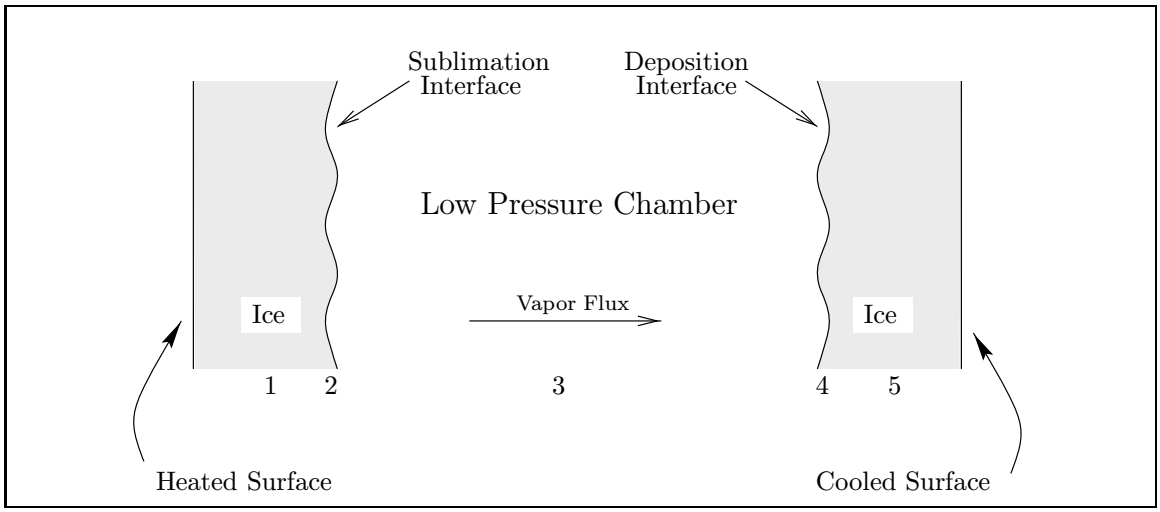


**Figure 3.4** Illustration of a simple sublimation process where mass transfer is driven by a concentration gradient and heat transfer is driven by a temperature gradient in the ice.

given temperature at 1.

Ice subjected to a low pressure will sublimate when the water vapor pressure of the gas in the drying chamber is lower than the saturated vapor pressure of the ice. Since the saturated vapor pressure of the ice increases with increasing temperature, simply heating the ice can raise its Gibbs energy above the Gibbs energy of the water vapor in the chamber. The vapor pressure in the chamber is kept low by continuous pumping of the chamber and by using a condenser. Both will remove water vapor from the drying chamber as it is generated by sublimation occurring at the surface of the ice. The condenser provides a surface that is cold enough to allow deposition of water from the gas phase to the solid phase on a cold surface.

Applying a thermodynamic analysis to this situation is relatively straightforward. If it is assumed that nearly equilibrium conditions are present, then the sublimation rate $W$ is determined by

$$W = \frac{q}{\Delta H_{\text{sub}}}, \tag{3.5}$$

where $q$ is the rate of heat input. From this analysis, it is obvious that the sublimation rate would increase as the rate of heat input is increased.

In order for the thermodynamic analysis to be valid, the Stefan number, $St$, of the

ice phase must be very small ($St \ll 1$). The Stefan number, defined as

$$St = \frac{c_p \Delta T}{\Delta H_{\text{sub}}}, \tag{3.6}$$

is the ratio of sensible heat to latent heat. A small Stefan number would indicate that latent heat was dominant and that sensible heat could be neglected. In this case, the Stefan number would be small if the temperature difference, $\Delta T$, in the ice is small which requires a low rate of heat input.

If the conditions under which sublimation is taking place are not near the equilibrium conditions, then the thermodynamics analysis does not apply and a more complicated transient analysis is required. Now we can assume that there are significant gradients in temperature across the sublimating ice and significant gradients in vapor pressure between the sublimation interface and deposition interface. This analysis links the vapor pressure at the deposition interface and the heat input to the sublimation rate.

### 3.2.2 Conventional Pharmaceutical Freeze-Drying

The case of ice subliming under a low pressure is a much simpler case than that of a real freeze-drying application. What makes a real application more complicated is the existence of a porous dried layer between the ice in the frozen layer and the drying chamber as well as the difficulties associated with transferring heat to the sublimation interface within the porous material. The materials of interest typically have maximum temperature constraints which prevent the use of high temperatures on the surface to increase heat transfer.

Figure 3.5 illustrates the various components of vial freeze-drying. Heat is conducted from the shelf to the sublimation interface within the product. Water vapor travels up through the dried layer and goes on to the condenser. At the condenser surface, water vapor is converted back to ice. Continuous pumping keeps the vapor flowing out of the vacuum chamber, thus preventing a significant increase of vapor pressure above the product due to the generation of vapor.

Based on the description of the process, there are five physical mechanisms that could control the rate of drying:

1. heat flow to the sublimation interface,

2. phase change from solid to vapor (sublimation),

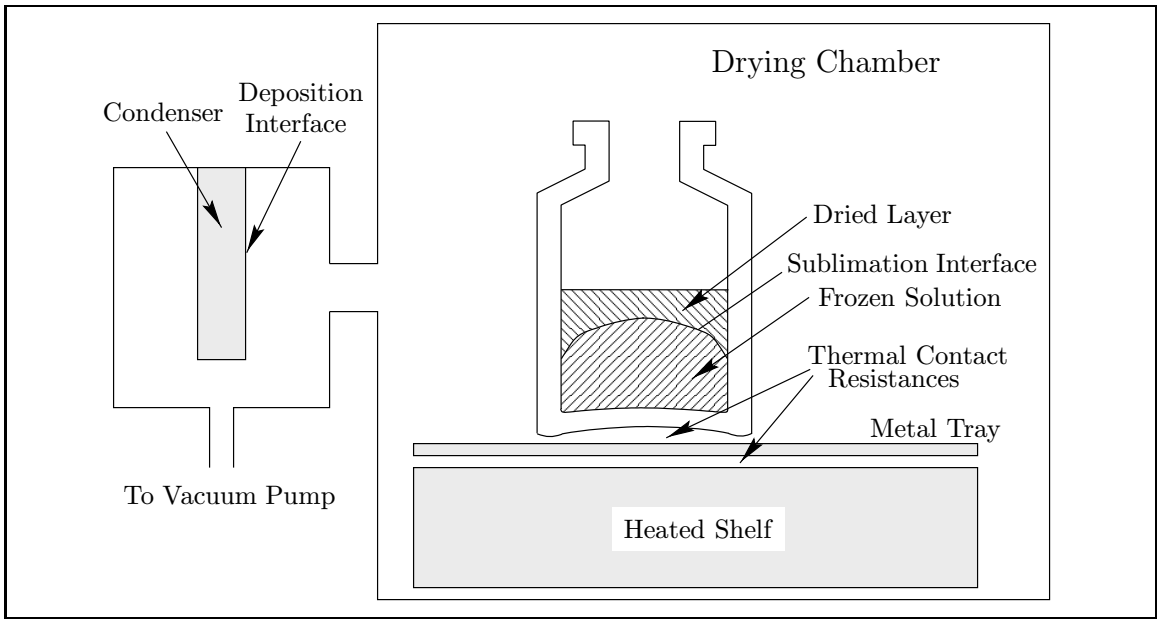


**Figure 3.5** Illustration of a conventional vial freeze-drying process without the vial stopper

3. mass transport of vapor from the sublimation interface to the deposition interface,

4. phase change from vapor to solid (deposition) and,

5. heat flow from the deposition interface.

Of these mechanisms, the rate limiting processes are heat flow to the sublimation interface and mass transport from the sublimation interface to the condensing surface (Pikal et al., 1983, 1984).

It is apparent that there is more to freeze-drying than just the thermodynamics. Maintaining nearly equilibrium conditions does not maximize the drying rate. Temperature, pressure and mass concentration gradients are necessary to maximize drying rates. Thus, heat and mass transfer play important roles in the process. One or the other is the rate limiting mechanism during the primary drying stage. In fact, it is likely that each will serve as the rate limiting process at different times during primary drying (Livesey and Rowe, 1987). The following sections present a discussion of the heat and mass transfer in vial freeze-drying.

## 3.3 Heat Transfer in Vial Freeze-Drying

From the discussion on sublimation and particularly Fig. 3.3, it is obvious that maintaining the maximum allowable temperature of the frozen region during freeze-drying is an essential part of maximizing the drying rate. Pikal (1985) determined that a 1°C increase in temperature can reduce the primary drying time by as much as 13% for the cases studied. Determination of the maximum allowable temperature in pharmaceutical freeze-drying is discussed in Chapter 4. The present section focuses on the issues pertaining to maintaining the desired temperature of the frozen layer in vial freeze-drying.

### 3.3.1 Heat Conduction and Contact Resistance

The dominant mode of heat transfer to the sublimation interface of a product being freeze-dried is conduction (Nail, 1980). In Fig. 3.5, a vial freeze-drying situation is illustrated. Heat is supplied to the sublimation interface using a metal shelf heated by circulating a temperature controlled fluid through it. Heat is conducted from the shelf up through the material and to the sublimation front where that energy is used to supply the latent heat of sublimation.

In this case the heat must travel though several different materials and across several contact resistances. These thermal resistances are the air gap between the tray and the shelf and air gap between the tray and the vial. The thermal circuit is illustrated in Fig. 3.6 showing the contact resistances combined. Measurements and calculations made by Nail (1980) for this situation are presented in Table 3.1. The effect of pressure is clear. At the lower pressure, there is a significant increase in thermal contact resistance and a decrease in the drying rate. Also, it is obvious that the most significant thermal resistance is the contact resistance.

In the low pressure environment of freeze-drying, the contact resistance between the vial and the metal tray as well as the contact resistance between the metal tray and the heated shelf become dependent on the total pressure of the gas in the chamber (Nail, 1980). As the pressure decreases, the number of molecules between two surfaces is reduced. This results in a lower thermal conductivity of the interstitial gas and thus a higher resistance to heat transfer.

Heat can also travel through the dried layer to the sublimation interface. Here again

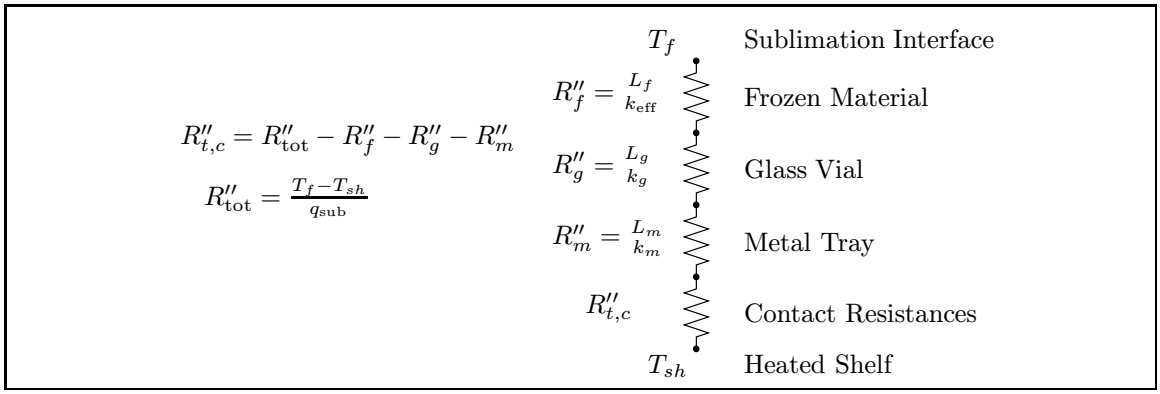


**Figure 3.6** Diagram of thermal resistances in a one dimensional vial freeze-drying process. All thermal contact resistances have been included in the parameter $R''_{t,c}$.

**Table 3.1** Measurements and calculations made by Nail (1980) in the analysis of heat transfer in vial freeze-drying

| | **1.3 Torr** | **0.04 Torr** | **units** |
|---|---|---|---|
| measured drying rate ($W$) | $5.83\times10^{-4}$ | $2.25\times10^{-4}$ | $\frac{\text{kg}}{\text{m}^2\text{s}}$ |
| average product temp ($T_f$) | -10 | -18 | °C |
| $\Delta T = T_f - T_{sh}$ [a] | 55 | 63 | °C |
| $q = W\Delta H_{\text{sub}}$ [b] | 1.634 | 0.631 | $\frac{\text{kJ}}{\text{m}^2\text{s}}$ |
| $R''_{\text{tot}} = \frac{\Delta T}{q}$ | 33.66 | 99.88 | $\frac{^\circ\text{C m}^2}{\text{kW}}$ |
| $R''_{t,c} = R''_{\text{tot}} - R''_f - R''_g - R''_m$ [c] | 27.76 | 93.98 | $\frac{^\circ\text{C m}^2}{\text{kW}}$ |
| $\frac{R''_{t,c}}{R''_{\text{tot}}} \times 100\%$ | 82.5% | 94% | |

[a] $T_{sh} = 45^\circ$C

[b] $\Delta H_{\text{sub}} = 2803.3\frac{\text{kJ}}{\text{kg}}$

[c] $R''_f = 3.7, \quad R''_g = 2.2, \quad R''_m = 0.015 \quad \left(\frac{^\circ\text{C m}^2}{\text{kW}}\right)$

the effective thermal conductivity of the porous material with a gas flowing through it can be increased by increasing the gas pressure within the material. This can be achieved by increasing the total pressure in the drying chamber. However, supplying heat through the frozen layer is much more effective, since the thermal conductivity of the frozen layer is much higher than the effective thermal conductivity of the dried layer (Mellor, 1978).

### 3.3.2 Thermal Capacitance

The driving potential for heat conduction is a temperature gradient. Initially, when the frozen product starts to dry, there is little resistance to mass transfer since the dried layer is small. In this state, the sublimation process can move very quickly if heat is supplied at a high rate. However, since the rate of heat transfer is dependent on a temperature gradient, this means that a large temperature gradient must exist from the shelf to the sublimation interface. Due to the temperature limits of the material, the required gradient cannot be achieved since it would require a high surface temperature on the bottom of the frozen sample.

Livesey and Rowe (1987) discussed the required temperatures for maintaining the maximum rate of sublimation at the start of primary drying. Using a mathematical model, they determined that shelf temperatures greater than 500°C would be required to achieve the maximum rate of sublimation.

Another problem associated with the use of high initial temperatures is the slow response of the shelf temperature. If the sublimation rate is to be kept at a maximum, fast accurate control of the heat transfer would be required. This can be explained by considering a fast sublimation rate as causing a rapid increase in the thickness of the dried layer.

As the dried layer thickness increases, the resistance to vapor flow from the sublimation interface increases. This will cause a reduction in the mass flow rate. If the mass flow rate is decreasing then the rate of heat input should also be decreasing to maintain a constant frozen layer temperature.

If the sublimation process occurs very rapidly, then the shelf temperature needs to fall rapidly. Given the large thermal capacitance of the shelf and subsequent slow response to temperature adjustments, high initial sublimation rates cannot be obtained. In fact, the shelf temperature is typically held constant for the entire primary drying stage and thus is

much lower than necessary at the start of primary drying (Nail, 1980; Livesey and Rowe, 1987).

### 3.3.3 Volumetric Heating

As a means of circumventing the problems associated with thermal contact resistance and conduction heat transfer, it is proposed to use microwave energy to volumetrically heat the material being dried. With volumetric heating, the heat can be generated within the material, thus no large temperature gradients are required to supply heat at a high rate. This also circumvents the problem of response time associated with adjusting the shelf temperature, since the main thermal capacitance is the material and vial combination, which, by itself, is much smaller than the thermal capacitance of the heated shelf and its fluids.

Microwave, or dielectric, heating works by rapid reorientation of polarized molecules in a material that is exposed to a rapidly changing electric field. The most significant type of polarization is dipolar polarization. In a material such as water, there exists a molecular dipole moment due to the differing electronegativities of the oxygen and hydrogen atoms. This dipole moment is the source of dipolar polarization.

In the frequency range of microwaves, the time response of the field changes is similar to the time response of the dipoles. When the field changes, the dipoles realign with the direction of the field. However, the dipoles will lag behind the field. This lag indicates that energy from the field is being transfered to the water, resulting in increasing temperatures.

The dielectric properties of a material characterize the heating of the material in a microwave field. The complex dielectric permitivity, $\epsilon^*$, is given by (Metaxas and Meredith, 1983)

$$\epsilon^* = \epsilon' - j\epsilon''_{\text{eff}} \tag{3.7}$$

where $\epsilon'$ is the dielectric constant and $\epsilon''_{\text{eff}}$ is the effective loss factor. The average power absorbed by a material, $P_{\text{avg}}$, is given by (Metaxas and Meredith, 1983)

$$P_{\text{avg}} = \omega\, \epsilon_0\, \epsilon''_{\text{eff}}\, E^2_{\text{rms}} V \tag{3.8}$$

where $\omega$ is the angular frequency, $\epsilon_0$ is the permitivity of free space ($\epsilon_0 = 8.8 \times 10^{-12}$ F/m), $\epsilon''_{\text{eff}}$ is the effective loss factor including the effects of conductivity, $E_{\text{rms}}$ is the r.m.s. value of the electric field strength in V/m and V is the volume in $\text{m}^3$.

**Table 3.2** Dielectric properties of representative materials in vial freeze-drying. $f = 3 \times 10^9$ Hz

| Material | $\epsilon'$ | $\epsilon''$ | $D_p$ (m) |
|---|---|---|---|
| fused silica (25°C) | 3.78 | 0.0002 | 189.5 |
| manitol (25°C) | 1.82 | 0.0011 | 23.9 |
| ice (-10°C) | 3.2 | 0.003 | 11.6 |
| water (25°C) | 76.7 | 12.00 | 0.014 |

The dielectric constant is a function of frequency, electric field strength, temperature and time history of the material and applied electric field. It is well known that water in its liquid state heats very well. The dielectric properties of ice and other materials common to vial freeze-drying are shown in Table 3.2. It can be seen that liquid water has a very high loss factor compared to the other materials. This indicates that if melting did occur during a microwave freeze-drying process, most of the energy would be absorbed by the liquid water.

Another important parameter to consider when attempting to heat volumetrically with microwaves is the penetration depth. If the penetration depth is small, then most of the heating will be on the surface of the material. In the case being considered here, uniform volumetric heating is desired. The penetration depth for a low loss material can be approximated by the expression (Metaxas and Meredith, 1983)

$$D_p = \frac{\lambda_0'(\epsilon')^{\frac{1}{2}}}{2\pi\epsilon_{\text{eff}}''} \tag{3.9}$$

where $\lambda_0'$ is the free space wavelength of the microwave radiation and is related to the frequency of the microwaves by $f = \frac{c}{\lambda_0'}$ (c is the speed of light in free space). The penetration depths are also included in Table 3.2. For the materials used in freeze-drying, the penetration depths are very large compared to the actual dimensions of common vials ($\sim 15$ mm diameter).

## 3.4 Mass Transport in a Porous Material

As previously mentioned, mass transport in porous materials is an important part of freeze-drying. In fact, it has been determined that approximately 90% of the resistance to vapor flow from the sublimation interface to the condenser is due to the porous dried layer that

| flow regime | | mechanisms | driving potential |
|---|---|---|---|
| Knudsen | ↑ | Knudsen diffusion | concentration gradient |
| transition | surface flow | slip flow (Knudsen+viscous) | concentration gradient pressure gradient |
| continuum | ↓ | viscous flow binary diffusion | pressure gradient concentration, temperature gradient |

**Figure 3.7** Chart showing the three flow regimes, the independent flow mechanisms and the driving potential for each flow mechanism

forms as the interface recedes into the material (Nail, 1980; Pikal et al., 1983). Accelerating the sublimation process means providing conditions for a maximum rate of mass transfer through the dried layer. Thus, a clear understanding of gas flow in a porous material is essential.

To maximize the rate of vapor flow through the dried layer, we must first understand the mechanisms by which the vapor moves through a porous material. There are three flow regimes. In each flow regime, there is more than one mechanism by which mass transport can take place. The three flow regimes are (Mason and Malinauskas, 1983):

1. **Knudsen flow**, where molecule-wall interactions are dominant,
2. **transition flow**, where both molecule-molecule interactions and molecule-wall interactions are important, and
3. **continuum flow**, where molecule-molecule interactions are dominant.

The flow regimes and several mass transport mechanisms along with driving potentials are listed in Fig. 3.7.

The Knudsen number, $Kn$, is used to determine the flow regime. It is defined as

$$Kn = \frac{\lambda}{d} \tag{3.10}$$

where $d$ is a characteristic length of the porous material, usually taken to be the average pore diameter, and $\lambda$ is the mean free path of the gas molecules. For $Kn \gg 1$ the flow is Knudsen flow, for $Kn \ll 1$ the flow is in the continuum regime and for $Kn \approx 1$ the flow is transitional.

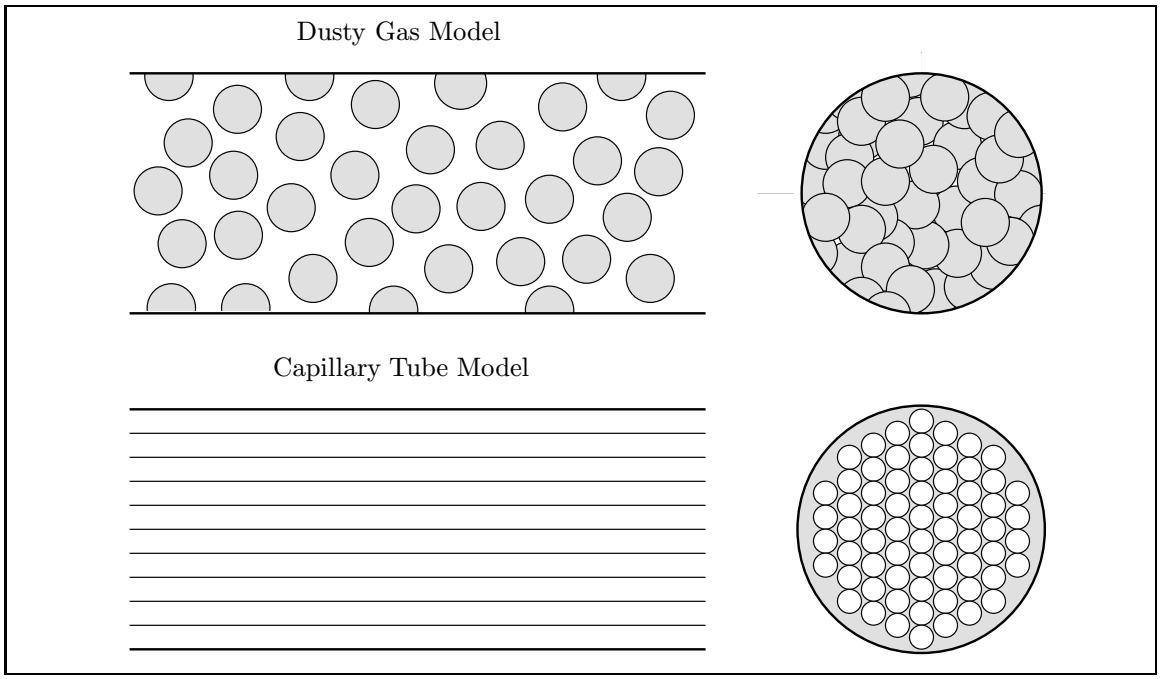


**Figure 3.8** Illustration of common models used to represent the structure of a porous material

In deriving the equations of mass transfer for the mechanisms mentioned above, the porous structure is modeled to simplify the mathematical description of the structure. The most popular models for the transitional flow regime in which all three mechanisms are important are the capillary tube model and the dusty gas model as illustrated in Fig. 3.8. The capillary tube model treats the porous material as a bundle of capillary tubes. It is not used here since a better representation of the porous material is provided by the dusty gas model.

The dusty gas model treats the porous material as a matrix of very large spheres (dust particles). The large spheres can be treated as a third component of a ternary mixture to derive equations for a binary diffusion problem. In this case, the two components of the binary diffusion problem are water vapor and an inert component representing air. This type of model is applicable to all three flow regimes, but does not include surface flow. Also, it does not include inertial terms or turbulence when modeling viscous flow.

In deriving the equations, the conditions imposed on the large spheres are: zero velocity and no concentration gradient

$$N''_D = 0; \qquad \frac{dC_D}{dx} = 0 \tag{3.11}$$

where $N''_D$ is the molar flux of the dust molecules and $C_D$ is the molar concentration of the dust molecules.

The dusty gas model was used by Evans et al. (1961) to derive the mass transport equations in a porous material, for binary diffusion with no pressure gradient. It allows unknown mass transport parameters to be reduced to two simple parameters that are independent of pressure and are determined by the structure of the porous material. These equations are (Evans et al., 1961)

$$N''_v = -\frac{c_2 D_{va} K_v}{(K_v + c_2 D_{va})\, RT} \frac{\partial P_v}{\partial x} + \frac{y_v K_v}{K_v + c_2 D_{va}} \left(N''_v + N''_a\right) \tag{3.12a}$$

and

$$N''_a = -\frac{c_2 D_{va} K_a}{(K_a + c_2 D_{va})\, RT} \frac{\partial P_a}{\partial x} + \frac{y_a K_a}{K_a + c_2 D_{va}} \left(N''_v + N''_a\right) \tag{3.12b}$$

where the subscripts $v$ and $a$ refer to water vapor and air respectively and the Knudsen diffusivities, $K_v$ and $K_a$, are

$$K_v = c_1 \sqrt{\frac{RT}{M_v}}; \quad K_a = c_1 \sqrt{\frac{RT}{M_a}} \tag{3.13}$$

and the coefficients $c_1$ and $c_2$ are dependent only on the structure of the porous material. These equations, while providing diffusion flux due to a concentration gradient, do not contain the effects of hydrodynamic flow induced by the total pressure gradient.

The first step toward including hydrodynamic flow is to put these equations into a form that contains the total pressure gradient, which supplies the driving force for hydrodynamic flow. This can be done by using the following identities and solving Eqn. 3.12a and Eqn. 3.12b simultaneously:

$$P_v = y_v P \tag{3.14}$$

$$P_a = y_a P \tag{3.15}$$

$$y_v + y_a = 1 \tag{3.16}$$

After some algebraic manipulation, the result for component $v$ is

$$N''_v = \frac{-1}{RT} \left( \frac{c_2 D_{va} K_v}{(c_2 D_{va} + K_m)} \frac{\partial P_v}{\partial x} + \frac{y_v K_v K_a}{(c_2 D_{va} + K_m)} \frac{\partial P}{\partial x} \right) \tag{3.17}$$

where $K_m = K_v y_a + K_a y_v$. A similar result can be obtained for component $b$. At this point, it is useful to introduce $D^o_{va} = D_{va} P$, since this quantity is independent of pressure. This

yields

$$N_v'' = \frac{-1}{RT}\left(\frac{c_2 D_{va}^o K_v}{(c_2 D_{va}^o + K_m P)}\frac{\partial P_v}{\partial x} + \frac{K_v K_a P_v}{(c_2 D_{va}^o + K_m P)}\frac{\partial P}{\partial x}\right) \tag{3.18}$$

The hydrodynamic flow can be modeled using the D'Arcy equation. For component A in a gas mixture, the D'Arcy equation is (Gunn and King, 1969)

$$y_v N''(\text{viscous}) = N_v''(\text{D'Arcy}) = -\frac{c_0\, P\, y_v}{\mu_m R T}\frac{\partial P}{\partial x} \tag{3.19}$$

where $c_o$ is determined by the structure of the porous material and is related to the permeability.

The diffusion flux and viscous flux can be shown to be independent in the first approximation of the dusty gas model (Mason et al., 1967). Therefore, the total molar flux can be determined by adding the equations of diffusion flux and viscous flux:

$$N''(\text{total}) = N''(\text{diffusive}) + N''(\text{viscous}) \tag{3.20}$$

A similar relationship can be written for a single component of a binary mixture:

$$N_i''(\text{total}) = N_i''(\text{diffusive}) + y_i N''(\text{viscous}) \tag{3.21}$$

where $y_i$ is the mole fraction of component $i$.

Substituting Eqn. 3.19 and Eqn. 3.18 into Eqn. 3.21, the following equations give the total molar fluxes of component $v$, $N_v''$, and component $a$, $N_a''$:

$$N_v'' = -\frac{1}{RT}\left(k_1\frac{\partial P_v}{\partial x} + k_2 P_v\frac{\partial P}{\partial x}\right) \tag{3.22a}$$

$$N_a'' = -\frac{1}{RT}\left(k_1\frac{\partial P_a}{\partial x} + k_2 P_a\frac{\partial P}{\partial x}\right) \tag{3.22b}$$

where $k_1$ and $k_2$ are

$$k_1 = \frac{c_2 D_{va}^o K_v}{(c_2 D_{va}^o + K_m P)} \quad \text{and} \quad k_2 = \frac{K_v K_a}{(c_2 D_{va}^o + K_m P)} + \frac{c_0}{\mu_m} \tag{3.23a}$$

and

$$k_3 = \frac{c_2 D_{va}^o K_a}{(c_2 D_{va}^o + K_m P)} \quad \text{and} \quad k_4 = k_2 \tag{3.23b}$$

These equations describe the mass transfer rate as a function of the pressure gradient in the porous material. To apply these equations, the parameters $c_0$, $c_1$ and $c_2$ must be determined experimentally. Obtaining these parameters can be difficult. However, it is possible that the

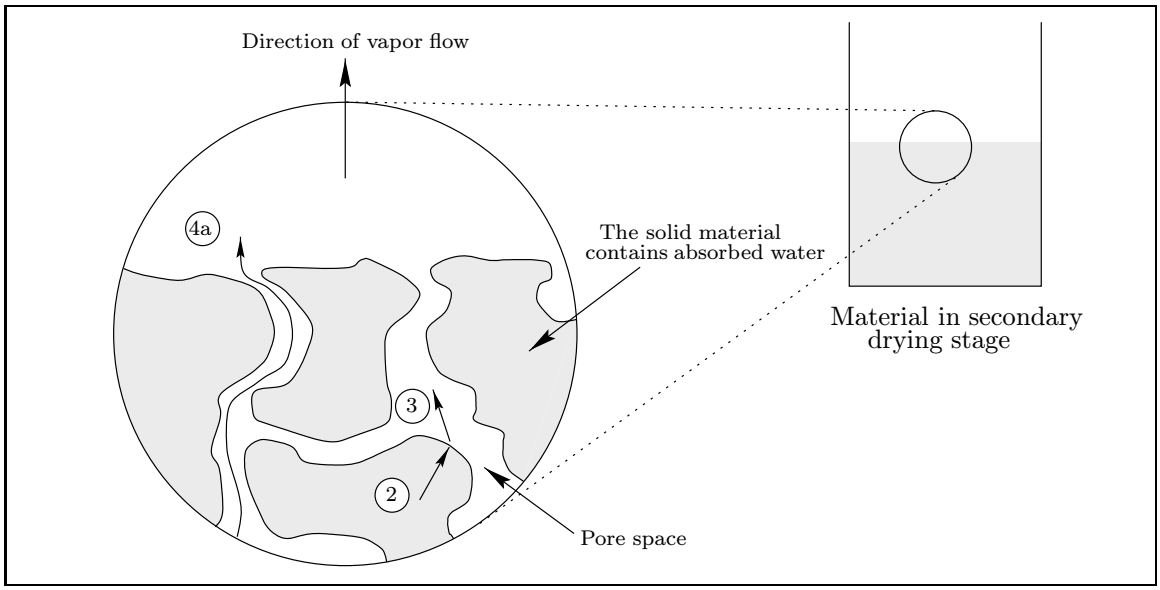


**Figure 3.9** A microscopic view of the secondary drying process where diffusion ② and desorption ③ are the rate limiting processes

problem can be simplified by using only the D'Arcy equation if the other flow mechanisms do not make significant contributions to the vapor flow through the dried region. This would result in the relative permeability, $c_0$, being the only parameter needed and would also greatly simplify the solution of model equations.

## 3.5 Desorption and Mass Diffusion in Secondary Drying

During the freezing process, ice crystals form from the water in the solution. As these ice crystals form, the remaining solution becomes more concentrated. This process of freeze concentration continues until the solution becomes so concentrated that the material is in a glassy state and is a true amorphous solid. Further cooling of the product beyond this point does not cause any measurable changes in the amorphous material.

Secondary drying is the process of removing the unfrozen or 'bound' water contained in the amorphous material. For the bound water to be removed, it must first diffuse from within the solid material to the surface of a pore. At this point, the water will desorb from the surface. The rate of diffusion and desorption is determined by the temperature of the material and the amount of moisture in the pore.

The mechanism for removal of the unfrozen residual moisture is primarily desorption. This means that release of the residual moisture can be predicted by desorption isotherms

(MacKenzie, 1977). A desorption isotherm gives the residual moisture content as a function of humidity for a given temperature. Using these data one can determine a temperature-pressure protocol for secondary drying that will bring the residual moisture content to the required level.

Water will follow the same path as in primary drying, from the material to the condenser. However, in secondary drying, diffusion of unfrozen water from within the material to its surface and subsequent desorption of that water become the most important mechanisms. Figure 3.9 shows how absorbed water diffuses to the solid-vapor interface, then desorbs and flows out of the material.

The possibilities for rate controlling mechanisms are

1. heat flow to the solid,

2. diffusion of the unfrozen water to the solid-vapor interface,

3. desorption from the solid surface to the vapor flow,

4a. diffusion through the porous material,

4b. mass transport from the porous material to the condensing surface,

5. phase change from vapor to solid (deposition), and

6. heat flow from the deposition interface.

The numbers in Fig. 3.9 correspond to the numbers in the above list. Pikal et al. (1990) concluded that water transport is not the rate limiting process in the secondary drying stage. The rate limiting process in secondary drying is either molecular diffusion of water molecules from within the solid to a pore surface or desorption of the water molecules from the surface of the solid.

Pikal et al. (1990) determined that the effect of chamber pressure on the secondary drying rate was insignificant, but that the effect of temperature was found to be significant. However, without desorption-isotherm data, the temperature must be determined by trial and error (Snowman, 1993).

## 3.6 Summary

The basis of the freeze-drying process is sublimation. Sublimation is a phase change from a solid to a gas. The conditions for the sublimation of ice to occur are temperature and vapor pressure below the water triple point. Also, since sublimation is an endothermic process, it requires heat input. The rate of sublimation during freeze-drying is dependent on many parameters, such as ice temperature, chamber pressure, resistance to vapor flow and resistance to heat flow.

There are two important process variables used to control the freeze-drying process: temperature and pressure. The ideal situation for maximizing the drying rate during primary drying is to maintain the maximum allowable temperature and lowest practical pressure. The maximum allowable temperature is determined by the material being dried and will be discussed in the next chapter. The pressure is determined by the effect of pressure on the mass transfer rate through the dried layer. Pressure should be decreased to the point where further decreasing the pressure has no effect on the drying rate.

In conventional freeze-drying, the pressure is not kept low, but in fact is used to control temperature. This is done mostly because the pressure controls the heat transfer to the drying product. Also, it is more important to maintain the maximum allowable temperature than it is to maintain a very low pressure.

A better solution might be to heat volumetrically and remove the dependence of heat transfer on pressure. Microwave energy can be used to supply heat volumetrically to pharmaceutical products during vial freeze-drying. Considering the dielectric properties of the material involved, it appears that the use of microwaves may be a viable solution.

# Chapter 4

# Application of Materials Science to Freeze-Drying

The product temperature during freeze-drying and the final moisture content determine the product quality. Both low temperature and low moisture content enhance product quality, but degrade process economics. Therefore, it is important to find operating conditions that not only provide acceptable quality but also minimize processing cost.

Recent research has shown that maintaining an acceptable product quality usually requires that freeze-drying be performed at temperatures below the glass transition temperature of the frozen product (Franks, 1989; Franks et al., 1991; Pikal and Shah, 1990). Thus, this temperature is usually taken as the upper temperature limit during primary drying. However, to minimize drying time, the primary drying temperature should be maintained as close as possible to its upper limit set by the glass transition temperature.

## 4.1 Glass Transition

When a material is not allowed to crystallize upon freezing, it forms an amorphous phase. In this case, the material remains as a liquid below its normal freezing temperature but eventually goes through a rapid increase in viscosity as the temperature continues to fall. This transition is known as a *glass transition* since the material is a glass.

A glass is a true solid that has the chemical composition of a crystalline solid but does not have the ordered molecular structure of the crystalline solid. Figure 4.1 shows how a material that would normally be expected to crystallize under slow freezing might form

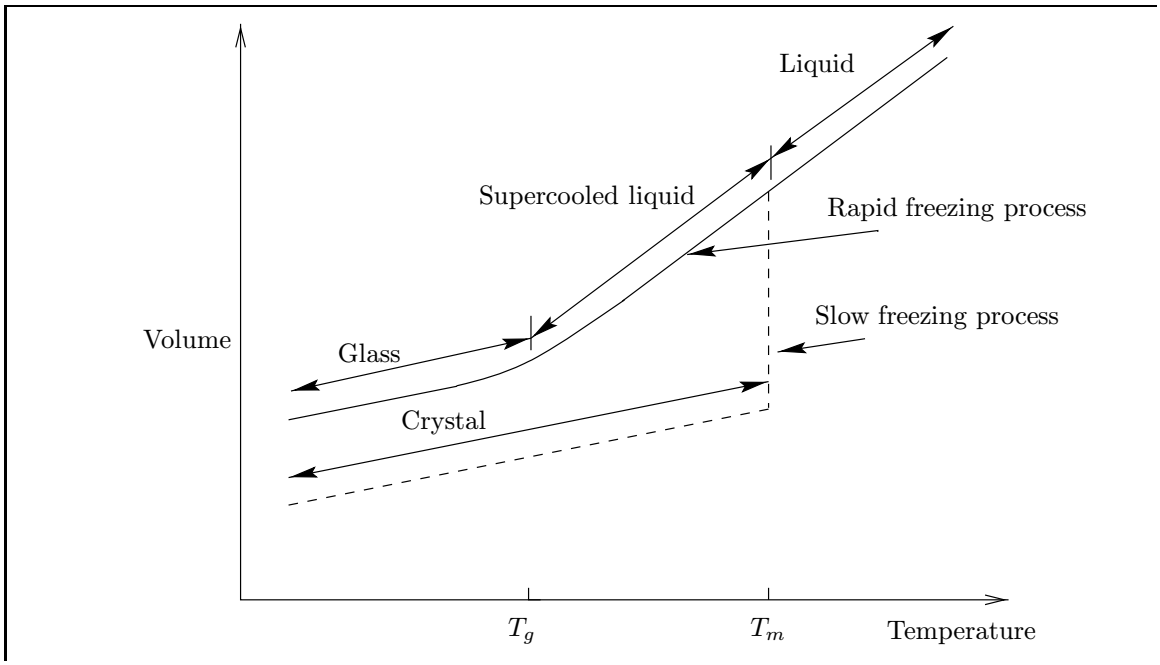


**Figure 4.1** A comparison of thermal expansion curves for a material undergoing crystallization and for the same material forming a glass (Shackelford, 1988)

a glass if it is rapidly frozen (Shackelford, 1988). The glass transition temperature, $T_g$, is usually taken as the midpoint of this transition region. There is often significant variability in $T_g$ measurements since the beginning and ending of the transition region are not well defined.

In the case being studied here, the material of interest is the porous material that forms upon freezing. The glass transition temperature of this material depends strongly on the amount of residual moisture contained in the material. Since the product is being dried, the amount of residual moisture changes during freeze-drying, especially during the secondary drying process. Thus, there is not one single value for $T_g$ but rather a range of $T_g$ values corresponding to the range of residual moisture content. The highest residual moisture content occurs after freezing and results in the lowest $T_g$ while the lowest moisture content is achieved at the end of the drying process and results in the highest $T_g$. The most important points in the range of $T_g$ values encountered are the initial value after freezing and the final value at the end of the secondary drying stage.

The following section describes the formation of the porous material upon freezing and its glass transition temperature.

## 4.2 Freeze-Concentration

Freezing is a separation process. In an aqueous solution, freezing forms ice crystals of pure water. As the freezing process continues, more and more water contained in the solution freezes. This results in an increasing concentration of the remaining solution. As the solution becomes more concentrated, its viscosity increases. Eventually, the solution reaches a point where further cooling will no longer change the concentration of the solution. A small percentage of the initial water remains in the solution and does not freeze out: it is called the residual moisture or sometimes the *bound* water.

This point, where further cooling will not further increase the concentration of the solution, is also referred to as the point of maximal freeze-concentration. At temperatures below this point, it is important to note that the concentrated solution has become an amorphous solid (a glass) with an associated glass transition temperature and a specific amount of residual moisture that is independent of the original concentration of the solution. The specific amount of residual moisture is termed $w'_g$, and the glass transition temperature of the material at this particular residual moisture content is termed $T'_g$.

Figure 4.2 shows a state diagram for a sucrose and water system. This diagram shows how a dilute sucrose solution will increase in concentration during freezing until the temperature reaches the $T'_g$ value. At this point the sucrose concentration is 80% and further cooling will not change this concentration. Note that $T'_g$ is reached during freezing for any concentration under approximately 80%.

It should also be noted that the temperature of the solution must be brought below $T'_g$ for freezing to go to completion, a requirement to maintain a high product quality throughout the freeze-drying process.

## 4.3 The Role of $T_g$ during Freeze-Drying

As previously indicated, the glass transition temperature is usually the upper limit for the primary drying temperature. For dried products, the glass transition temperature is the theoretical upper temperature limit for maintaining stability of the active components. This section discusses the relationship between the glass transition temperature and product quality.

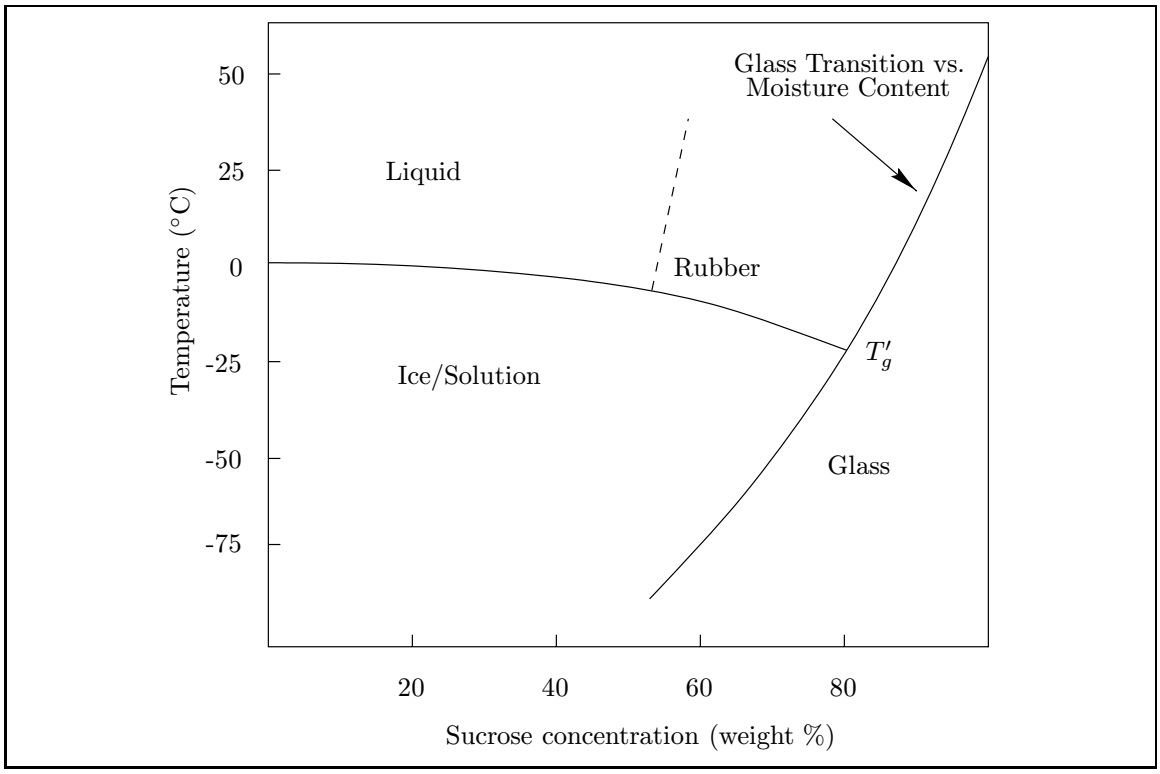


**Figure 4.2** State diagram for a binary system of sucrose and water showing the $T'_g$ value

### 4.3.1 Biological and Pharmacological Effects

Most of the chemical and biochemical changes that might affect the shelf life of a product occur as the temperature of the product rises above the glass transition temperature (Franks et al., 1991). However, if the material temperature remains close to the glass transition temperature without exceeding it at any time during the drying process, product stability is maintained. Thus, the glass transition temperature is an important consideration when developing a freeze-drying protocol designed to achieve maximum product quality.

### 4.3.2 Physical Effects

During primary drying, if the temperature of the product exceeds $T'_g$, collapse can occur. This phenomenon greatly increases the required time for the product to dry as well as the likelihood of in-process decomposition. Products that collapse typically have high residual moisture contents, longer rehydration times and low stability (Pikal and Shah, 1990). Figure 4.3 illustrates the structural difference between a product in which collapse has occurred and one in which collapse has not occurred.

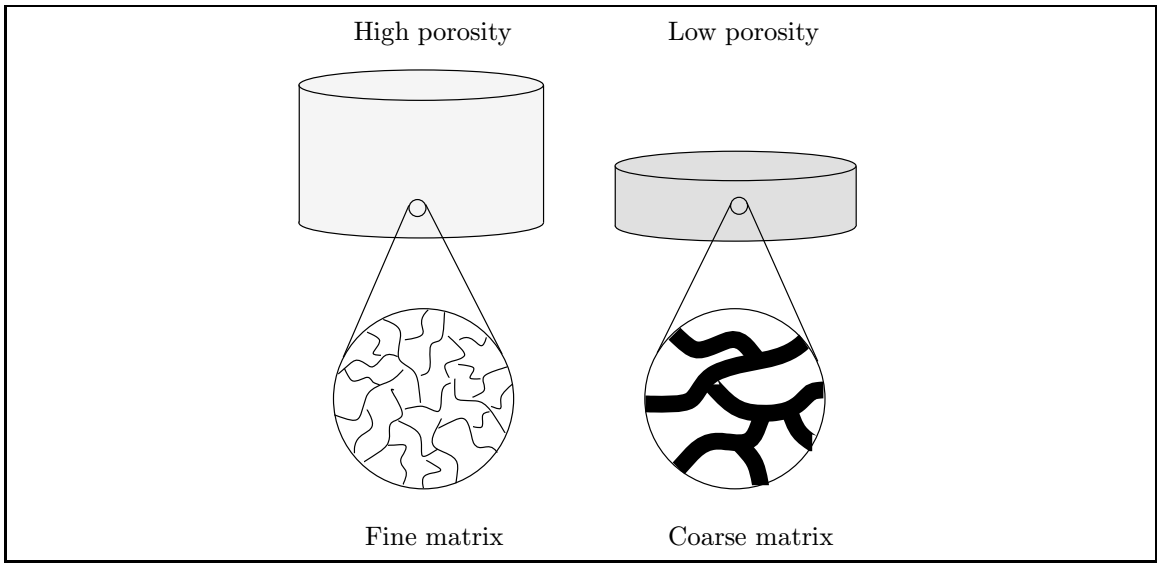


**Figure 4.3** A comparison of structure with and without collapse. In the collapsed structure, viscous deformation has occurred and the residual moisture content remains high after secondary drying.

Collapse, in pharmaceutical freeze-drying, refers to the degradation of the structure of the dried product as the sublimation interface passes through the material. This phenomenon is highly dependent on temperature and is usually associated with primary drying. It typically occurs when the temperature of the product is allowed to rise a few degrees above $T_g'$. Above $T_g'$, an increase in the viscosity occurs causing viscous deformation.

The collapse temperature, $T_c$, is related to the glass transition temperature, $T_g'$, in that the glass transition in the amorphous phase must take place, hence increasing the viscosity of the phase, before collapse can occur. Pikal and Shah (1990) make the distinction between $T_c$ and $T_g'$ by defining collapse as "the result of a glass transition in the dried region formed during primary drying, while $T_g'$ refers to a glass transition in the amorphous phase in contact with ice."

It is generally considered that $T_c$, the temperature at which collapse occurs, is slightly different from $T_g'$. However, some researchers have assumed that they are equal (Hatley and Franks, 1991). In their study on collapse, Pikal and Shah (1990) found that the collapse is dependent on the sublimation rate and often occurs at a temperature a few degrees higher than $T_g'$. It should also be kept in mind that $T_g'$ refers to the glass transition temperature of the amorphous phase *before* the ice has been removed. After the sublimation front passes a given point in the material, the amount of residual moisture can increase or decrease

**Table 4.1** Collapse temperatures of some common pharmaceuticals (MacKenzie, 1977; Hatley and Franks, 1991)

| **Substance** | $T_c$ (°C) | $T_g'$ (°C) |
|---|---|---|
| Dextran | -9 | |
| Ficoll | -19.5 | |
| Fructose | -48 | -42 |
| Gelatin | -8 | |
| Glucose | -40 | -43 |
| Inositol | -27 | |
| Lactose | -32 | |
| Maltose | -32 | -29.5 |
| Mannitol | -30 | |
| Monosodium glutamate | -50 | |
| Polyvinal pyrrolidine | -23 | |
| Raffinose | -26 | |
| Sorbitol | -45 | -43.5 |
| Sucrose | -32 | -32 |

through adsorption and desorption and subsequently change the glass transition temperature to either inhibit or promote collapse. It is also important to note that Pikal and Shah (1990) determined the glass transition temperatures of their samples with a freeze-drying microscope. Other researchers (Franks, 1989; Hatley and Franks, 1991) have used a differential scanning calorimeter (DSC) to measure $T_g'$ and assumed that $T_c = T_g'$.

Table 4.1 lists the collapse temperatures and glass transition temperatures of some common pharmaceuticals (MacKenzie, 1977; Hatley and Franks, 1991). The $T_g'$ values were measured with the use of a DSC, however the method of measurement used to determine collapse temperatures was not provided, but is most likely the freeze-drying microscope method.

### 4.3.3 Maximum Storage Temperature

The goal of freeze-drying is to produce a shelf-stable product, which means a product stable at room temperature. From previous sections, it is known that maintaining stability requires keeping the product temperature below its glass transition temperature. This avoids the detrimental effects of viscous deformation. The glass transition is dependent on residual moisture content. The purpose of secondary drying is to decrease the residual moisture content and thereby to increase the glass transition temperature which in turn results in a

more stable product.

For the product to be stable at room temperature, the glass transition temperature should be about 30°C above room temperature for maximum stability. This brings up the question of when to stop the drying process. Since freeze-drying is a very energy intensive process, it is advantageous to stop the drying process as soon as the required residual moisture content has been reached. Thus, knowledge of the glass transition temperature as a function of moisture content is important for optimizing the freeze-drying process.

## 4.4 Measurement of Glass Transition Temperatures

A differential scanning calorimeter (DSC) can be used to determine the glass transition temperature as a function of moisture content of a material. This curve can be very useful in developing a freeze-drying schedule that maintains a high product quality for a particular material.

Figure 4.4 shows and example of a DSC trace for a BHI/trehalose sample. This trace shows that an endothermic event begins at approximately 40°C. This is the start of glass transition. The dashed lines shown in the figure can be used to determine the glass transition temperature for this BHI/trehalose sample which is estimated to have an 11% residual moisture content.

### 4.4.1 Materials

In this work, experiments were conducted using a mixture of brain heart infusion (BHI) broth and trehalose, a sugar. This mixture was used to suspend the proposed vaccine strain of the noncapsulated bacterial mutant *A. pleuropneumoniae*, J45-C. The mixture contained 2 grams of trehalose for every 10 ml of BHI broth. The vaccine did not affect the drying characteristics since it was only a very small part of the solution. Therefore, most of the drying experiments as well as the glass transition measurements did not include the vaccine. The drying experiments and the results will be discussed in the following chapters while the discussion of the measurement of glass transition temperatures follows.

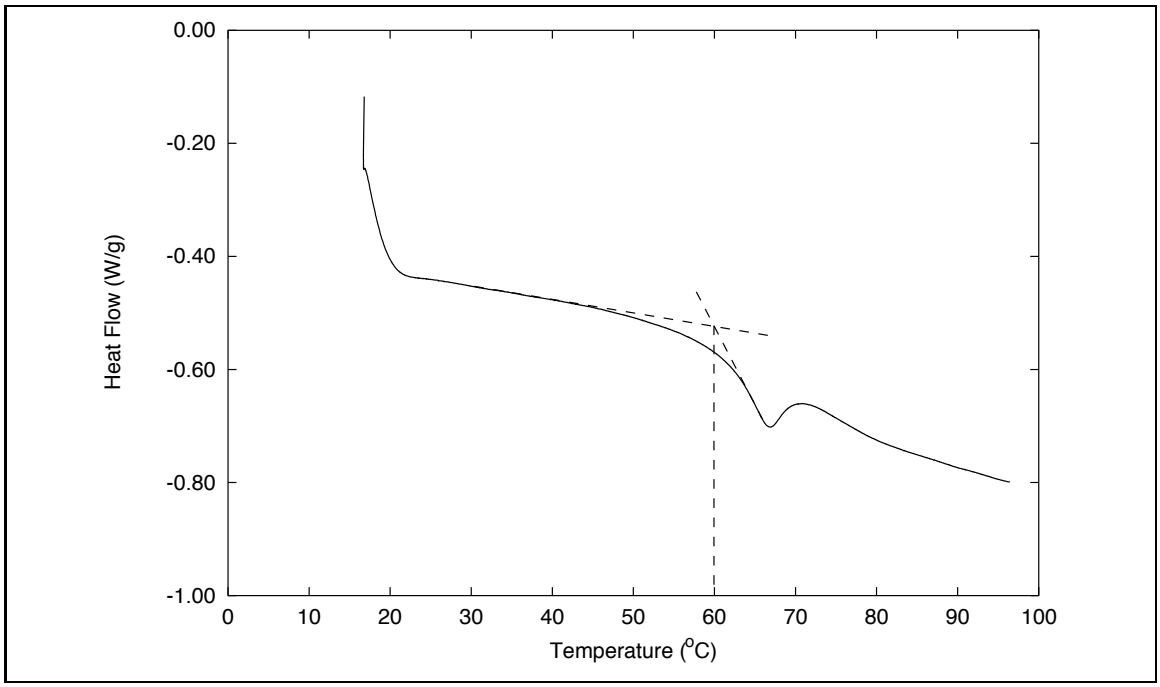


**Figure 4.4** Example of a DSC trace for a freeze-dried sample with 11% moisture content showing a glass transition at 60°C

### 4.4.2 Preliminary Measurements

The first step in conducting a thermal analysis of the materials was to obtain thermogravimetric analysis (TGA) and DSC measurements of each material individually, for a specific mixture of the materials and for the freeze-dried mixture of material. The mixture ratio for the material is always the same. The results of the tests discussed in this section are presented in Appendix E.

A thermogravimetric analysis measures the change in the weight of the material as the temperature of the material is slowly increased. These measurements record temperatures at which volatile components are given off. The results indicate that the mixture of the two materials behaves as a superposition of the two individual materials and that there is no complex interaction between the two materials.

DSC measurements were also taken for the individual components as well as for the mixtures. The results show a distinct difference between the dry mixture and the freeze-dried mixture containing about 11% residual moisture content. The freeze-dried mixture exhibits a glass transition at 60°C. This is indicated in Fig. 4.5.

### 4.4.3 Glass Transition Temperature versus Moisture Content

Based on the preliminary results, the glass transition temperature was measured as a function of moisture content. Measurements were made for residual moisture contents in the range of 7% to 18% moisture content and were compared to the results of the Fox equation (Sperling, 1992)

$$\frac{1}{T_g} = \frac{M_1}{T_{g1}} + \frac{M_2}{T_{g2}} \tag{4.1}$$

where $M_1$ is the mass fraction of water, $M_2$ is the mass fraction of the BHI/trehalose mixture, $T_{g1}$ is effective glass transition of water and $T_{g2}$ is the glass transition of the BHI/trehalose mixture at zero moisture content.

The Fox equation is plotted in Fig. 4.5 along with measured glass transition temperatures. The effective glass transition temperature of liquid water was estimated as -147.4°C (125.8 K). This is an *effective* value since water brought down to this temperature would actually freeze into a crystalline structure which does not have a glass transition temperature. The glass transition temperature of the dry BHI/trehalose mixture was measured as 71.0°C (344.1 K).

Figure 4.5 shows the correlation between the amount of residual moisture contained in a freeze-dried sample of BHI/trehalose versus the measured glass transition temperature. If the temperature at which the dried material will be stored is known, then the maximum allowable residual moisture content can be estimated using the DSC data and the Fox equation (Sperling, 1992) as a model. Likewise, if the required final moisture content is known, then the point at which the drying process can be stopped will be known.

The difference between the measured data and line predicted by the Fox equation (Fig. 4.5) can be explained by error in the DSC measurement of the glass transition temperature as well as error in the prediction of the residual moisture content. The residual moisture content is determined by estimating the initial mass fraction of the water in the solution based on the amount of dry ingredients used to prepare the solution. Once the initial amount of water is known for a given sample, subtracting the weight loss measured during the freeze-drying process gives the residual moisture content.

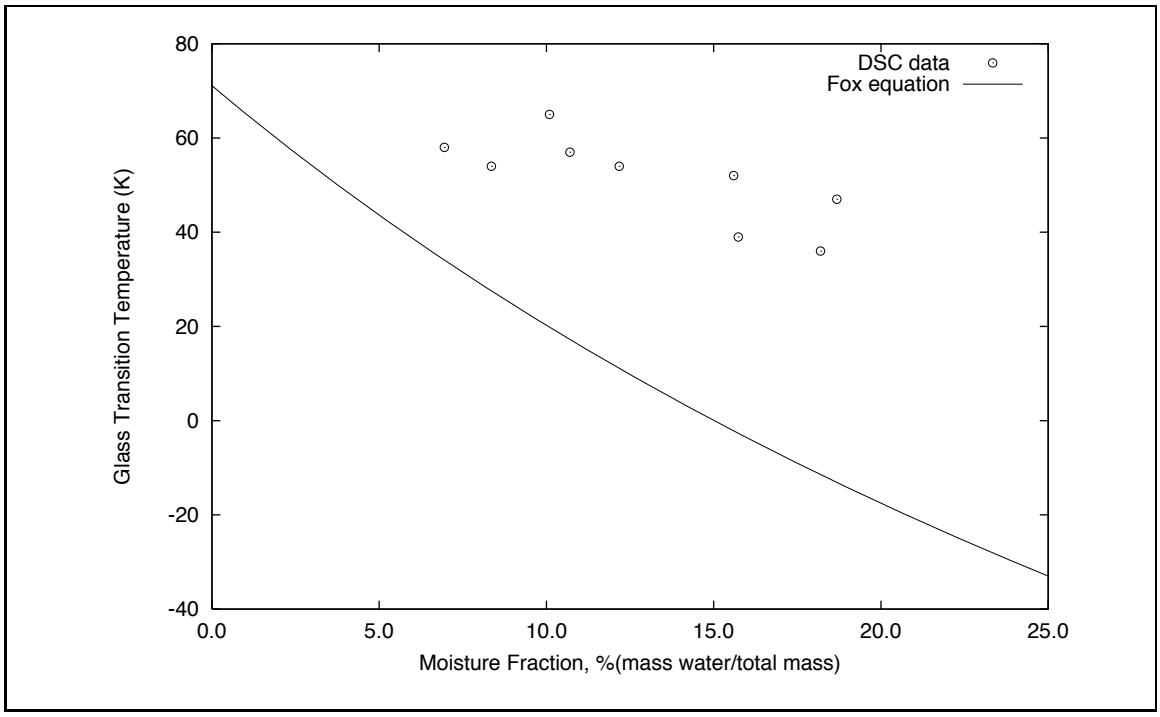


**Figure 4.5** Glass transition temperature as a function of residual moisture content

### 4.4.4 Measurement of $T_g'$

The measurement of $T_g'$ is a little more difficult than the measurements of $T_g$ versus moisture content. In this case, the sample must be frozen and placed in the DSC at a very low temperature. This was done by placing a small amount of the liquid solution into a DSC pan. The pan was then placed in a glass vial which was in turn held in liquid nitrogen until the solution in the DSC pan was frozen.

Hatley and Franks (1991) reported that $T_g'$ for trehalose is -32°C. This value can vary by several degrees depending on the procedures used to prepare the samples and to measure the transition temperatures. The $T_g'$ of the mixture being used in the current experiment could be either above or below the value for trehalose since it is not known how the addition of the BHI affects the trehalose. Other factors may influence the measurement of $T_g'$, such as the freezing rate and the heating rate utilized in the DSC measurement. Indeed, the freezing rate can influence the $T_g'$ measurement by causing differences in the amount of air trapped in the amorphous phase. The heating rate influences the measurement by increasing the glass transition measurement as the heating rate increases.

In the present work, the DSC apparatus was operated in sub-ambient mode using

liquid nitrogen, hence allowing to start the DSC scan at approximately -100°C. The DSC scan was run up to melting temperature, at a constant heating rate of 10°C/minute. The results of several DSC runs indicate that $T'_g$ is approximately equal to -50°C. Combining the previous experimental results with the Fox equation, the value of $w'_g$ is estimated equal to approximately 30% moisture content.

The results of this chapter will be an important consideration when analyzing the results of the viability study presented in Chapter 6. The $T'_g$ value is very low and the freeze-drying systems used in this study are currently not capable of freeze-drying at such a low temperature. However, the structural degradation caused by freeze-drying above the $T'_g$ may be prevented if the moisture content of the material falls very quickly as the sublimation interface recedes into the sample. However, the same would probably not hold true for the biochemical effects.

# Chapter 5

# Description of the Experimental Apparatus and Methods

In this work, it is proposed that microwave freeze-drying can be a viable alternative to conventional freeze-drying and that microwave freeze-drying offers an advantage over conventional freeze-drying. Demonstrating and evaluating these ideas are the purposes of the experimental work.

The experimental program is divided into two phases: I) a comparison of conventional and microwave freeze-drying on a laboratory scale and II) a demonstration of the potential of microwave freeze-drying to offer economic savings by reducing processing time. The experimental microwave freeze-drying apparatus and the experimental program are discussed in detail in this chapter.

## 5.1 Description of the Experimental Apparatus

Microwave freeze-drying was conducted in an experimental microwave freeze-drying system. The overall system, as shown in Fig. 5.1, is composed of four major subsystems: the vacuum system, the microwave power circuit, the temperature and weight measurement devices and the data acquisition system. The following sections describe the apparatus in detail. Appendix C contains a list of equipment with specifications.

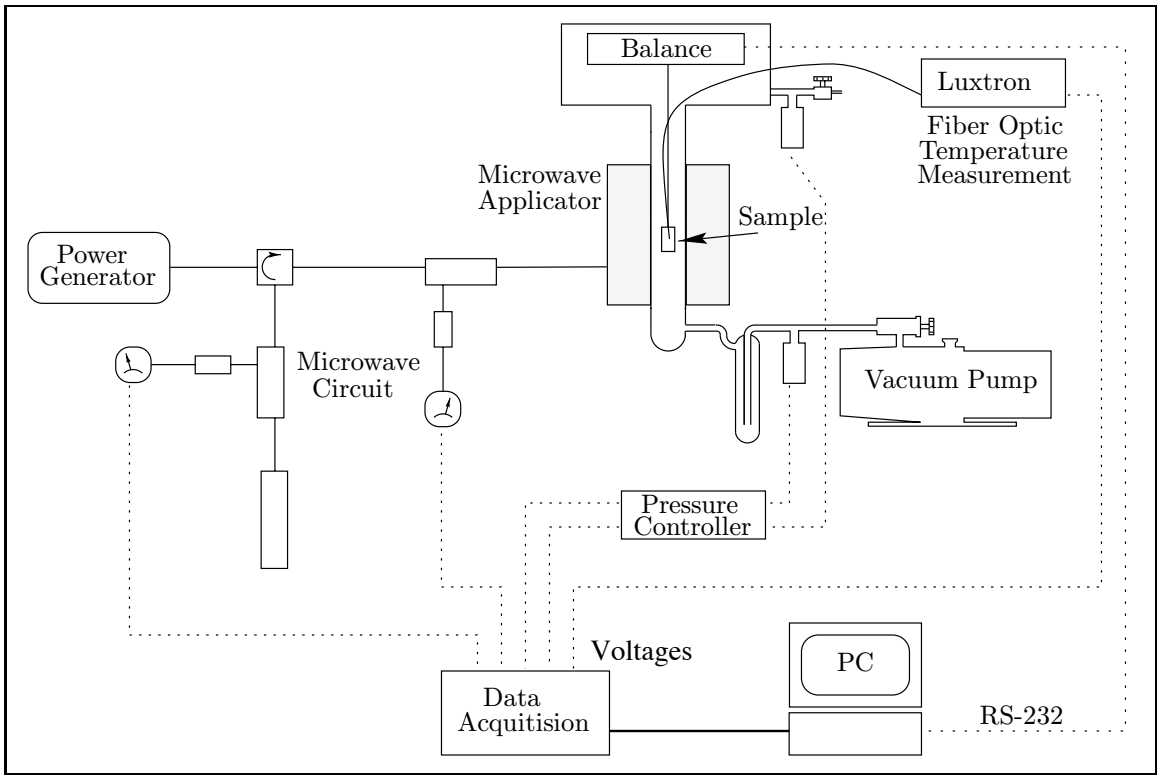


**Figure 5.1** Schematic of the experimental microwave freeze-drying system showing the major components

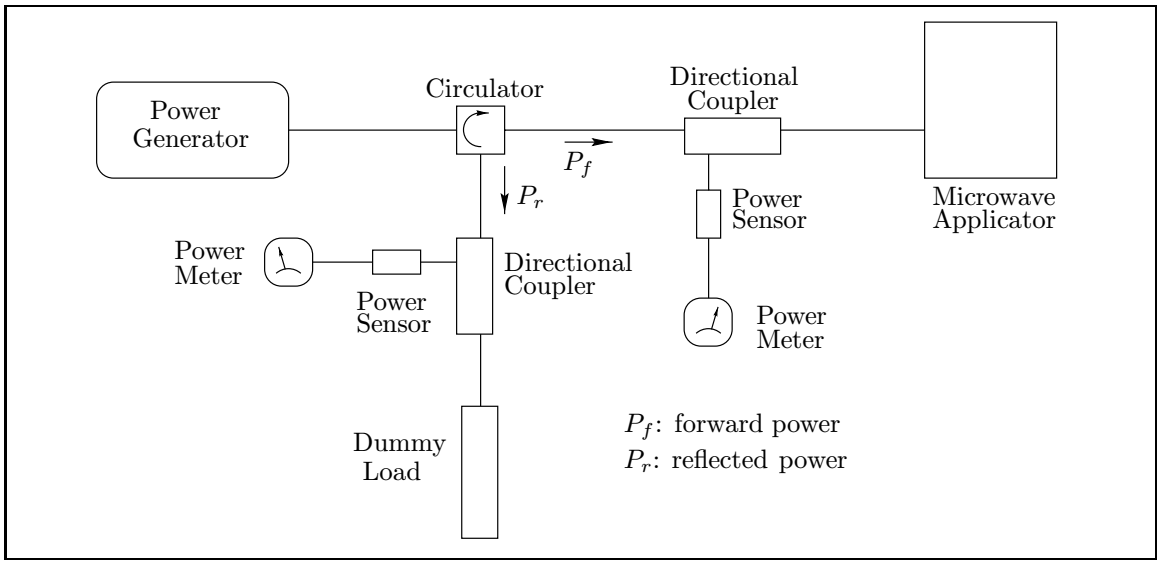


**Figure 5.2** Schematic of the microwave circuit used to provide power to the microwave applicator

### 5.1.1 The Microwave System

The microwave circuit is designed to transfer power from the microwave power generator to the applicator and prevent reflected power from returning to the power generator. The forward power is the total power supplied to the applicator. The reflected power is a fraction of the power which is not dissipated in the applicator. It is reflected back through the coaxial cable and directed to a dummy load by a circulator.

The major components of the microwave circuit are a 100 Watt microwave power generator (Opthos Instruments Inc., Model MPG-4M), a circulator (Microwave Associates Inc., Model MA-HC7238) used to prevent reflected power from returning to the power supply, two power sensors (Hewlett Packard, Model 8481A) and power meters (Hewlett Packard, Model 435B), two directional couplers (Narda Microwave Corp., Model 22611) used to break off a fraction of the power for the power sensors, a dummy load (Narda Microwave Corp., Model 369NF) for dissipating reflected power and finally the microwave applicator (Wavemat Inc., Model CMPR-150). A schematic of the circuit showing the major components is given in Fig. 5.2.

The applicator used in the microwave freeze-drying experiments is a cylindrical, resonant mode, microwave cavity. The main characteristic of this type of applicator is that if a microwave signal of the correct electromagnetic field polarization and frequency

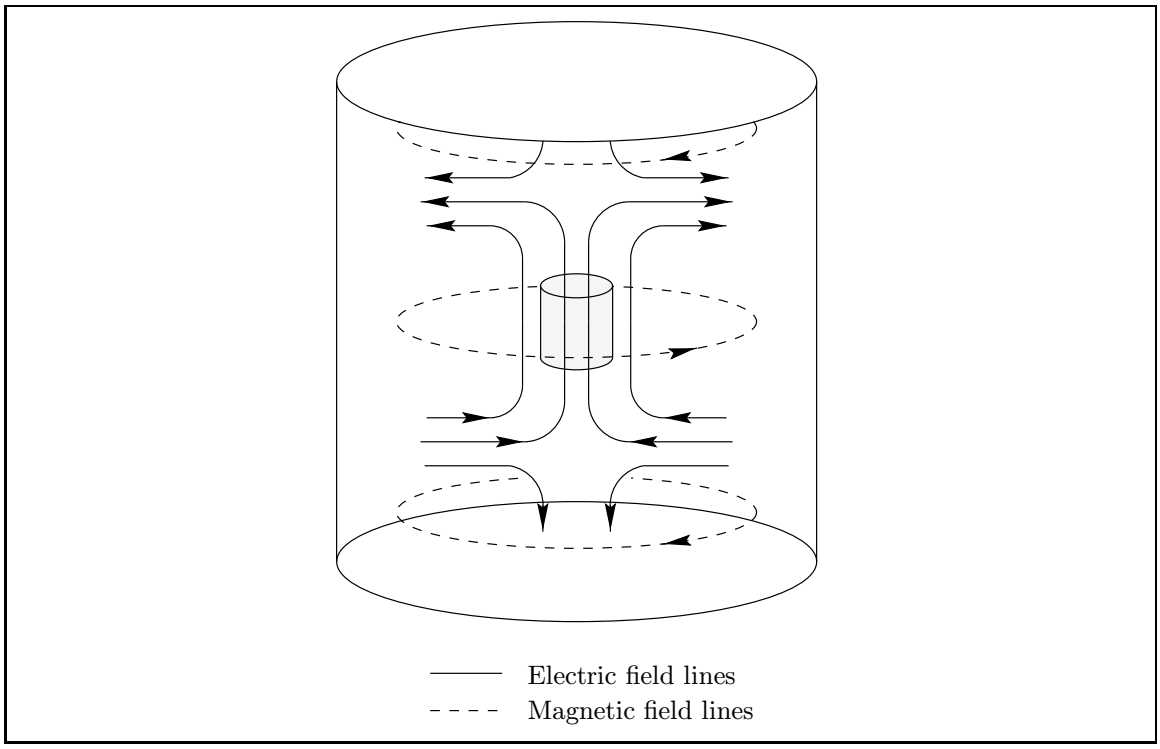


**Figure 5.3** Illustration of the $TM_{012}$ mode showing a sample suspended in the center of the cavity

is launched into the cavity, a geometrically simple standing wave pattern will be set up. There are several advantages to this situation. One advantage is that an appropriate field pattern can be chosen to provide uniform heating for the geometry of the sample. Another advantage is that for a relatively low input power high field strengths can be achieved. This is an important advantage for materials with low dielectric loss (Metaxas and Meredith, 1983).

In all of the experiments conducted in this work, the microwave applicator was tuned to a $TM_{012}$ mode. This mode provides a concentration of power axially down the center of the cavity. Figure 5.3 illustrates the field pattern of the $TM_{012}$ mode.

Figure 5.4 shows a cross section of the microwave applicator with overall dimensions. The important features of the applicator are the adjustable shunt plate (2), and the adjustable probe (6). The values of $L_c$ and $L_p$ determine the mode. The typical tuning used to achieve this mode is $L_p = 26\,\text{mm}$ and $L_c = 139$ to $142\,\text{mm}$. Small adjustments of the probe position do not affect the field pattern. However, as the sample dries, its dielectric properties change and the cavity height needs to be adjusted accordingly.

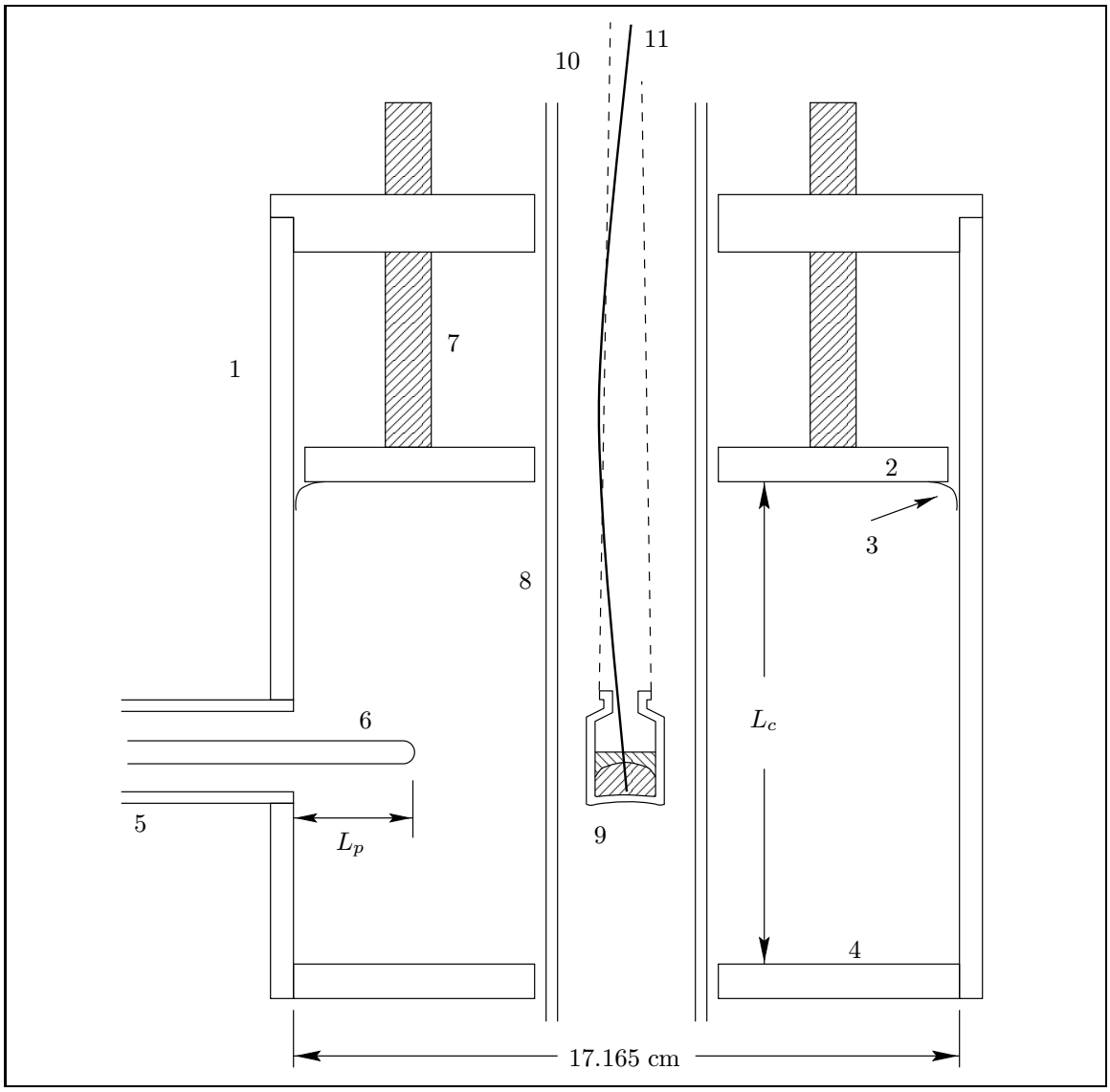


**Figure 5.4** A cross section of the cylindrical microwave applicator showing the adjustable shunt plate (2) and probe (6) used to tune the cavity. The sample is shown with an embedded fiber optic temperature probe.

| | | | | | |
|---|---|---|---|---|---|
| 1 | conducting cylindrical shell | 5 | coaxial input port | 9 | sample |
| 2 | adjustable shunt plate | 6 | adjustable coupling probe | 10 | cotton thread |
| 3 | silver finger stock | 7 | motion guide rods | 11 | fiber optic probe |
| 4 | base plate | 8 | quartz tube | | |

Other modes that can be used with this cavity are: $TM_{111}/TE_{011}$, $TE_{112}$, $TE_{212}$, $TE_{113}$ as well as several hybrid modes.

### 5.1.2 The Vacuum System

The vacuum system was designed to obtain low pressures very quickly as well as to evacuate water vapor generated by the sample very quickly. This was done by keeping the system volume small and using a pump with a high displacement. The vacuum pump (Leybold Vacuum Products, Model D16A) is a 1 HP pump with a 400 L/min displacement rating.

The vacuum system is shown in Fig. 5.5. Samples are suspended from an electronic balance into a quartz tube running axially through the cylindrical microwave applicator. A liquid nitrogen condenser is used to prevent water vapor from entering the pump. The condenser also acts as a pump for condensible vapors, aiding the pump in maintaining low pressure when the samples are generating vapor.

The samples are frozen outside the system. In order to limit the undesirable increase in temperature prior to the start of the experiment, the frozen sample must be placed into the system as fast as possible and low chamber pressure must be achieved quickly. As seen on Fig. 5.5, a custom vacuum fitting is placed under the aluminum box which contains the electronic balance. This allows a quick connection between the quartz tube and the aluminum box.

The aluminum box used to house the balance has a removable plate on one end. This plate is used to access the balance and also contains vacuum feed-throughs for two fiber optic probes, power for the electronic balance and an RS-232 connection for the balance. There is also a vacuum tube attachment for a pressure sensor and purge valve.

There are two Pirani pressure sensors (Edwards High Vacuum International, Model PRM10K) on the system. The upper and lower pressure gauges respectively monitor the chamber pressure and the performance of the pump and condenser. When the vacuum system is completely sealed, the pressure will vary as the rate of drying changes. The lower pressure sensor is between the condenser and the pump. Thus, when operating with the system completely sealed the pressure at this gauge is below its operating range. This condition is used to determine if the system is operating properly.

Both pressure sensors are connected to a pressure controller (Edwards High Vacuum International, Model 1101). This device is used to convert the sensor output to units of

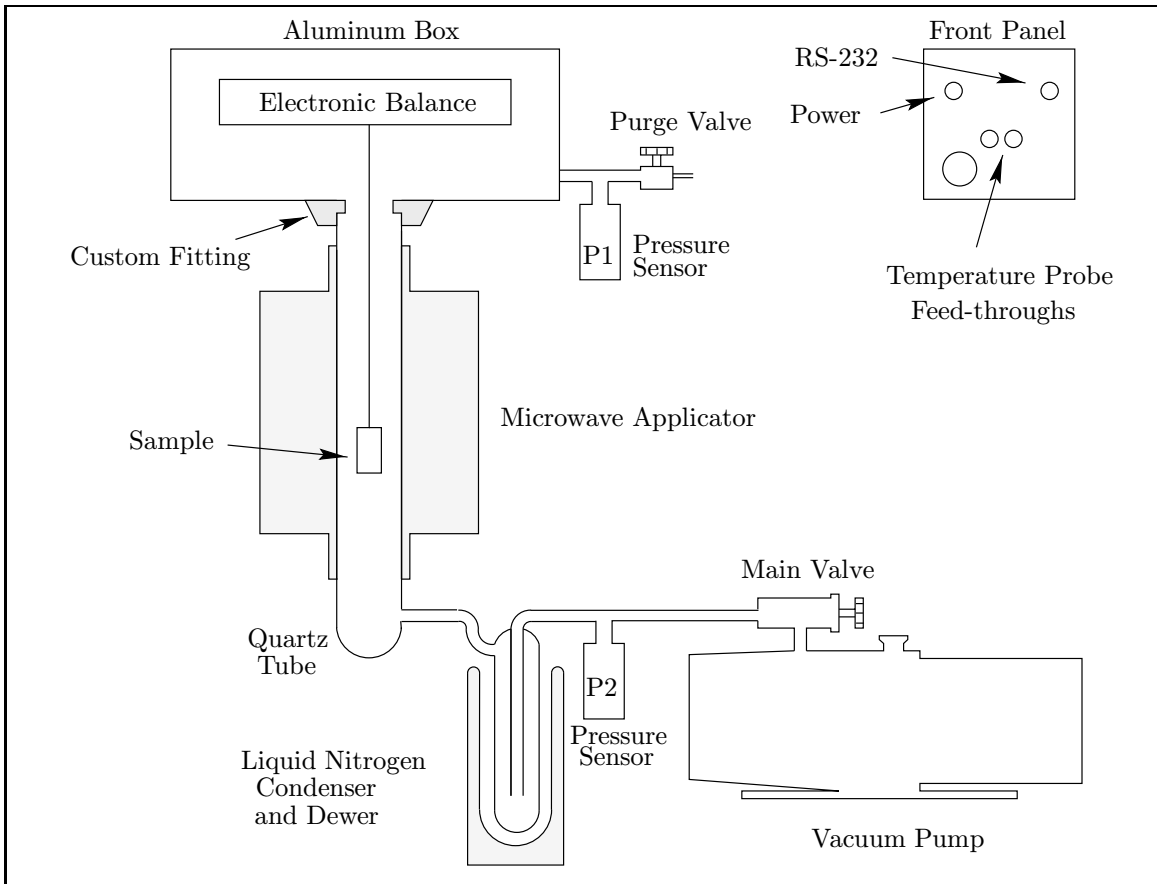


**Figure 5.5** The vacuum system of the experimental microwave freeze-drying apparatus. The sample chamber is a quartz tube 3.8 cm in diameter.

Torr. It also outputs a voltage for each sensor that is read by the data acquisition system.

### 5.1.3 Weight Measurements

The weight measurements were made using an electronic balance (Mettler Instrument Corp., Model PM200). The balance was placed in an aluminum box above the sample chamber. The sample was suspended from a small hook on the bottom of the balance. Even though the balance was not originally built for operating in a low pressure environment, it was proven to be adequate under a relatively constant pressure. The balance was tared only after the operating pressure was reached, because the initial pressure drop induces some error in the weight readings.

Data from the scale were recorded by the data acquisition system via an RS-232 port on the balance. The subsequent digital data which are output by the balance were read into the data acquisition board through the parallel port on the computer. The data acquisition program used to test and calibrate the balance is listed in Appendix D.

### 5.1.4 Temperature Measurements

Temperature measurements were made using a fiber optic temperature measurement system (Luxtron Corporation, Model 790 Floroptic Thermometer). The tip of the temperature sensor consists of a small amount of temperature sensitive phosphor which is excited with a blue-violet light. When excited, the phosphor emits a red fluorescence. The decay time of this red fluorescence is measured and correlated with the phosphor temperature by comparing the measured decay time with a digital look-up table (Luxtron Corp., 1992).

Fiber optic probes were chosen over thermocouples, because the Teflon coated silica glass fibers are relatively transparent to the microwave field. Conductive thermocouple wires could cause intense localized heating inside the sample.

When temperature measurements were made, the probe was frozen into the sample during the sample freezing stage. Before surrounding the vial with liquid nitrogen, the probe tip is placed near the bottom center of the vial. It was difficult to place the probe tip very precisely and thus there was some variability in the probe tip location among experiments.

The temperature data were converted to a voltage signal output by the Luxtron machine. This voltage was read and recorded by the data acquisition system.

### 5.1.5 Data Acquisition

The data acquisition system (National Instruments, Model AT-MIO-16F data acquisition board with National Instruments Labwindows software) was used to record data output from the instrumentation on the microwave freeze-drying system. This system was integrated into a 486DX-33MHz IBM compatible PC.

Except for the electronic balance, all the instruments output a voltage signal that was read by the data acquisition board through a terminal block. Voltage readings were recorded from the Luxtron temperature measurement system (2 channels), the pressure controller (2 channels) and the power meters (2 channels). Data were acquired at 20 second intervals. The main data acquisition program, vetdata.c, is listed in Appendix D.

## 5.2 Experimental Program

### 5.2.1 Phase I: A Comparison of Microwave and Conventional Freeze-Drying

To be a viable alternative to conventional freeze-drying, microwave freeze-drying must be able to be used in the same way and produce at least the same, if not better, results. The best way to demonstrate that microwave freeze-drying has the potential of replacing conventional freeze-drying is to take an existing use of a conventional freeze-dryer and instead, use the microwave process and compare the final product obtained in each case.

In this phase, the goal is to show that microwave freeze-drying can work at least as well as conventional freeze-drying on a laboratory scale. The approach taken to achieve this goal was to collaborate with Dr. Thomas Inzana and the Center for Molecular Medicine and Infectious Diseases of the Virginia-Maryland Regional School of Veterinary Medicine.

Dr. Inzana has been working with a proposed live vaccine developed for a specific swine disease. Freeze-drying in a conventional laboratory tray freeze-dryer is used to stabilize the live vaccine for storage and/or transport. A simple comparison can be made by using the experimental microwave freeze-dryer in place of the conventional freeze-dryer and comparing the results to those obtained with the conventional freeze-dryer.

The objectives for this phase are:

1. to test the experimental microwave freeze-drying apparatus with a live vaccine,

2. to compare viability loss with that of a conventional freeze-drying process, and

3. to compare the drying rates of the microwave freeze-drying system to those obtained with the conventional freeze-drying system.

These objectives are met when sufficient data have been collected to answer the following questions:

1. Can a live vaccine survive a microwave freeze-drying process?

2. Is there a statistically significant difference among viability losses?

3. Is there a statistically significant difference among drying rates?

### Materials

The materials used to prepare the samples were brain heart infusion (BHI) broth, trehalose, and the proposed vaccine strain of the noncapsulated bacterial mutant *A. pleuropneumoniae* J45-C. Two sample types were used: a 2 ml sample of BHI with 20% trehalose that contained no bacteria and a 2 ml sample of BHI with 20% trehalose that contained the *A. pleuropneumoniae* vaccine strain. Samples without the vaccine strain were used to conduct drying rate experiments. Samples with the vaccine strain were use to conduct viability study experiments.

The decision not to include the vaccine strain in the drying rate experiments was dictated by several observations. Firstly, and most importantly, the vaccine strain was not expected to significantly affect the drying characteristics due to its small volume in comparison with other components of the solution. Secondly, samples containing the vaccine strain required not only long preparation procedures (approximately 18 hours) but also sterile handling. Using only the BHI broth also facilitated the use of the same vial for each drying rate experiment, thus eliminating the differences in heating due to variations among vials.

### Bacterial Culture

The noncapsulated, vaccine strain of *A. pleuropneumoniae*, J45-C, was maintained in sterile skim milk at -80°C, and cultured onto brain heart infusion agar supplemented with 5 $\mu$g/ml of nicotinamide adenine dinucleotide (BHI-NAD) at 37°C overnight. The bacteria were

transformed to BHI-NAD broth in a side-arm flask and shaken at 37°C to the desired phase of growth.

### Sample Preparation and Freezing

The base solution was prepared by mixing BHI powder with distilled water. Trehalose was added to 20% (w/v). If the samples did not contain the vaccine strain, a pipet was used to place 2 ml of the BHI/trehalose solution in the appropriate number of vials. When the BHI/trehalose solution was prepared for the viability experiments, it was filter sterilized and handled aseptically.

For the viability tests, the bacteria were grown to mid-log phase in BHI containing NAD to $10^9$ colony forming units per ml (determined spectrophotometrically and confirmed by viable plate count). The bacteria were then washed once and resuspended with the original volume of BHI with 20% trehalose.

Once the samples were prepared and placed in the Wheaton 5 ml serum vials, they were placed in a small container of liquid nitrogen until the solution was completely frozen.

### Conventional Freeze-Drying

Conventional freeze-drying was conducted in a laboratory tray freeze-dryer (Labconco Corp., Model 75018-18). The typical procedure for the material under study does not utilize the shelf heating feature of the tray freeze-dryer. Shelf heating was not necessary to maintain a warm shelf since drying of only a few samples did not provide a significant thermal load on the shelf. This procedure was used to determine an average drying curve for the conventional process.

The drying curve was determined by placing four samples in the freeze-dryer and then removing them for weighing. During the primary drying stage, measurements were taken at regular half-hour intervals. Since melting occured upon removal of the samples from the system, a new batch of four samples was placed in the freeze-dryer until the next time interval was reached. This procedure continued until the secondary drying stage was reached. During the latter stage, one single batch of samples was used and measurements were taken at hourly intervals. Indeed, in the secondary drying stage, the samples had reached room temperature and no longer contained ice. Thus, they could be removed, weighed, and then placed back in the freeze-dryer without detrimental effects.

### Microwave Freeze-Drying

The procedure for using the microwave freeze-drying apparatus was determined by conducting preliminary experiments. These preliminary experiments were used to determine the required power schedule for maintaining temperature profiles similar to those measured during the experiments with the conventional freeze-dryer, with the exception that temperatures during the secondary drying were about 10°C higher for the microwave freeze-drying process. As the conventional process did not utilize shelf heating, the secondary drying temperature was equal to room temperature. The temperature in the secondary stage in the microwave apparatus was set higher than room temperature in order to determine the effect of an increased secondary drying temperature on the drying rate. The higher secondary drying temperature was not expected to affect the viability results since the maximum allowable temperature for the vaccine thought to be approximately 45°C. This was determined by Dr. Inzana through previous experience with the live vaccine.

The power schedule used for microwave freeze-drying experiments was 18 Watts for the first 2 hours (primary drying) and 6 Watts for the next 3 hours (secondary drying). It should be noted that these power values refer to the total power dissipated in the cavity, which is primarily used to heat the sample and the walls of the cavity. A small amount of energy dissipates in the quartz tube and the glass vial and some leaks through the openings of the cavity.

Similar pressures were maintained in both processes. These pressures were in the range of 0.1 Torr during primary drying to about 0.01 Torr during secondary drying. However, since the only pressure sensor on the conventional freeze-dryer was between the pump and the condenser, accurate measurements of the actual chamber pressure are not available.

### Viability Tests

The viability experiments involved drying simultaneously two identical samples containing the vaccine strain. One sample was frozen immediately and placed in the conventional tray freeze-dryer. The other was transported on wet ice to the microwave freeze-drying apparatus, where it was frozen and placed in the apparatus. The microwave freeze-dried sample was dried for 5 hours, while the other sample remained in the tray freeze-dryer for about 20 hours.

The 5 hour drying time for the samples placed in the microwave freeze-drying apparatus was chosen based on the drying rate experiments discussed previously. This time yielded a final moisture content of about 8% or less. The 20 hour drying time for samples placed in the conventional freeze-dryer was chosen based primarily on convenience. The samples were ready late in the morning, while the earliest time that the conventionally freeze-dried sample could be removed from the freeze-dryer was the next morning. This caused the conventional freeze-drying samples to have a lower final moisture content of approximately 5%.

The viability of both samples was assessed using a standard plate count assay. Upon completion of either freeze-drying process, the bacterial samples were resuspended in 2 ml of sterile distilled water, and then diluted 5 logs in phosphate buffered saline. Duplicate samples of 20 $\mu$l from each dilution were spread on quadrants of a BHI-NAD agar plate. The mixture was incubated overnight at 37°C and the colonies counted on plates yielding between 30 and 300 colonies.

### 5.2.2 Phase II: Demonstrating the Advantages of Microwave Heating

In this phase, the goal is to show that microwave freeze-drying has the potential to reduce overall drying times. The approach taken was to conduct experiments using only the microwave freeze-drying apparatus that will demonstate the potential of microwave freeze-drying. Specifically, it was intended to test the theory that a lower chamber pressure results in an increased drying rate if heating of the sample is not adversly affected by lowering the chamber pressure.

The objectives for this phase are:

1. to conduct freeze-drying experiments at two different pressures and
2. to compare drying rates obtained for the two different pressure cases.

These objectives will be met when enough data have been collected to determine if there is a statistically significant difference among the drying rates.

#### Materials

The materials used in the experiments of phase II were similar to that of phase I, i.e. BHI and trehalose, in the same mixture ratio and with no live vaccine. Indeed, the inclusion of

a very small amount of vaccine was irrelevant since the present experiments were designed to investigate the heat and mass transfer phenomena involved.

### Sample Preparation and Freezing

As in phase I, the base solution was prepared by mixing BHI powder with distilled water. Trehalose was added to 20% (w/v). After the BHI/trehalose solution was prepared, it was filter sterilized. Approximately 50 ml of the BHI/trehalose solution was prepared at a time. The solution was stored in a refrigerator at 3°C.

Samples were prepared by using an eye-dropper to place approximately 2.05 grams of the solution into a Wheaton 5 ml serum vial. The vial was then dipped in liquid nitrogen until the sample was completely frozen. When temperature measurements were required during the freeze-drying process, a fiber optic temperature probe was place in the center of the solution before freezing.

### Microwave Freeze-Drying Pressure Experiments

The experiments were designed to show how a moderate difference in pressure can affect the drying rate during the primary drying stage. According to Fig. 3.3 on page 26, the ice temperature plays a significant role in determining the sublimation rate. Therefore, in order to isolate the effect of pressure, it is necessary to run all the experiments at the same primary drying temperature.

Keeping the primary drying temperatures identical between the high pressure and low pressure experiments is not only difficult to implement but also limits the upper pressure. The lower pressure is limited by the capabilities of the vacuum system. Given these requirements, initial experiments were conducted to determine suitable pressures and primary drying temperatures for each of the two cases.

The upper limit on pressures used in industry ranges from 1 to 1.5 Torr (Nail, 1980; Snowman, 1993; Pikal et al., 1983). Ideally, pressures in this range should have been used for the high pressure experiments. However, with such pressures, the sample temperature increases above the safe limit of -20°C and foaming occurs. Indeed, when the safe limit temperature is exceeded, melting of the sample at the sublimation interface occurs and foaming is observed.

Foaming is the result of a build up of pressure at the sublimation interface and a

simultaneous increase in temperature above the glass transition temperature. The increase in temperature results in viscous flow in the dried layer. The build up of pressure causes the now viscous material in the dried layer to flow outward into the low pressure environment above the sample. The outward flow of the viscous material gives the sample the appearance of foaming.

It was found that in the conventional freeze-dryer, the pressure could be increased up to about 0.3 Torr without increasing the temperature of the sample above -20°C and causing subsequent foaming or collapse of the sample. This pressure could be maintained by controlling the appropriate air leak rate with a purge valve. However, the use of such pressure with the microwave heating could not be implemented because the temperatures were already close to the upper temperature limit. Therefore, it was decided that, to have a significant difference between the high and low pressure cases, 0.3 Torr would be used as the high pressure without microwave heating.

In determining power schedule for the low pressure experiments, the goal was to match the temperature profile of the high pressure experiment. This was done by closing the purge valve and adjusting the microwave power input until the appropriate temperature for primary drying was achieved. The forward power used in the low pressure experiments was 15 Watts while reflected power was 8 Watts.

There are two basic experiments: one for temperature data and one for weight data. The reason for the two types of experiments is that if temperature is being measured, then the weight data is corrupted by the presence of the fiber optic temperature probe in the sample. A detailed procedure for these experiments is listed in Appendix A.

# Chapter 6

# Experimental Results and Discussion

The experiments discussed in the previous chapter were broken down into two phases: I) a comparison of conventional and microwave freeze-drying on a laboratory scale and II) a demonstration of the effect of reducing pressure on the primary drying rate.

The comparison of phase I is composed of two parts: A) a comparison of drying rates and B) a comparison of viability loss. Part A focuses on the drying curves and corresponding drying rates of each process. A discussion of the temperatures and pressures associated with the drying rates is included.

Part B of phase I focuses on the viability loss inherent to each process. The viability loss is a fundamental measure of the performance of the drying process. If a significant viability loss occurs, either the process parameters need to be changed or an alternate method of stabilization should be used.

In phase II, minimum and maximum pressures are chosen such that similar primary drying temperatures are maintained. Drying rates are determined from measured drying curves, i.e. from the measurement of the moisture content of the sample as a function of time. As in part A of phase I, the temperatures and pressures are discussed.

## 6.1 Phase I, Part A: Comparison of Drying Rates

The primary interest was to study the effect of the volumetric heating mode on the drying rates of the samples. It was expected that the drying rates obtained with the experimental

microwave freeze-drying system would be higher than those obtained in the conventional freeze-drying system. In order to investigate this premise, BHI/trehalose samples were dried in a conventional tray freeze-dryer and an experimental microwave freeze-drying apparatus under similar conditions.

### 6.1.1 Analysis of Temperature Curves

The first step in comparing the microwave and conventional freeze-drying processes is to determine a power schedule for the microwave freeze-drying experiments that produces similar temperature profiles during the primary drying stage. Similar temperature profiles are required to eliminate the effect of temperature.

Temperature profiles were measured for the conventional process and repeated in the microwave freeze-drying apparatus with the exception that temperatures during secondary drying were about 10°C higher in the microwave process. As discussed in Chapter 5, this difference is the result of microwave heating being applied in the secondary drying stage for the purpose of investigating the effect of temperature during this stage. Figure 6.1 shows measured temperature profiles for each process. Similar trends in the temperature measurements are obtained for both processes.

The initial rapid increase in temperature is due to the warming that occurs once the sample is removed from the liquid nitrogen and placed in the drying chamber which is at room temperature. The temperature continues to increase during the quick reduction of the chamber pressure. Eventually, the temperature is sufficiently high and the pressure is low enough for the sublimation process to begin. At this point the temperature stops increasing as seen at approximately 0.2 hours in Fig. 6.1. The temperature then begins to slowly decrease.

The slowly decreasing temperature that occurs during the primary drying stage indicates that more energy is being used in the phase change than is being supplied to the sample. This is typical of a system which is in a non-equilibrium state moving toward equilibrium. Thus, the process is driven by the low chamber pressure and the sample temperature is falling toward the saturation temperature corresponding to the chamber pressure.

As shown in Fig. 6.1, the primary drying temperatures are well above the glass transition of the material, $T_g'$, determined to be approximately -50°C in Chapter 4. The

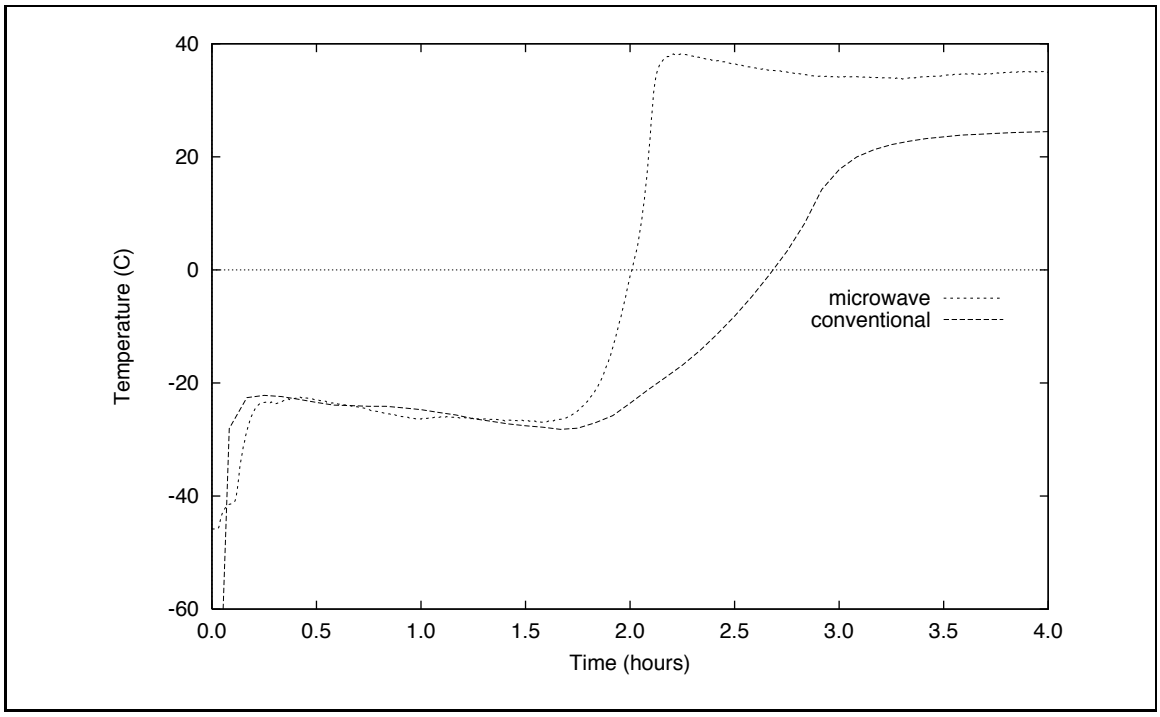


**Figure 6.1** Typical temperature profiles for the microwave and conventional processes

temperature profiles used in the experiments were chosen based on the process used by researchers at the veterinary school. It was not the aim of this work to modify their process and then conduct a comparison. There did not seem to be any negative effects on the physical structure of the dried material.

Primary drying was typically complete after about 2.5 hours for the microwave process and 3 hours for the conventional process. Just before the end of the primary drying stage, the temperatures rise again as the ice phase has completely sublimed. For the microwave process, the change from the primary drying temperature to the secondary drying temperature takes about 15 minutes, which is relatively short compared to approximately one hour obtained for the conventional process.

After the transition from primary to secondary drying, the temperature levels out. In the conventional case, the secondary drying temperature was room temperature, i.e. 25°C because shelf heating was not used. In the microwave case, the secondary drying temperature was about 35°C. This temperature is below the maximum allowed temperature of the vaccine and is significantly higher than the secondary drying temperature utilized in the conventional apparatus. As a consequence, the effect of the secondary drying temperature could be determined.

### 6.1.2 Comparison of Drying Curves

Under similar operating conditions, it was expected that the performance of the two processes would be similar, but that the microwave freeze-drying process would provide a decrease in the drying times due to the volumetric heating mode and the slightly higher temperatures during secondary drying. To make the comparison, an end point was chosen based on preliminary data. The chosen end point was 8% moisture content, which provided reasonable durations for the experiments.

The microwave experiments required at least 5 hours to be sure that the end point was reached. The conventional freeze-drying experiments ran overnight for a total of 20 hours since this was the most convenient way to run these experiments.

The moisture content is defined in terms of a dry basis moisture content. The dry basis moisture content, $X$, is defined as the mass of the water contained in the material divided by the mass of the dry material:

$$X = \frac{M_w}{M_s}. \tag{6.1}$$

By combining the dry mass of the sample and its weight data as a function of time, the moisture content can be calculated and plotted as a function of time.

Figure 6.2 shows a comparison of drying curves, i.e. moisture content as a function of time, obtained with each process. The drying curve for the conventional freeze-drying process was obtained by the method previously explained. The drying curve for the microwave process is an average of 16 curves. The comparison illustrates the difference between the conventional process, which supplies heat by conduction, and the microwave process, which supplies heat volumetrically. Figure 6.2b is the same data plotted with a log y scale to make the difference between the two curves in the secondary drying stage more apparent.

With similar temperatures during primary drying and similar pressure profiles, it was expected that the drying curves for each process would also be similar. However, it was also expected that the drying curves for the microwave case would show an increased drying rate. The drying curves presented in Fig. 6.2a show that the microwave freeze-drying case caused roughly a half hour reduction in primary drying time. However, the times required to reach the end of the secondary drying phase in each process are significantly different, as shown in Fig. 6.2b. It appears that the moisture content at the beginning of secondary drying is much closer to the end point in the microwave case, thus decreasing the necessary

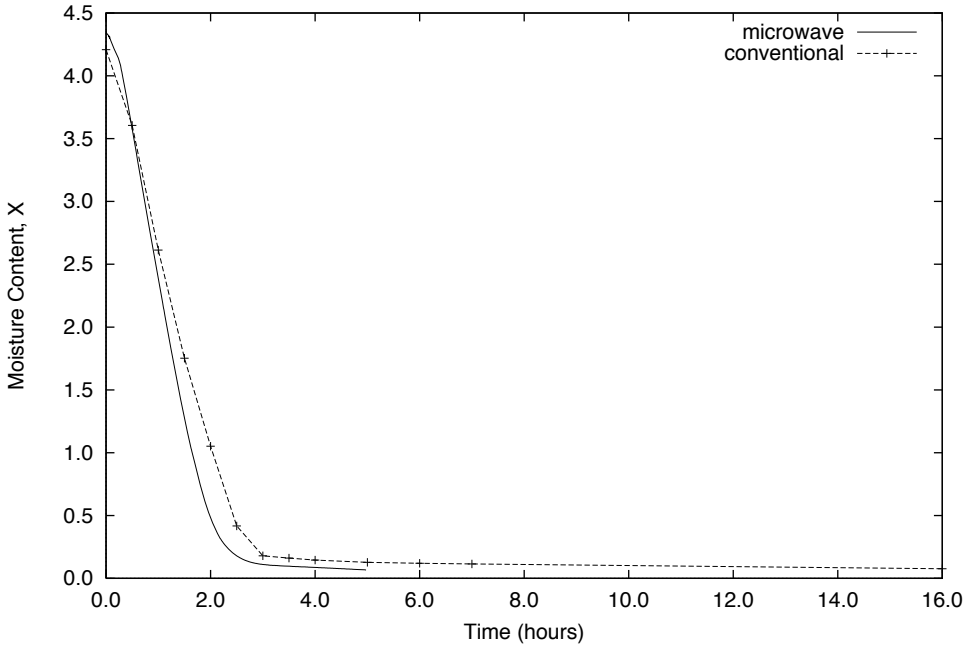


(a) Drying curves for the conventional and microwave processes

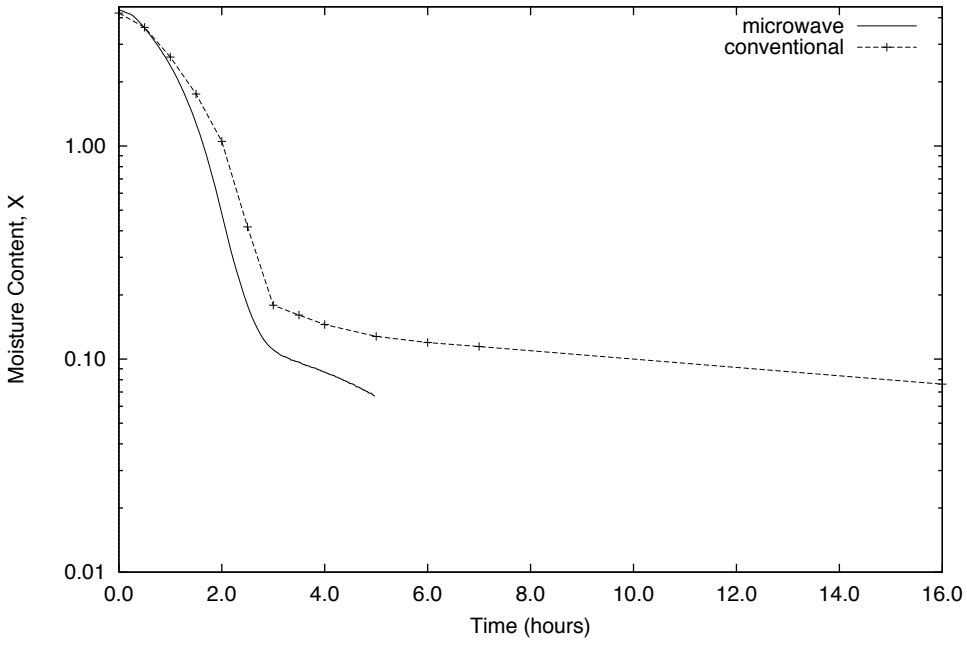


(b) Drying curves plotted with a log y scale

**Figure 6.2** A comparison of drying curves of BHI/trehalose samples for each process. The chamber pressure is approximately 0.01 Torr.

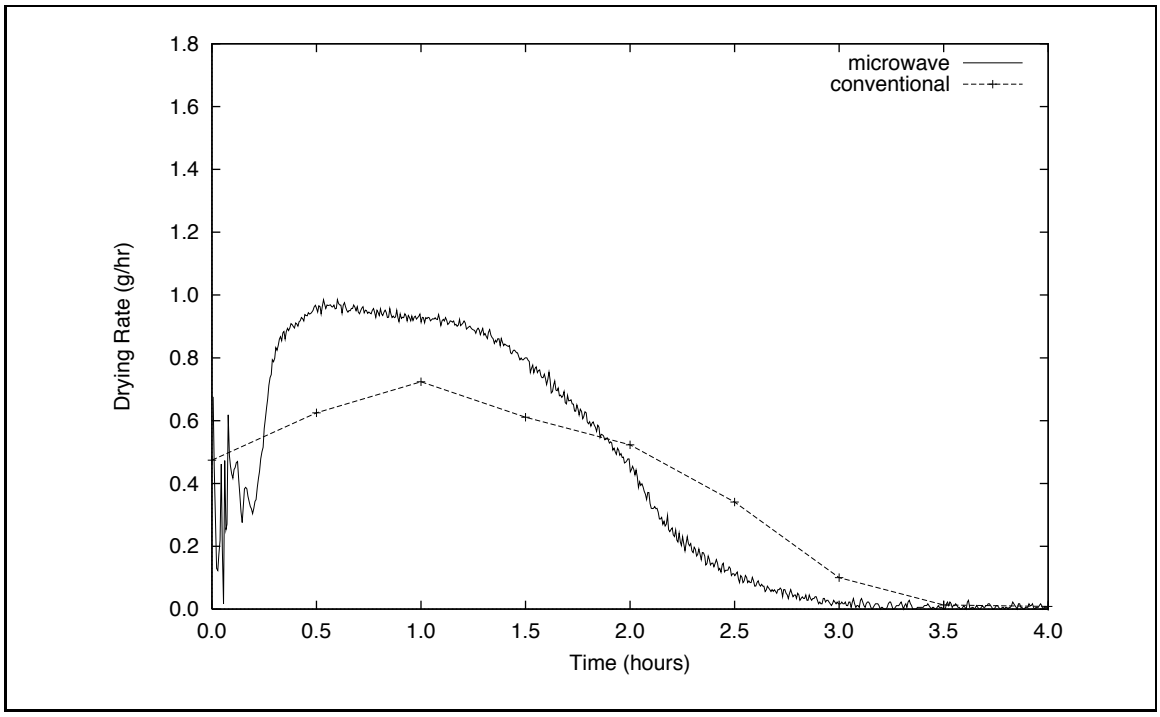


**Figure 6.3** Comparison of drying rates for the microwave and the conventional cases. These curves are the derivatives of the curves in Fig. 6.2.

secondary drying time and producing a significant overall time savings.

The drying rates for the primary drying stage are plotted in Fig. 6.3. The drying rate for the microwave case reaches a maximum value of 1 g/hr and maintains this drying rate for about 1 hour. The conventional drying rate shows a peak of about 0.8 g/hr.

Based on Fig. 6.2 and Fig. 6.3, the secondary drying stage starts around the 3 hour point. This is where the moisture content curves have leveled off, indicating that all ice has been removed. During the secondary drying stage the moisture content is very low. Also, the residual moisture is absorbed into the material. This situation results in very low drying rates.

Figure 6.4 shows a comparison of secondary drying rates. Microwave freeze-drying starts out at a lower rate. This is explained by the lower moisture content at the start of secondary drying. However, the plot shows that the microwave process operates at an approximately constant drying rate. This is attributed to the higher secondary drying temperature (35 °C). The drying rate in the conventional process decreases rapidly. This is explained by the fact that in the conventional case, the secondary drying stage starts out with a higher moisture content but has a lower secondary drying temperature.

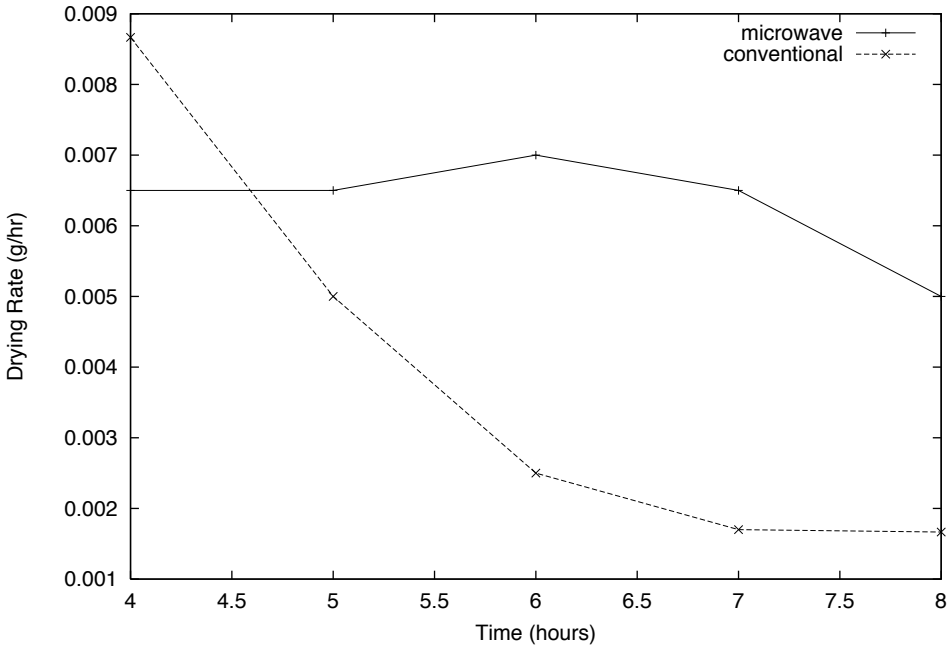


**Figure 6.4** Comparison of secondary drying rates for the microwave and the conventional cases

The significant results of Fig. 6.4 are the effect of the moisture content at the start of secondary drying and the effect of temperature. Since the secondary drying rates are very low, a low moisture content at the start of secondary drying can result in a significant reduction of secondary drying time. Also, the effect of higher temperature is to maintain a higher drying rate throughout much of secondary drying.

Table 6.1 contains statistical data describing the results of the drying experiments for the two different drying processes. The mean drying time represents the time necessary to yield an 8% residual moisture content. Since the two data sets are independent, a comparison of the 95% confidence intervals illustrates a significant difference between the two means. The significant difference in the mean drying times shows that the BHI/trehalose samples were dried much faster using the microwave freeze-drying process. It should also be noted that the confidence intervals for these means are relatively small for number of observations, showing the repeatability of the experiments is good.

**Table 6.1** A comparison of overall drying times between the conventional and microwave processes in hours for a final residual moisture content of 8%.

| | Conventional | Microwave |
|---|---|---|
| Number of samples, $N$ | 12 | 16 |
| Mean drying time | 10.752 | 4.131 |
| Standard deviation | 0.751 | 0.394 |
| 95% Confidence interval | (10.275, 11.230) | (3.921, 4.342) |

## 6.2 Phase I, Part B: Viability Study

When live vaccines are being preserved, it is very important that the viability of the vaccine remain as high and stable as possible. Therefore, it is important to include a viability study in the comparison of microwave and conventional freeze-drying. The tests performed were used to evaluate the impact of each process on cell viability. It was expected that there would not be any significant difference in the viability losses between the two processes.

There were three main parts to the viability experiments: 1) growing the bacteria and preparing the sample, 2) freeze-drying the samples (one in the conventional freeze-dryer and one in the microwave freeze-drying apparatus) and 3) resuspending the bacteria and conducting a plate count assay. The samples freeze-dried in the microwave apparatus also had to be transported from the microbiology lab to the heat transfer lab.

Table 6.2 contains the results of the viability tests in terms of concentration, $C$. Table 6.2 also lists basic statistical calculations, i.e. the mean, the standard deviation, and a 95% confidence interval for the mean. Note that the standard deviation is significant and that the confidence intervals for the means, $\overline{C}_c$ and $\overline{C}_m$, overlap. However, since the data sets of $C_c$ and $C_m$ are not independent, it is also important to note that the confidence interval for the mean of the differences, $\overline{W}$, does not contain zero which indicates that there is a difference among viability loss for each process.

A paired-sample t-test was used to determine the probability that the two data sets produced by the two processes are from the same distribution. Since the concentration measurements are related by the initial concentration within each test, but each test is independent, a paired-sample t-test was appropriate. The test was performed using the differences, $W$, between the final concentration for the conventional process, $C_c$, and the final concentration for the microwave process, $C_m$. The test statistic, $T$, is defined as (Hogg

**Table 6.2** The results of viability tests.

| Initial Conc. | Conventional | Microwave | Differences |
|---|---|---|---|
| $C_i \times 10^{-8}$ (cfu/ml) | $C_c \times 10^{-8}$ (cfu/ml) | $C_m \times 10^{-8}$ (cfu/ml) | $W \times 10^{-8}$ (cfu/ml) |
| 6.60 | 6.80 | 4.30 | 2.50 |
| 12.0 | 3.40 | 1.40 | 2.00 |
| 9.9 | 0.73 | 0.52 | 0.21 |
| 8.87 | 5.27 | 3.02 | 2.25 |
| 6.39 | 3.02 | 0.594 | 2.43 |
| 10.2 | 2.64 | 2.07 | 0.57 |
| 18.0 | 8.54 | 3.77 | 4.77 |
| 8.97 | 3.68 | 2.13 | 1.55 |
| Mean | 4.26 | 2.225 | 2.035 |
| Std Dev | 2.49 | 1.39 | 1.39 |
| 95% CI | (2.18, 6.34) | (1.06, 3.39) | (0.87,3.20) |

and Ledolter, 1992)

$$T = \frac{W}{S_W/\sqrt{N}}, \tag{6.2}$$

where N is the number of data points and $S_W$ is the standard deviation. The hypothesis being tested is $H_0 : \ \mu_c = \mu_m$ versus $H_a : \ \mu_c > \mu_m$. The resulting $p$ value indicates the probability that the null hypothesis, $H_0$, is true.

The results of the paired t-test are: $T = 4.127$ and $p = 0.0023$. The $p$ value is the probability that the two data sets, $C_c$ and $C_m$, are from the same distribution. Thus, it can be concluded that the microwave freeze-drying process resulted in a higher viability loss than the conventional process with level of significance $p = 0.0023$, according to results presented in Table 6.2.

Possible explanations for this observation include: the microwave apparatus was not close to the microbiology laboratory where the samples were prepared, thus the microwave samples required transportation and about a 20 minute delay before freezing; the microwave process exposed samples to higher temperatures; samples dried in the conventional freeze-drier were dried to a lower moisture content. It is suspected that the exposure to higher temperatures (above the $T_g$ during the initial part of the secondary drying) and the differences in final moisture content were the primary reasons for the differences observed in the viability results. Note also that the microwave process was not optimized and that the combination of reduced process temperatures and an optimized process could resolve the

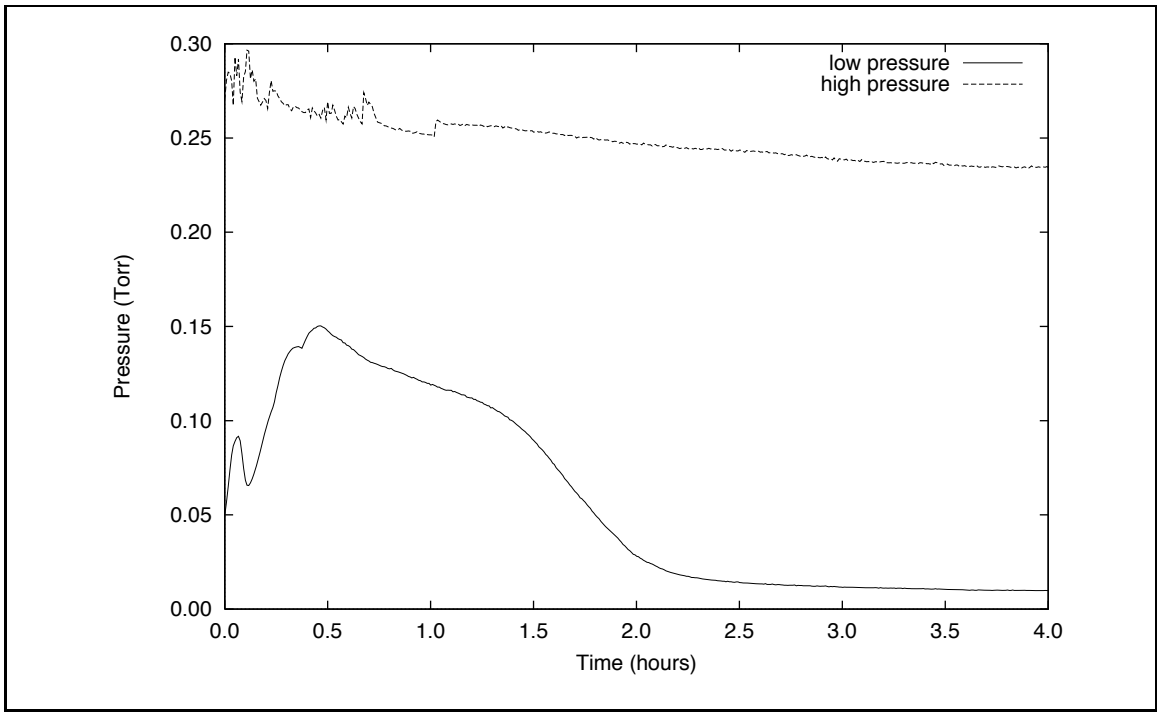


**Figure 6.5** Average pressure profiles for the high pressure and low pressure experiments

differences in the viability results.

## 6.3 Phase II: Effect of Pressure

The results of phase II are expected to demonstrate one of the advantages of volumetric heating: the ability to control the heating independently of the chamber pressure during primary drying. The results presented here are representative output of the experiments.

### 6.3.1 Comparison of Pressure Curves

The discussion of the results for phase II focuses on the comparison of drying rates obtained at two different pressures. These two sets of experiments are thereafter referred to as the high pressure case and the low pressure case. In this section, the differences between these two cases are presented and discussed.

Figure 6.5 shows the difference between the pressure curves for the high and low pressure cases. The difference between the two cases is not very large, but it is the largest difference that could be achieved with the experimental system in its current state as discussed in Chapter 5.

Low pressure in the chamber is easily achieved. The purge valve is closed and the vacuum system is completely sealed. Under these conditions, the vapor generated by the subliming ice significantly affects the total chamber pressure. This explains the rise in pressure observed during the first half hour. The decreasing pressure from 0.5 to 2 hours indicates that the rate of sublimation is decreasing during this time period. The decreasing rate is due to increasing mass transfer resistance and decreasing temperature.

To increase the pressure in the high pressure case, air was admitted into the chamber through the purge valve. Control of the chamber pressure was difficult since the leak rate could not be precisely controlled with the purge valve. This is evident in Fig. 6.5 from the variations in pressure observed for the high pressure curve during the first hour. A precision leak valve would have been a better alternative. However, this was not an economically viable option. The pressure profile for the high pressure case does not show the large increase in pressure during the initial phase of primary drying. In this case, sublimation rate is expected to be lower, thus the changes in the vapor pressure probably do not have a significant impact on the total pressure.

### 6.3.2 Comparison of Temperature Curves

The trends seen in the temperature profiles for phase I are also present in the temperature profiles of phase II. Again, the goal is to keep the temperature profiles similar during primary drying to remove the effect of temperature differences from the sublimation rate results.

Figure 6.6 shows the temperature versus time curves for the high pressure and low pressure cases. The primary drying stage of the high pressure case is from 0.25 hours to about 3 hours. The primary drying stage of the low pressure case is from about 0.25 hours to about 2 hours. The temperature profile in the low pressure case shows a transition to secondary drying much earlier than in the high pressure case. This indicates that the ice is completely removed much earlier in the low pressure case.

The low pressure case, however, shows a higher secondary drying temperature. As in phase I, the difference in secondary drying temperature is used to investigate the effect of temperature on secondary drying.

In the low pressure case, the power schedule is as follows. For the first 2 hours, the forward power was set to 12 Watts while the reflected power was about 6 Watts. At 2 hours, the forward and the reflected powers were respectively decreased to 6 and 3 Watts.

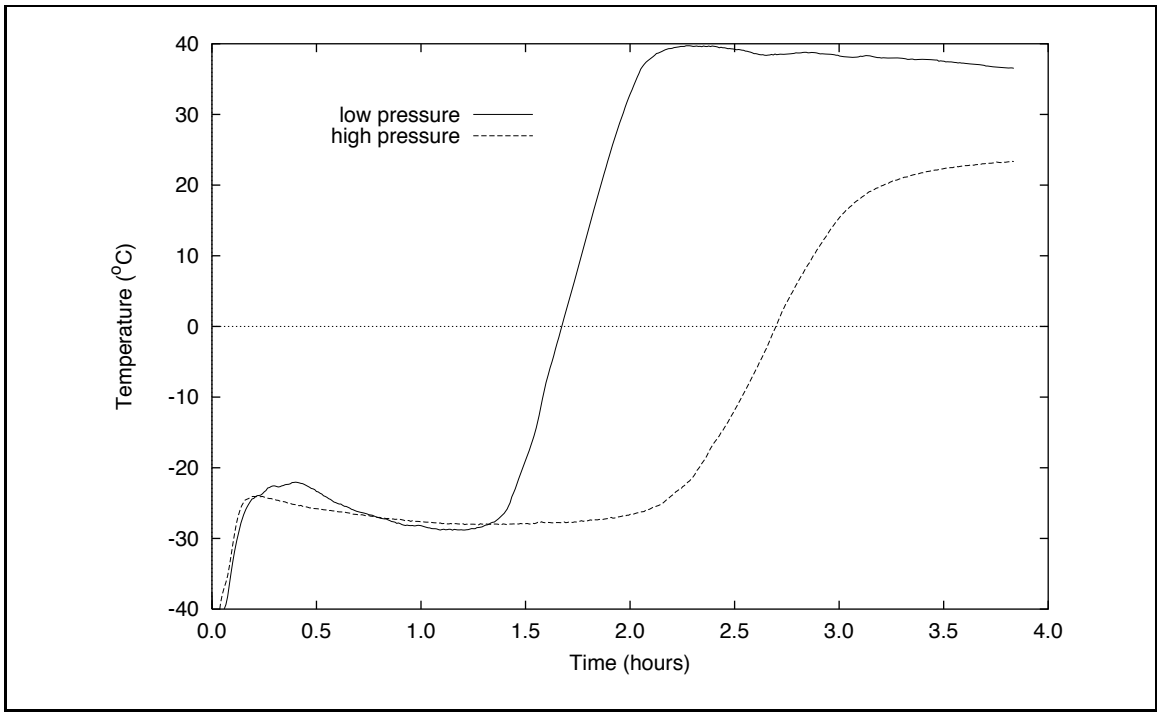


**Figure 6.6** Average temperature profiles for the high pressure and low pressure experiments

The high pressure experiments were run without power.

The high pressure curve of Fig. 6.6 shows the reduction of the slope during the primary drying stage. This is a result of having the chamber pressure closer to the saturation pressure of the ice at the sublimation interface. Also, there is a smaller total pressure gradient driving the moisture transfer through the dried layer and a smaller driving potential to move the system towards equilibrium conditions.

### 6.3.3 Comparison of Drying Rates

The primary interest in phase II was to show that higher sublimation rates could be achieved by lowering the chamber pressure. This could serve as a demonstration of the benefits of volumetric heating over conductive heating. Indeed, as explained in Chapter 3, when conductive heating is used, lowering the sample pressure results in reduced heating.

Figure 6.7 shows the results of the weight measurements during the drying process. The weight curve for the low pressure case shows an increased rate of weight loss over the high pressure result. The primary drying stage ends after about 2 hours in the low pressure case whereas it lasts about 3 hours in the high pressure case. The lower pressure resulted

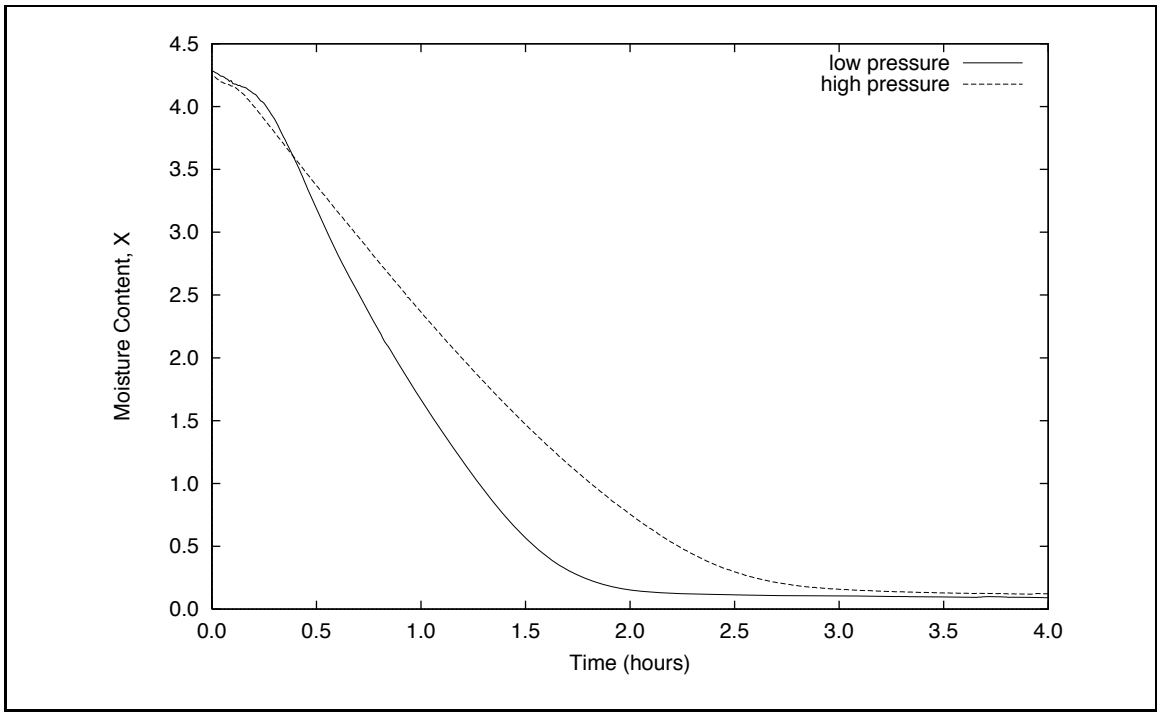


**Figure 6.7** Average weight profiles for the high pressure and low pressure experiments

in a one-third time savings.

The secondary drying stage shows results similar to the comparison in phase I. The low pressure case starts the secondary drying stage at a lower moisture content. Thus, for the entire secondary drying stage the low pressure case remains at a lower moisture content and reaches the end point of drying sooner than the high pressure case.

The drying rate results are shown in Fig. 6.8. The drying rates are calculated by the same method as in phase I. The low pressure case shows a sharp peak at 0.5 hour. This maximum value of the drying rate is approximately double the maximum value of the drying rate obtained in the high pressure case.

The high initial peak of the low pressure case is the desired trend over the more broad and flat curve of the high pressure case. The high initial peak indicates that under low pressure, it is possible to drive the sublimation to a high rate at the start of primary drying when the resistance to vapor flow is low. This was discussed in Chapter 3 and is an advantage of volumetric heating.

Even though the power input to the microwave cavity was constant, the amount of power being absorbed by the sample changes during drying. This is because power absorption is proportional to the volume of the sample. In this case, the volume of the ice is

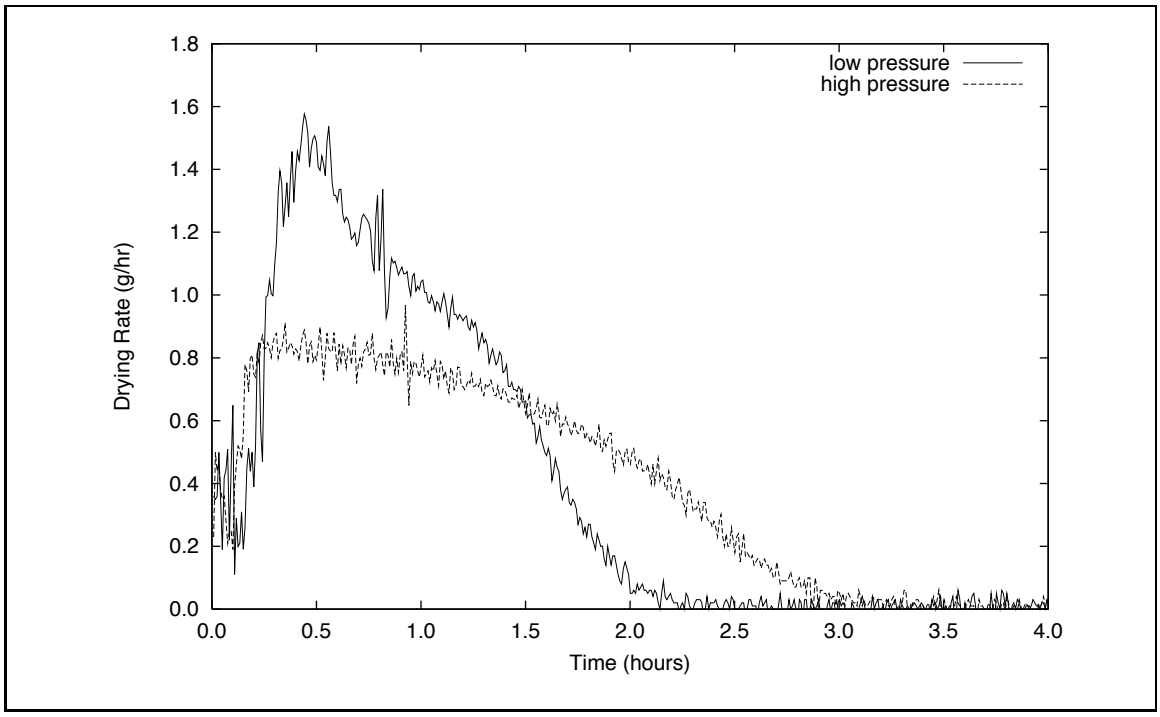


**Figure 6.8** Average drying rate profiles for the high pressure and low pressure experiments

decreasing during the drying process, thus the highest heating rate is expected at the start of primary drying before any ice has been sublimated.

# Chapter 7

# Development of a Mathematical Model

The primary goal of this section is to show that volumetric heating can provide an advantage over conductive heating in the freeze-drying process. The experimental results of Chapter 6 suggest that a lower chamber pressure yields higher drying rates under volumetric heating. Since it was determined in Chapter 3 that temperature has a significant effect on the sublimation rate, it needs to be shown here that the difference in sublimation rates presented in Chapter 6 is not due exclusively to slight differences in sublimation temperatures.

A mathematical model of the sublimation process allows the simulation of experiments which are difficult to conduct. In this case, identical temperature profiles are desired during primary drying to isolate the effect of pressure. This situation can be investigated using a mathematical model.

In this chapter, several models are presented, starting with a very simple model and eventually arriving at a very complex model. Results from all but the most complex models are presented and discussed.

## 7.1 Freeze-Drying Models

The simplest models are based on a pseudo steady-state assumption, the uniformly retreating ice front (URIF) models. In these models, steady-state heat transfer is assumed during a sufficiently small time step. From the known heat of sublimation and calculated total amount of heat transfer during the time step, a new position for the ice front is calculated.

These models work fairly well for a very slow process. However, since they only take into account sublimation, the product is considered dry at the end of the primary drying stage. The benefit of URIF models is that they are very simple.

The use of the URIF model can be extended by including a linear approximation to secondary drying. When the drying process is very slow this combination works reasonably well. This method was used by Bruttini et al. (1991) to model freeze-drying in a conventional freeze-dryer.

The next type of model is based on a transient analysis. This type of model is also used only for modeling sublimation, thus the product is again considered dry at the end of primary drying. The analysis is based on transient heat transfer and moisture concentration equations. This type of model generally gives slightly better predictions than URIF models (Liapis, 1980). The transient sublimation models give reasonable results, especially when applied to freeze-drying of meat (Liapis, 1980; Ma and Peltre, 1975b; Ang et al., 1977b).

The most comprehensive type of model is the sorption-sublimation model. This type of model includes a transient sublimation model combined with simultaneous moisture desorption from areas in the material where the ice has been sublimated. This model has been shown to give better results than the URIF and transient sublimation models (Liapis and Litchfield, 1979; Liapis and Bruttini, 1994; Sadikoglu and Liapis, 1997).

The approach adopted in this work is to start with a simple steady state model based on thermodynamics and then slowly increase its level of complexity until a model based on transient heat conduction and mass transfer is developed. Adsorption and desorption in the dried layer will not be considered. While this is important to secondary drying, it should not have a significant effect on the accuracy of the model during primary drying (Sadikoglu and Liapis, 1997).

## 7.2 Sublimation of Ice

The first step to building a mathematical model of the primary drying stage is to look at a mathematical description of sublimation occurring one-dimensionally from one end of a cylinder of ice. This analysis illustrates the concepts discussed in Chapter 3. Two analyses are presented in this section: the first one is based on thermodynamics alone and the second one incorporates Knudsen's equation of the form given by Eqn. 3.4 on page 25.

A unique aspect of the models presented here is that the heating source is volumetric. With a volumetric heat source the rate of heating is dependent on the volume of the material. This heating mode results in a decreasing heating rate as sublimation occurs. It is also assumed that the dielectric properties remain constant, thus the volumetric heating rate is constant for a constant electric field strength.

### 7.2.1 A Simple Model

A steady-state analysis provides the most simple model of sublimation. It assumes a constant, uniform temperature throughout the ice/vapor system and it is assumed that thermodynamic equilibrium exists. Other assumptions include one-dimensional behavior, a flat phase interface of infinitesimal thickness and a constant, uniform volumetric heat generation within the ice. It is also assumed that the chamber pressure remains constant throughout the sublimation process.

The model is derived by applying an energy balance. The form of this energy balance is given as

$$\dot{E}_{\text{in}} - \dot{E}_{\text{out}} + \dot{E}_{\text{g}} = \dot{E}_{\text{st}}, \tag{7.1}$$

where $\dot{E}_{\text{in}}$ is the rate of energy entering the system, $\dot{E}_{\text{out}}$ is the rate of energy leaving the system, $\dot{E}_{\text{g}}$ is the rate of energy being volumetrically generated within the system and $\dot{E}_{\text{st}}$ is the rate of change of the amount of energy stored in the system. The system is defined by a control volume boundary. The goal is to use the energy balance to derive an equation that describes the position of the sublimation interface, $s$, as a function of time, $t$, for a given sublimation temperature and volumetric heating rate.

Applying the energy balance to the ice for steady-state conditions results in

$$\begin{aligned} \dot{E}_{\text{in}} &= 0 \\ \dot{E}_{\text{out}} &= \rho_i \Delta H_{\text{sub}} A_c \frac{ds}{dt} \\ \dot{E}_{\text{g}} &= A_c (h - s) \dot{q}_i \\ \dot{E}_{\text{st}} &= -(\rho c_p)_i T A_c \frac{ds}{dt} \end{aligned} \tag{7.2}$$

where $A_c$ is the cross sectional area, $\Delta H_{\text{sub}}$ is the latent heat of sublimation, $\rho_i$ is the density of the ice, $h$ is the height of the cylinder of ice and $\dot{q}_i$ is the volumetric heating rate.

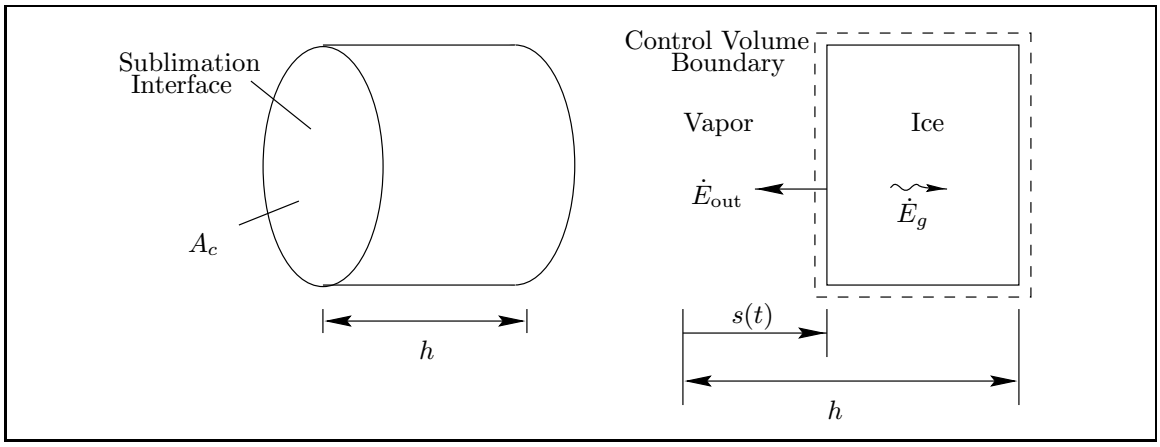


**Figure 7.1** A cylindrical ice plug with a constant uniform temperature and sublimation occurring from one surface

An illustration of the system is shown in Fig. 7.1 with the control volume boundary shown as a dashed line.

The energy balance can be reduced to the following linear first order ordinary differential equation for the distance that the sublimation interface, s, has moved during time, t, yielding

$$\frac{ds}{dt} + \left[\frac{\dot{q}_i}{\rho_i \Delta H_{\text{sub}} - (\rho c_p)_i T}\right] s = \left[\frac{\dot{q}_i}{\rho_i \Delta H_{\text{sub}} - (\rho c_p)_i T}\right] h \qquad s(0) = 0 \tag{7.3}$$

By using the thermal properties of ice, the solution to this model equation can be plotted to illustrate trends in drying curve.

It is given that sublimation is taking place at 240 K (-33°C) which determines that $\Delta H_{\text{sub}} = 2839.0 \times 10^3$ J/kg. The density is taken as $\rho_i = 920\,\text{kg/m}^3$, the specific heat as $(c_p)_i = 2040$ J/kg · K, the volumetric heating rate as $\dot{q}_i = 9 \times 10^5\,\text{W/m}^3$ and the height as $h = 0.009\,\text{m}$. Substituting these values into Eqn. 7.3 and solving for $s(t)$ results in

$$\frac{ds}{dt} + 0.000416s = 3.747 \times 10^{-6} \qquad s(0) = 0 \tag{7.4}$$

yielding as a solution

$$s(t) = 0.009\,(1 - \exp\,(-0.000416t)) \tag{7.5}$$

Equation 7.5 is plotted in Fig. 7.2 as $h - s(t)$. The quantity $h - s(t)$ yields a result that is similar to the measurement of sample weight versus time discussed in the experimental section.

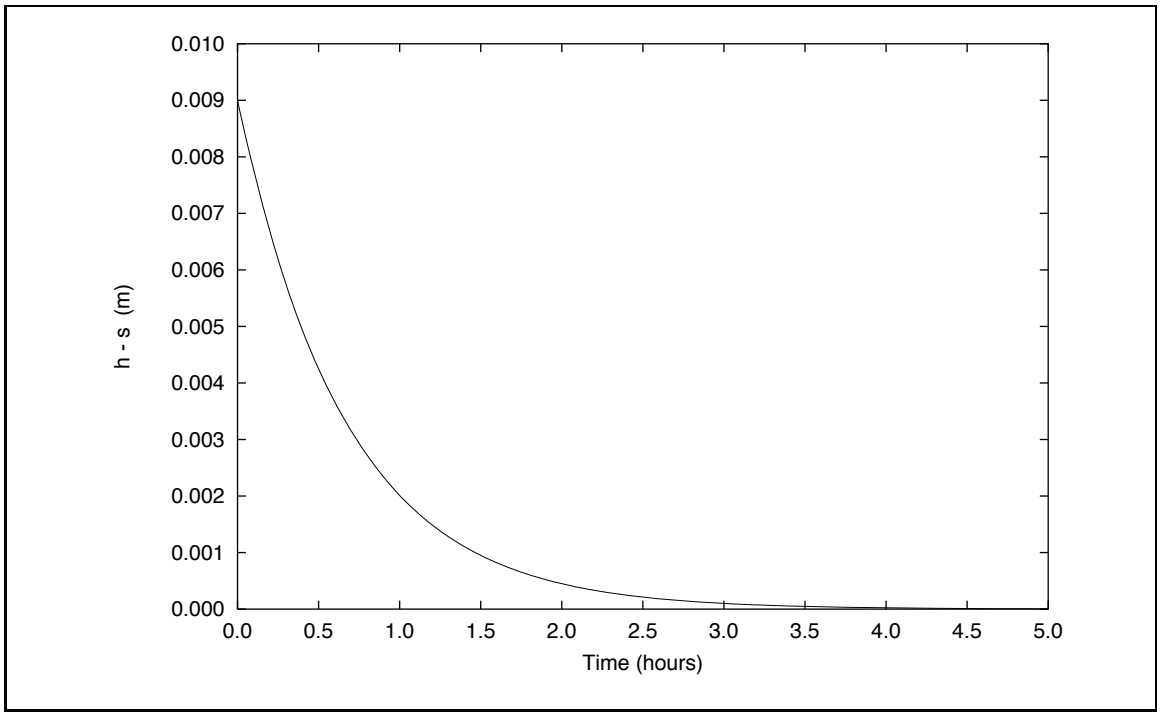


**Figure 7.2** Thickness of the ice layer versus time during ice sublimation using a steady-state model as described in Section 7.2.1.

Figure 7.2 shows the effect of volumetric heating. As the position of the sublimation interface recedes, the rate of heat input decreases since heating is dependent on the volume of ice. As the rate of heat input decreases, the sublimation rate decreases.

During a real freeze-drying situation, the pressure in the drying chamber is often much lower than the saturation pressure of the ice. Thus, equilibrium conditions do not exist. Including Knudsen's equation in the model accounts for the non-equilibrium conditions.

### 7.2.2 Knudsen's Equation

To remove the restriction imposed by the assumptions of constant temperature and equilibrium conditions between the vapor and the ice, Knudsen's equation is introduced. Knudsen's equation in the form given in Eqn. 3.4 (page 25) relates the sublimation rate to the chamber pressure and the ice temperature. The resulting model better simulates the actual situation encountered when conducting experiments. However, the uniform temperature assumption is still enforced.

Knudsen's equation requires the saturation pressure. This pressure is a function

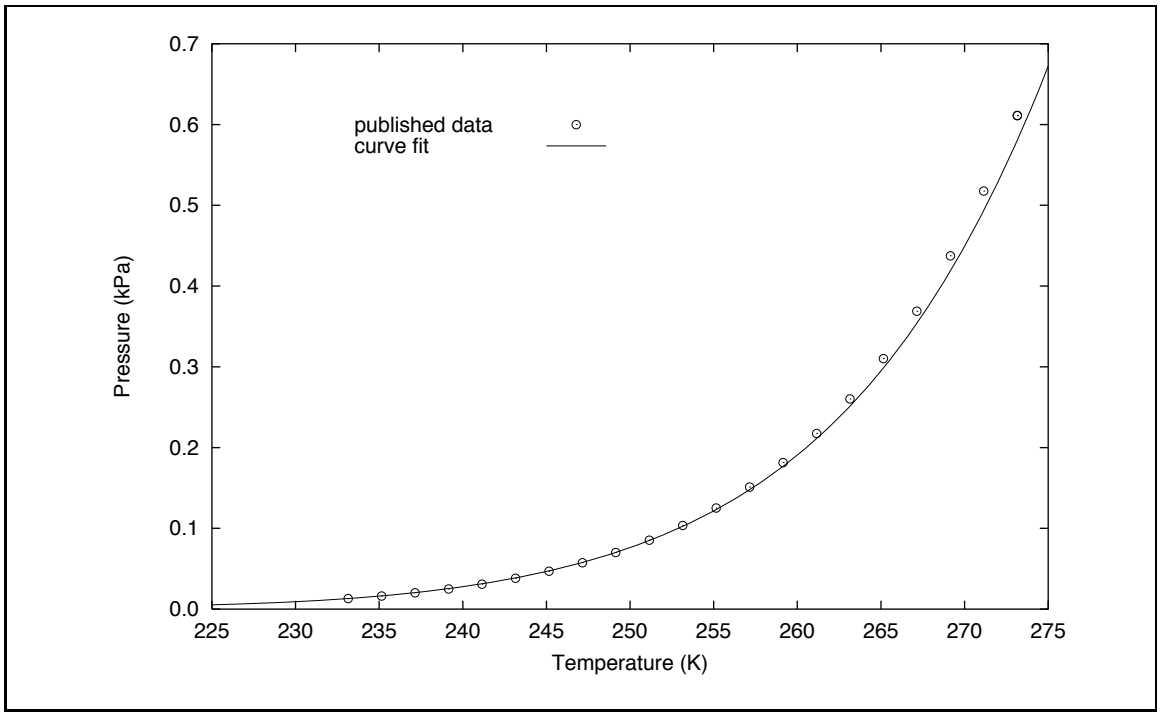


**Figure 7.3** Approximation of published pressure-temperature data for the phase equilibrium line between ice and water vapor

of the ice temperature and is plotted in Fig. 7.3. The following function represents the saturation pressure line plotted in Fig. 7.3 (Liapis and Litchfield, 1979):

$$P_{\text{sat}}(T) = 0.1333 \exp\left(\frac{-6001.0}{T} + 23.44\right). \tag{7.6}$$

Application of the energy balance now yields

$$\begin{aligned} \dot{E}_{\text{in}} &= 0 \\ \dot{E}_{\text{out}} &= \rho_i \Delta H_{\text{sub}} A_c \frac{ds}{dt} \\ \dot{E}_{\text{g}} &= A_c (h - s) \dot{q}_i \\ \dot{E}_{\text{st}} &= -(\rho c_p)_i T A_c \frac{ds}{dt} + (\rho c_p)_i A_c (h - s) \frac{dT}{dt} \end{aligned} \tag{7.7}$$

which can be reduced to

$$\frac{dT}{dt} = \frac{\dot{q}_i}{(\rho c_p)_i} - \begin{bmatrix} \rho_i \Delta H_{\text{sub}} - (\rho c_p)_i T \\ (\rho c_p)_i (h - s) \end{bmatrix} \frac{ds}{dt}. \tag{7.8}$$

The mass flux generated at the sublimation interface is given by Knudsen's equation as

$$\rho_i \frac{ds}{dt} = \kappa \left(P_{\text{sat}}(T) - P_c\right) \left(\frac{M}{2\pi RT}\right)^{-\frac{1}{2}} \tag{7.9}$$

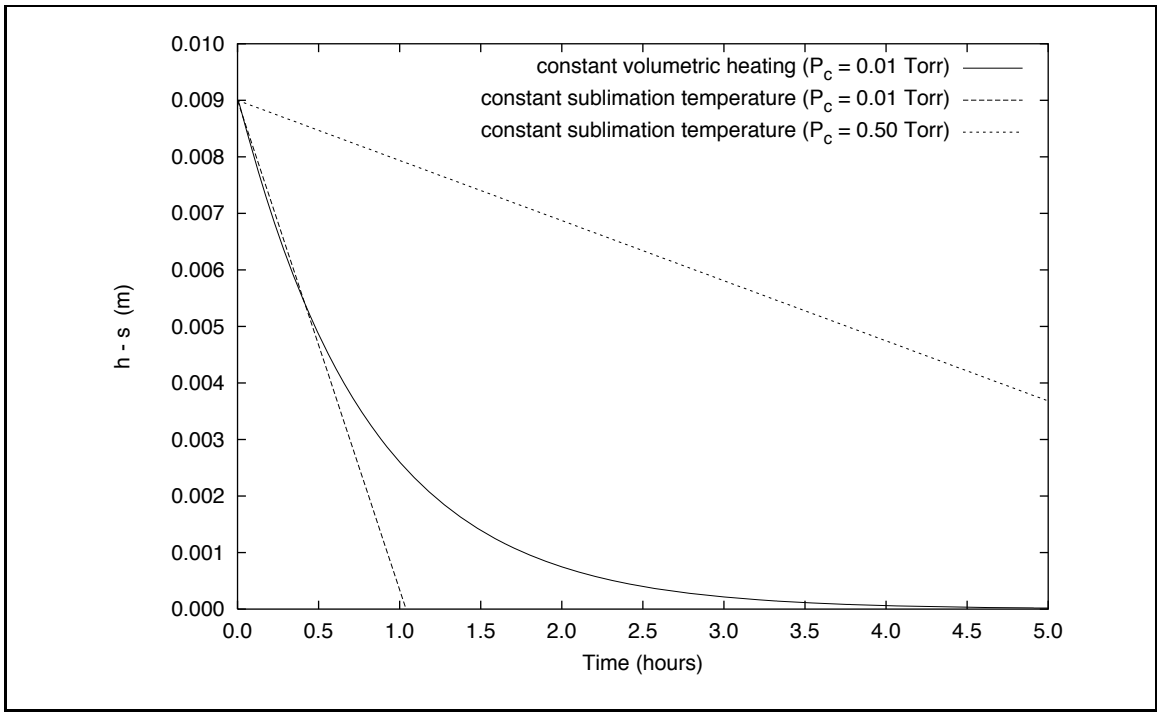


**Figure 7.4** The thickness of the frozen layer versus time for two constant temperature cases ($T = 250\,\mathrm{K}$) and a constant volumetric heating case (Section 7.2.2)

where $\kappa$ is Knudsen's evaporation coefficient ($\kappa = 0.8$), $P_c$ is the chamber pressure ($P_c = 0.01$ Torr), $R$ is the universal gas constant, $M$ is the molecular weight of water and $T$ is the ice temperature.

The solution to this set of equations is plotted in Figs. 7.4 and Fig. 7.5. The result is almost identical to the previous model except when considering the ice temperature. With the previous model, the ice temperature was considered constant. With the current model, Fig. 7.5 shows that the ice temperature decreases during the drying process. For comparison purposes, the constant temperature case ($T = 250\,\mathrm{K}$) is plotted in Fig. 7.4. A constant ice temperature leads to a constant drying rate.

As in the previous model, the effect of heating volumetrically is apparent. When the ice volume decreases, the heating rate and subsequently the sublimation rate decrease. When the volumetric heating is varied to maintain a constant temperature, the result is a constant sublimation rate that leads to a significantly shorter drying time. Also shown in Fig. 7.4 is the sublimation curve for the same constant temperature, but for a higher chamber pressure. The comparison of the two constant temperature cases shows how a lower chamber pressure can increase the sublimation rate.

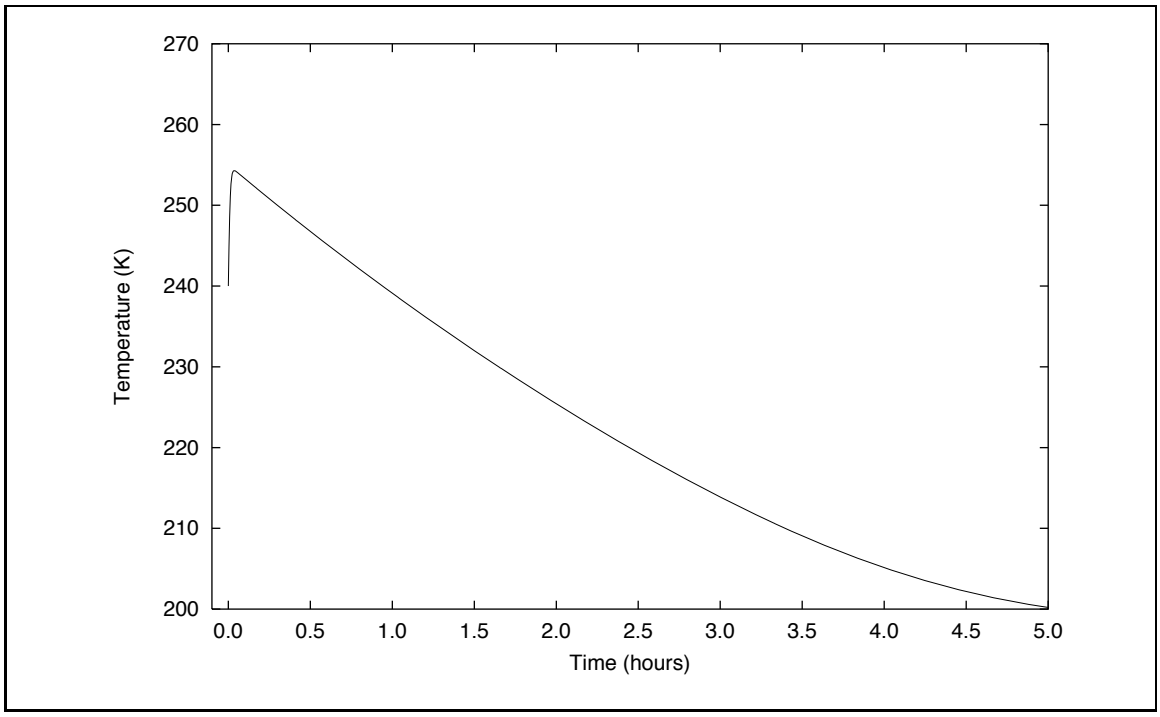


**Figure 7.5** The temperature of the ice as a function of time given by the model described in Section 7.2.2. The temperature of the system is considered uniform and the mass transfer is modeled with Knudsen's equation.

The next step in developing a mathematical model of sublimation in a porous material is to include the porous material. The following section gives a brief description of the porous material.

## 7.3 Sublimation in a Porous Material

Including the porous material is an essential part of the model. It influences both the volumetric heating and the mass transfer rate from the sublimation interface. This section discusses the effect of including the porous material in the model.

### 7.3.1 Description of the Sample

The model of the porous material assumes that the material is homogeneous and porous with a constant pore size distribution. As seen on Fig. 7.6, the sample is assumed cylindrical with diameter $d = 15\,\text{mm}$ and height $h = 9\,\text{mm}$. The porosity, $\epsilon$, defined as the volume of the void space divided by the total volume of the sample, is estimated as 0.7. The ice volume is $1.11 \times 10^{-6}\,\text{m}^3$.

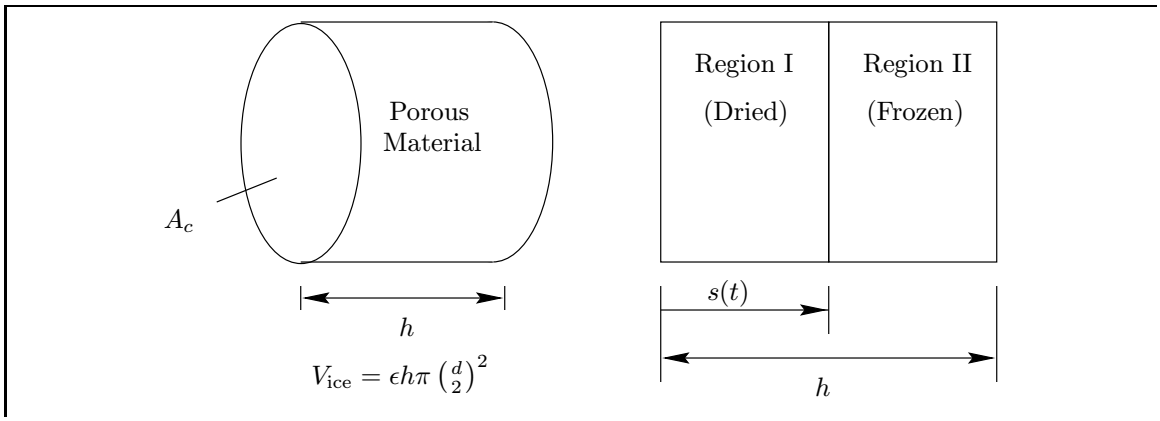


**Figure 7.6** Description of the sample used in the application of the mathematical models that include the porous material

In its starting condition, the sample is assumed completely frozen at 260 K (-13°C). The pores are assumed to be filled with ice. The structure of the porous material is considered to be rigid and unaltered with time.

### 7.3.2 A Modified Simple Model

The simple model presented in Section 7.2.1 can easily be extended to include the porous material. However, it is again assumed that the temperature is uniform and constant. It is also assumed that the vapor flowing through the porous dried layer has no effect on the energy balance.

Figure 7.7 shows a diagram of the system. The heat generated volumetrically in the dried region (region I) is assumed to be transfered to the sublimation interface, maintaining the dried layer at a constant temperature. This is represented by the $\dot{E}_{\text{in}}$ term which can be determined by drawing a control volume boundary around the dried layer and applying an energy balance.

Application of the energy balance to the control volume surrounding the frozen region (region II) results in

$$\begin{aligned}
\dot{E}_{\text{in}} &= A_c \dot{q}_s (1-\epsilon) s - (\rho c_p)_s (1-\epsilon) T A_c \frac{ds}{dt} \\
\dot{E}_{\text{out}} &= \rho_i \Delta H_{\text{sub}} \epsilon A_c \frac{ds}{dt} \\
\dot{E}_{\text{g}} &= A_c (h-s) \left[ (1-\epsilon)\dot{q}_s + \epsilon \dot{q}_i \right] \\
\dot{E}_{\text{st}} &= -\left[ (\rho c_p)_i \epsilon + (\rho c_p)_s (1-\epsilon) \right] T A_c \frac{ds}{dt}
\end{aligned} \tag{7.10}$$

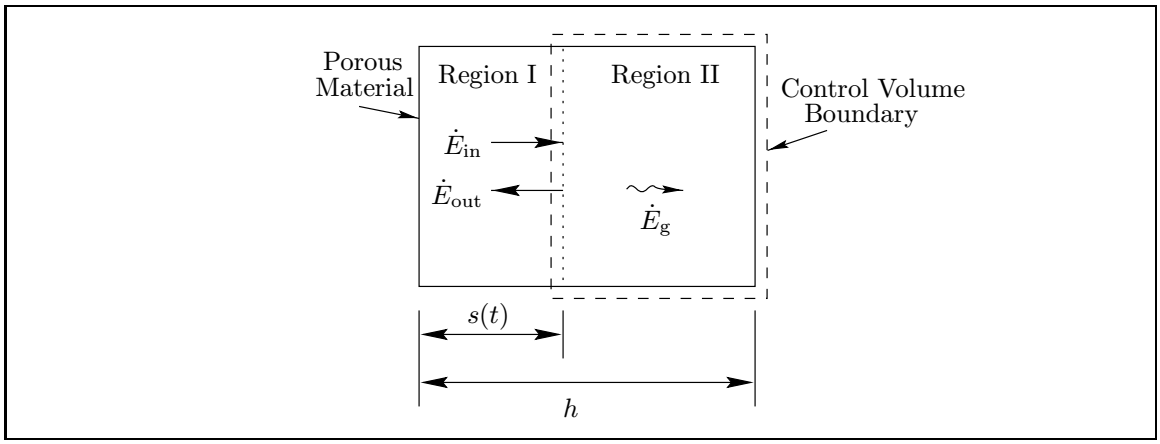


**Figure 7.7** Diagram of a cylindrical porous plug with ice sublimating from the pores

where $\dot{q}_s$ is the volumetric heating rate in the solid material of the porous structure. The volumetric heating rate can be estimated from the drying rate data of Chapter 6. Multiplying the peak sublimation rate by the latent heat of sublimation and dividing this result by the volume of the sample gives a reasonable estimate of the volumetric heating. Using this method, $9 \times 10^5$ W/m$^3$ was taken for $\dot{q}_i$. Since $\dot{q}_s$ is expected to be lower, $5 \times 10^5$ W/m$^3$ was chosen for this value.

The energy balance can be reduced to the following linear first order ordinary differential equation

$$\frac{ds}{dt} + \begin{bmatrix} \dot{q}_i\epsilon \\ \rho_i \Delta H_{\text{sub}}\epsilon - (\rho c_p)_i \epsilon T \end{bmatrix} s = \begin{bmatrix} \dot{q}_i\epsilon + \dot{q}_s(1-\epsilon) \\ \rho_i \Delta H_{\text{sub}}\epsilon - (\rho c_p)_i \epsilon T \end{bmatrix} h \tag{7.11}$$

where $\rho_s = 145.0\,\text{kg/m}^3$ and $c_{p_s} = 2600$ J/kg $\cdot$ K. Substituting the numerical values into Eqn. 7.11 yields

$$s(t) = 0.0111\,(1 - \exp\,(-0.000416t)) \tag{7.12}$$

Equation 7.12 is plotted in Fig. 7.8. Comparing this curve with the curve presented in Fig. 7.2 (page 86), it is obvious that the porous material has a significant affect on the drying rate. Now, heat is generated within the volume of the solid that makes up the porous structure as well as within the ice. Since the porous material does not decrease in volume during the drying process, as the ice does, it provides a source of constant heat flow to the ice. This prevents the trailing off of the sublimation rate as seen in Fig. 7.2.

The next step is to include an equation modeling the vapor flow through the porous dried layer. Knudsen's equation cannot be used for this purpose because it describes only

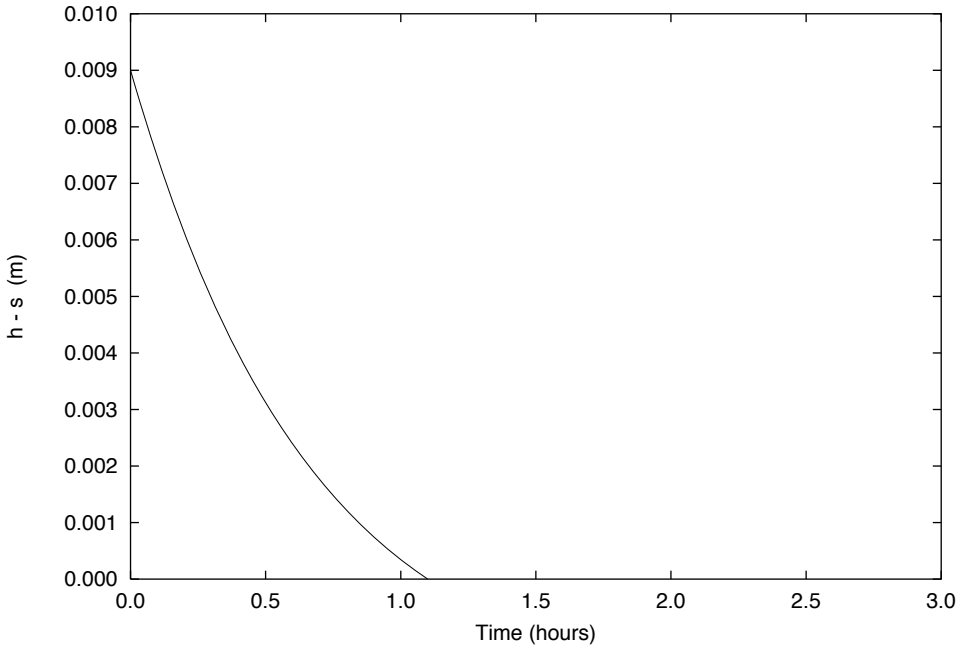


**Figure 7.8** The thickness of the frozen layer as a function of time when considering the porous material and a steady-state model as described in Section 7.3.2.

sublimation of ice into a low pressure chamber. Flow through a porous material is most often modeled by the D'Arcy equation.

### 7.3.3 The D'Arcy Equation

Initially, neglecting other forms of mass transport, the D'Arcy equation, Eqn. 3.19, can be used to describe the mass flux traveling through the dried layer. If a linear pressure gradient and a constant water vapor density are assumed, the D'Arcy equation is reduced to

$$\rho_i \frac{ds}{dt} = \rho_v \frac{c_0}{\mu_v} \frac{P_{\text{sat}}(T) - P_0}{s} \tag{7.13}$$

where the subscript $v$ refers to water vapor, $c_0$ is the relative D'Arcy flow permeability and $\mu$ is the viscosity.

Again, with the assumption of a uniform temperature, the energy balance results in

$$\begin{aligned}
\dot{E}_{\text{in}} &= A_c \dot{q}_s (1-\epsilon) s - (\rho c_p)_s (1-\epsilon) \left[ T A_c \frac{ds}{dt} + A_c s \frac{dT}{dt} \right] \\
\dot{E}_{\text{out}} &= \rho_i \Delta H_{\text{sub}} \epsilon A_c \frac{ds}{dt} \\
\dot{E}_{\text{g}} &= A_c (h-s) \left[ (1-\epsilon) \dot{q}_s + \epsilon \dot{q}_i \right] \\
\dot{E}_{\text{st}} &= \left[ (\rho c_p)_s (1-\epsilon) + (\rho c_p)_i \epsilon \right] A_c \left[ -T \frac{ds}{dt} + (h-s) \frac{dT}{dt} \right]
\end{aligned} \tag{7.14}$$

which can be reduced to

$$\frac{dT}{dt} = \frac{(\rho c_p)_i \epsilon T - \rho_i \Delta H_{\text{sub}} \epsilon}{(h-s)(\rho c_p)_i \epsilon + h(\rho c_p)_s (1-\epsilon)} \frac{ds}{dt} + \frac{\dot{q}_i \epsilon (h-s) + \dot{q}_s (1-\epsilon) h}{(h-s)(\rho c_p)_i \epsilon + h(\rho c_p)_s (1-\epsilon)} \tag{7.15}$$

Figure 7.9 shows the thickness of the frozen layer, equivalent to the position of the sublimation interface, as a function of time. This result is identical to the previous result (Fig. 7.8) except that the ice temperature is no longer constant. Figure 7.10 displays a plot of the temperature of the ice as a function of time. This plot shows a quick drop in the temperature to a point where the energy loss due to sublimation is equal to the energy input due to the volumetric heating. From there, the temperature increases until the ice volume has decreased to the point where, again, the energy loss due to sublimation is equal to the energy input due to the volumetric heating. From there till the end of the drying process, the temperature decreases.

The use of the D'Arcy equation allows for the investigation of the effect of chamber pressure. Assuming a constant temperature, Eqn. 7.13 can be solved for $s(t)$ yielding

$$s(t) = \sqrt{\frac{2 c_0 \rho_v}{\mu_v \rho_i} (P_{\text{sat}}(T) - P_0) t} \tag{7.16}$$

In Fig. 7.11, drying curves are plotted versus time for different chamber pressures. In each case, the sublimation temperature is 260 K. These results still consider that the pressure gradient is linear. It is important to note that decreasing pressure has the most effect when the chamber pressure is above 0.1 Torr (13.33 $\text{N/m}^2$). Reducing the chamber pressure below 0.01 Torr (1.333 $\text{N/m}^2$) does not result in any further increase of the drying rate.

The results shown in Fig. 7.11 correspond to those in Fig. 6.7. In both cases the effect of lowering the chamber pressure is to increase the sublimation rate. Thus, the results of the this section confirm the observations in phase II of the experimental results of Chapter 6.

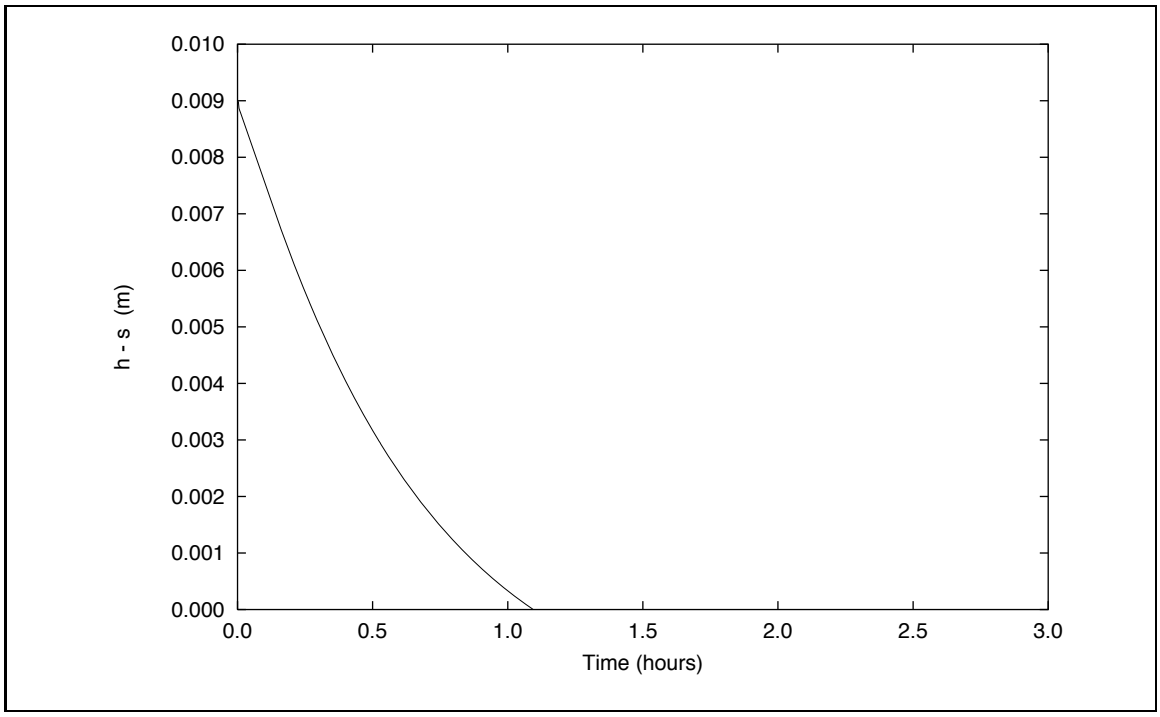


**Figure 7.9** The thickness of the frozen layer as a function of time during primary drying using a model that includes the D'Arcy equation for a porous material as described in Section 7.3.3

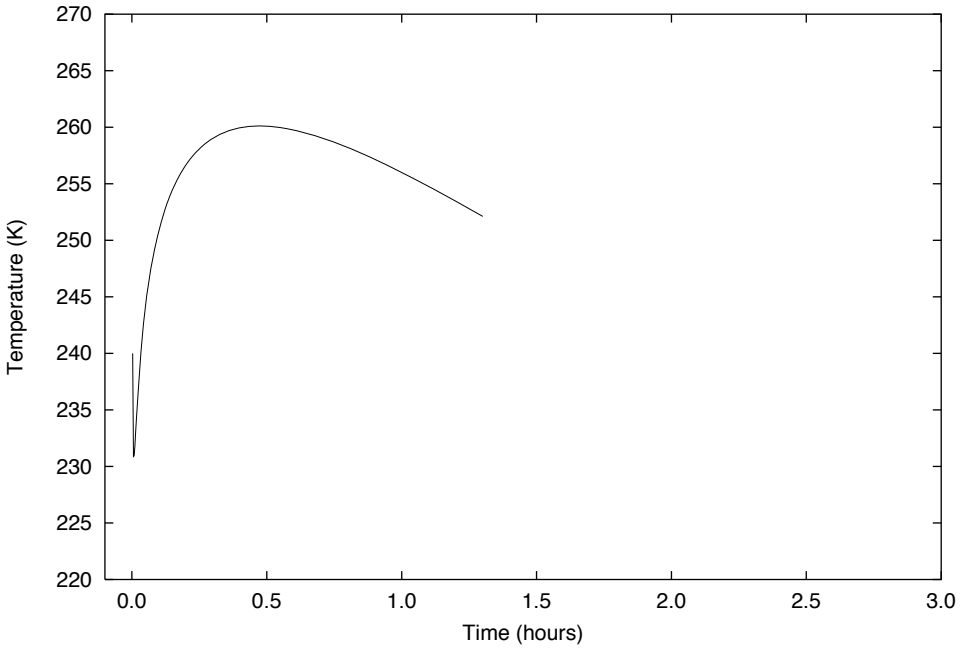


**Figure 7.10** Temperatures predicted by the model that includes the D'Arcy equation for a porous material (Section 7.3.3)

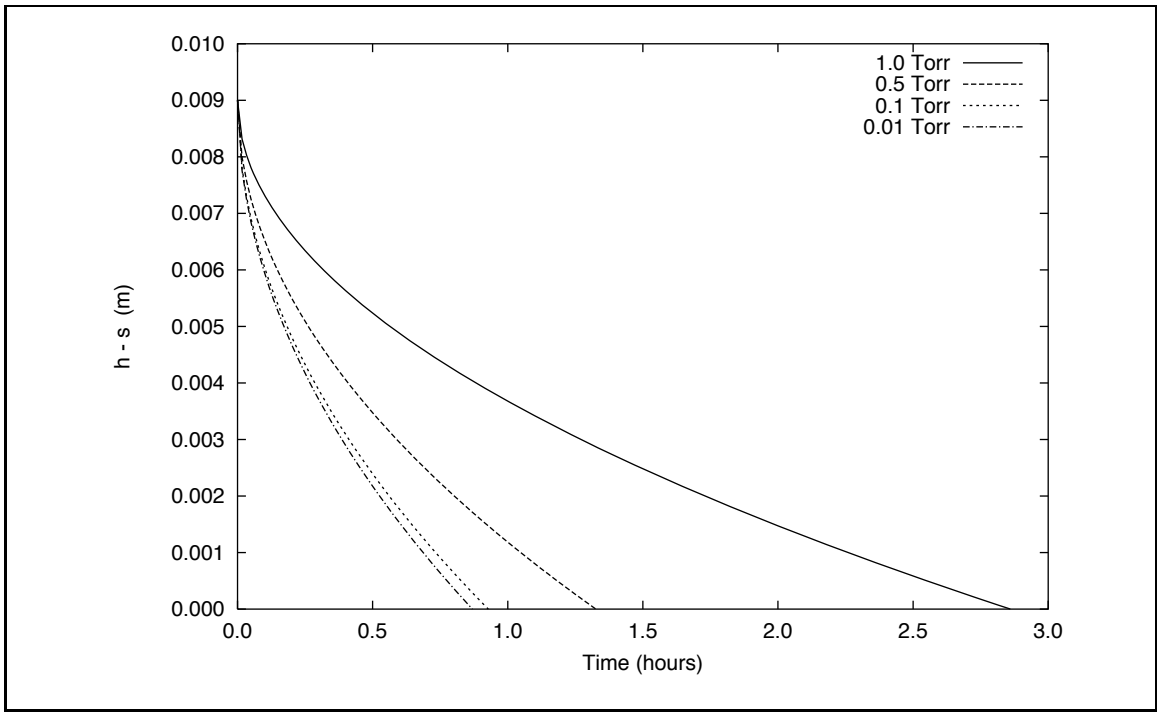


**Figure 7.11** Comparison of drying curves predicted by the D'Arcy equation (Section 7.3.3). The sublimation temperature is constant (260 K) and the pressure distribution in the dried layer is assumed linear.

### 7.3.4 The Heat Equation in the Porous Dried Region

The next step in the development of the model is to remove the uniform temperature assumption in the dried layer. A uniform temperature throughout the entire sample is not a good assumption since the effective thermal conductivity of the porous dried region (region I) is very low, of the order of $10^{-1}$ or $10^{-2}$ W/m $\cdot$ K (Liapis and Litchfield, 1979). The effective thermal conductivity of the frozen region (region II) is of the order of 1 W/m $\cdot$ K (Liapis and Litchfield, 1979). Therefore, the assumption of a uniform temperature is retained for the frozen layer. Thus, region II can be modeled as a lumped capacitance, while in region I, the heat equation is required to describe heat conduction and predict the rate of heat being input to the sublimation interface from the dried layer.

The heat transfer problem in region I can be described as

$$(\rho c_p)_{I,\text{eff}} \frac{\partial T_I}{\partial t} = \dot{q}_s + k_{I,\text{eff}} \frac{\partial^2 T_I}{\partial x^2} \tag{7.17}$$

The effective thermal properties are defined as (Nozad et al., 1985)

$$\begin{aligned}(\rho c_p)_{I,\text{eff}} &= (\rho c_p)_s(1-\epsilon) + (\rho c_p)_v\epsilon \\ k_{I,\text{eff}} &= k_s(1-\epsilon) + k_v\epsilon\end{aligned} \tag{7.18}$$

where the subscript $v$ refers to water vapor. The following initial condition and boundary conditions are taken to completely specify the problem:

$$\begin{aligned}T_I(x,0) &= 240\,\text{K} \\ \frac{\partial T_I}{\partial x}(0,t) &= 0 \\ -k_{I,\text{eff}}\frac{\partial T_I}{\partial x}(s,t) &= q''_{I\text{out}}(t)\end{aligned} \tag{7.19}$$

The heat flux boundary condition at $x = s$ can be determined by applying an energy balance to region II that includes the moving boundary

$$\begin{aligned}\dot{E}_\text{in} &= q''_{I\text{out}}A_c \\ \dot{E}_\text{out} &= \rho_i\Delta H_\text{sub}\epsilon A_c\frac{ds}{dt} \\ \dot{E}_\text{g} &= A_c(h-s)\left[\dot{q}_s(1-\epsilon) + \dot{q}_i\epsilon\right] \\ \dot{E}_\text{st} &= (\rho c_p)_{II,\text{eff}}A_c\left[(h-s)\frac{dT_{II}}{dt} - T\frac{ds}{dt}\right]\end{aligned} \tag{7.20}$$

where

$$(\rho c_p)_{II,\text{eff}} = (\rho c_p)_s(1-\epsilon) + (\rho c_p)_i\epsilon \tag{7.21}$$

Solving for $q''_{I\text{out}}$ leads to

$$q''_{I\text{out}} = -(h-s)\left[(1-\epsilon)\dot{q}_s + \epsilon\dot{q}_i\right] + \left[\rho_i\Delta H_\text{sub}\epsilon - (\rho c_p)_{II,\text{eff}}T\right]\frac{ds}{dt} + (\rho c_p)_{II,\text{eff}}(h-s)\frac{dT_{II}}{dt} \tag{7.22}$$

As in the previous section, the D'Arcy equation (Eqn. 7.13) is used to model the water vapor flow through region I. To solve this problem, the moving boundary is immobilized by applying a coordinate change

$$\xi = \frac{x}{s(t)} \qquad 0 \le x \le s \tag{7.23}$$

which yields

$$\frac{\partial T_I}{\partial t} = \frac{\alpha_{I,\text{eff}}}{s^2}\frac{\partial^2 T_I}{\partial \xi^2} + \frac{\xi}{s}\frac{ds}{dt}\frac{\partial T_I}{\partial \xi} + \frac{\dot{q}_s}{(\rho c_p)_{I,\text{eff}}} \tag{7.24}$$

**Table 7.1** Parameter values used in calculations

| **Parameter** | Value | Units |
|---|---|---|
| $R$ | 8314.41 | $\mathrm{J/kmol \cdot K}$ |
| $M$ | 18.02 | kmol/kg |
| $c_0$ | $7.219 \times 10^{-10}$ | $\mathrm{m^2}$ |
| $\mu_v$ | $1.0 \times 10^{-8}$ | $\mathrm{kg/s \cdot m}$ |
| $\rho_v$ | $8.7 \times 10^{-4}$ | $\mathrm{kg/m^3}$ |
| $\epsilon$ | 0.7 | |
| $h$ | 0.009 | m |
| $P_0$ | 1.333 | $\mathrm{N/m^2}$ |
| $\Delta H_{\mathrm{sub}}$ | $2839.0 \times 10^3$ | J/kg |
| $\rho_i$ | 920.0 | $\mathrm{kg/m^3}$ |
| $c_{p_i}$ | 2040.0 | $\mathrm{J/kg \cdot K}$ |
| $\rho_s$ | 145.0 | $\mathrm{kg/m^3}$ |
| $c_{p_s}$ | 2600.0 | $\mathrm{J/kg \cdot K}$ |
| $k_s$ | 0.17 | $\mathrm{W/m \cdot K}$ |
| $\dot{q}_i$ | $9 \times 10^5$ | $\mathrm{W/m^3}$ |
| $\dot{q}_s$ | $5 \times 10^5$ | $\mathrm{W/m^3}$ |

where

$$\alpha_{I,\mathrm{eff}} = \frac{k_{I,\mathrm{eff}}}{(\rho c_p)_{I,\mathrm{eff}}} \tag{7.25}$$

The technique used to solve this problem is a collocation method where the heat equation was discretized in the spatial coordinate, hence resulting in a set of ordinary differential equations. The discretization of the heat equation was done by applying the conservative control volume method of Patankar (1980).

The resulting set of ODE's was solved using the Mathematica numerical ODE solver NDSolve. The solutions are plotted in Figs. 7.12 and 7.13. Figure 7.12 shows the position of the phase front versus time while Fig. 7.13 shows the variation of the ice temperature in region II versus time. The parameter values are given in Table 7.1.

The results now show a much steeper drying curve as well as a steeper temperature curve compared to Fig. 7.9. The drying time predicted by this model is about 0.7 hours compared to 1.1 hours predicted by the previous model presented in Section 7.3.3.

The next step in the development of a model is to remove the restriction of a linear pressure gradient in the dried layer. The temperature gradient can be used along with the ideal gas law and the D'Arcy equation to specify the vapor flux in the dried layer as a function of both position and time without a linear assumption.

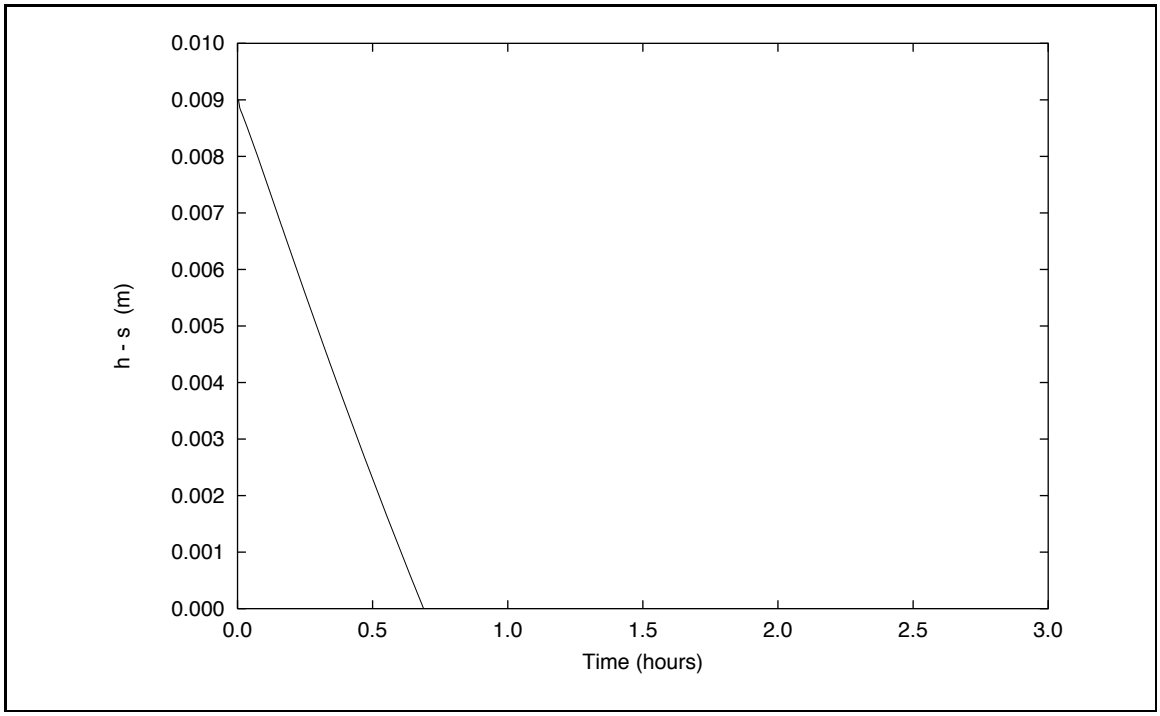


**Figure 7.12** The thickness of the frozen layer as a function of time during primary drying using a model that includes the D'Arcy equation and a transient heat conduction equation for the frozen region as described in Section 7.3.4

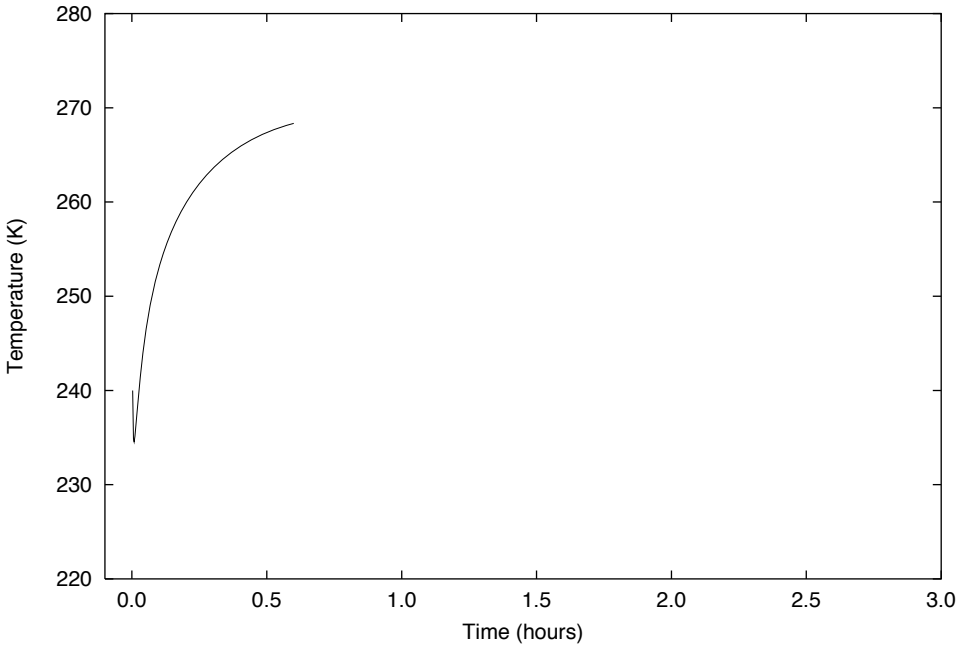


**Figure 7.13** Temperature of the frozen region predicted by the model that includes the D'Arcy equation and a transient heat conduction equation for the frozen region (Section 7.3.4)

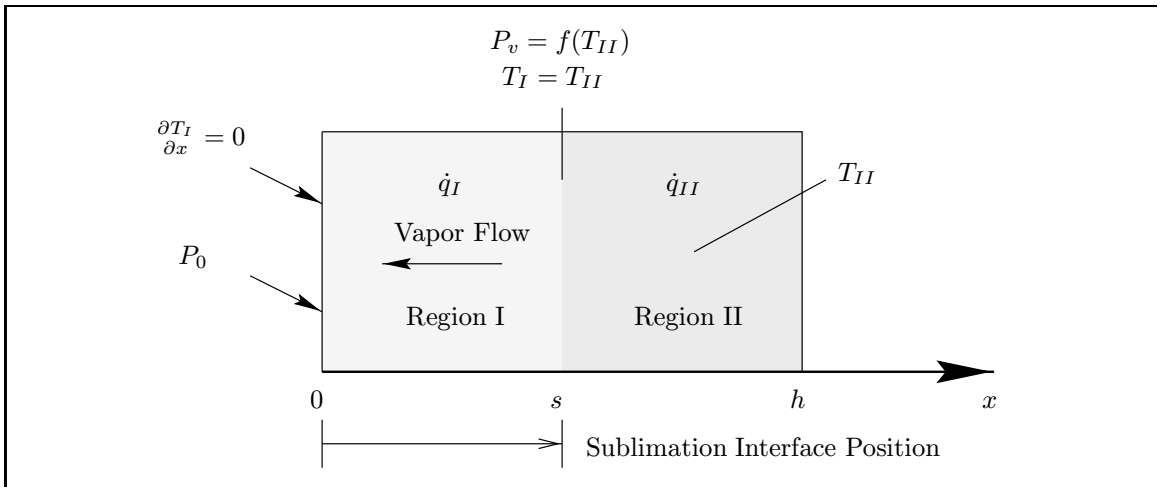


**Figure 7.14** Schematic of the problem

## 7.4 The Dusty Gas Model

The use of the dusty gas model equations developed in Chapter 3 provides a detailed model of the vapor flow through the dried layer and allows for the consideration of a second gas component in the dried layer. Maximizing the vapor flow is an important part of optimizing the freeze-drying process for maximum drying rates. The model presented in this section eliminates two of the previous model's assumptions: a linear pressure gradient and a constant water vapor density. Also, by incorporating the dusty gas model equations, diffusional flow mechanisms are taken into account. However, the model is still restricted to a one-dimensional system.

A schematic of the problem is given in Fig. 7.14. Now considering convective heat transfer in the dried layer, the heat equation for region I can be written as

$$\frac{\partial T_I}{\partial t} = -n_t'' \frac{c_{p_g}}{(\rho c_p)_{I,\text{eff}}} \frac{\partial T_I}{\partial x} + \alpha_{I,\text{eff}} \frac{\partial^2 T_I}{\partial x^2} + \frac{\dot{q}_I}{(\rho c_p)_{I,\text{eff}}} \tag{7.26}$$

where convection is included and $n_t''$ is the total mass flux of gas through the porous dried layer. The thermal boundary conditions are

$$\begin{aligned} \frac{\partial T_I}{\partial x} &= 0 \quad \text{at} \quad x = 0, \quad t > 0 \\ \frac{\partial T_I}{\partial x} &= q_{I\text{out}}'' \quad \text{at} \quad x = s, \quad t > 0 \end{aligned} \tag{7.27}$$

where $q_{I\text{out}}''$ is given by Eqn. 7.22. The initial condition is

$$T_I = T_{II} = T^0 \quad \text{at} \quad t = 0, \quad 0 \le x \le h \tag{7.28}$$

The continuity equations for the water vapor and air moving through the dried layer are given by

$$\frac{M_v}{RT}\frac{\partial P_v}{\partial t} + \frac{\partial n_v''}{\partial x} = 0, \quad 0 \le x \le s \tag{7.29}$$

$$\frac{M_a}{RT}\frac{\partial P_a}{\partial t} + \frac{\partial n_a''}{\partial x} = 0, \quad 0 \le x \le s \tag{7.30}$$

where the temperature dependent terms have been dropped since they are not significant compared to the other terms (Liapis and Litchfield, 1979).

Equations for the mass fluxes, $n_v''$ and $n_a''$, can be derived by combining the diffusion equations of Evans et al. (1962) and the D'Arcy equation for viscous flow through a porous medium. This results in

$$n_v'' = -\frac{M_v}{RT}\left(k_1\frac{\partial P_v}{\partial x} + k_2 P_v\left(\frac{\partial P_v}{\partial x} + \frac{\partial P_a}{\partial x}\right)\right) \tag{7.31}$$

$$n_a'' = -\frac{M_a}{RT}\left(k_1\frac{\partial P_a}{\partial x} + k_2 P_a\left(\frac{\partial P_a}{\partial x} + \frac{\partial P_a}{\partial x}\right)\right) \tag{7.32}$$

These equations were developed in Chapter 3. The boundary and initial conditions for the mass transport equations are given by

$$P_v = P_{v0}, \qquad P_a = P_0 - P_{v0} \qquad \text{at} \quad x = 0 \tag{7.33}$$

$$P_v = f(T_{\text{sat}}), \quad \frac{\partial P_a}{\partial x} = 0 \qquad \text{at} \quad x = s \tag{7.34}$$

$$P_v = 0 \qquad \text{at} \quad t = 0, \qquad 0 \le x \le s \tag{7.35}$$

$$P_a = 0 \qquad \text{at} \quad t = 0, \qquad 0 \le x \le s \tag{7.36}$$

Finally, the velocity of the sublimation interface is

$$\frac{ds(t)}{dt} = \frac{-n_t''}{\rho_{II} - \rho_I} \tag{7.37}$$

These model equations can be solved by transforming the moving boundary problem to a problem of a fixed domain as was done for the model in the previous section. After the equations are transformed, they can be solved by using a finite difference method or the collocation method used in the previous section.

The benefit of this model is that it accurately models the significant processes that occur during freeze-drying. The mass transfer equation can combine independent mass transport mechanisms which occur in a porous material under low pressure. This is the most important part of the model since it is to be used to show how changes in the chamber pressure affect the mass flow rate through the porous layer.

# Chapter 8

# Summary and Conclusions

## 8.1 Project Summary

Much of the previously published work on pharmaceutical freeze-drying focuses on developing a better understanding of the freeze-drying process. The knowledge gained by studying the freeze-drying process was then used for process optimization in a effort to improve product quality and reduce processing cost. However, significant changes in the design of the equipment used in pharmaceutical freeze-drying have not been studied. This is the significance of this work. By supplying heat volumetrically rather than through conduction a very different approach to conducting the freeze-drying process has been studied.

The goal of this project was to show that volumetric heating can be used in pharmaceutical freeze-drying and that this mode of heating offers some advantages. There were two approaches taken to the work, one experimental and one analytical. The experimental approach was broken into two phases, one focused on comparing microwave and conventional freeze-drying and the other focused on demonstrating the advantages of volumetric heating. In the analytical approach, a mathematical model was used to confirm the trends observed in phase II of the experimental work.

Experiments were conducted in a conventional laboratory freeze-dryer and the drying rate results were compared to the results obtained with an experimental microwave freeze-drying apparatus. Experiments were also conducted with the vaccine strain *A. pleuropneumoniae*. A viability study was conducted, comparing the viability loss caused by each process. The viability study showed a slightly higher viability loss for the microwave process.

A comparison of drying curves showed that the microwave process resulted in a slight improvement in primary drying time: 2.5 hours for the microwave process compared to 3 hours for the conventional process. There was a significant difference in overall drying times: 4 hours for the microwave process compared to 11 hours for the conventional process. This result was caused by a lower residual moisture content at the start of secondary drying and a higher secondary drying temperature for the microwave process.

Experiments were also conducted to show that using lower chamber pressure results in higher drying rates. This is not the case in a conventional freeze-dryer since heating is dependent on the chamber pressure in the low pressure environment of freeze-drying. Thus, an advantage of volumetric heating was demonstrated. The results show that a modest increase in pressure, from 0.05 to 0.3 Torr, caused a one third reduction in primary drying time.

The mathematical model developed in the analytical work relied on the D'Arcy equation to describe the flow of vapor in the porous dried layer. The results of the model confirm trends seen in the measured temperature and weight profiles. Analyzing the effect of varying the chamber pressures shows that lowering the pressure in the range of 1 to 0.01 Torr results in a significant increase in drying rate giving as much as a two thirds reduction in drying time for the case studied. A model incorporating mass transport equations derived from the dusty gas model was also presented. This model offers the benefit of a more accurate prediction of mass transport through the porous dried layer.

## 8.2 Conclusions

The goal of investigating the feasibility and advantages of using microwave freeze-drying as an alternative to conventional freeze-drying in the pharmaceutical industry was reached. The experimental and analytical results support the expectations based on the theory presented in Chapter 3. The following list contains the conclusions for each of the two phases of the project.

### 8.2.1 Experimental Investigation

**Phase I: Comparison of Microwave and Conventional Freeze-Drying**

1. Under similar operating conditions, microwave freeze-drying results in a significantly shorter drying time, as much as a one-third times savings for primary drying.

2. Under the operating conditions studied, the microwave freeze-drying process resulted in a slightly lower viability compared to the conventional process. This result can be attributed to the higher secondary drying temperature and a slightly higher residual moisture content in the microwave case.

**Phase II: The effect of pressure on drying rate**

1. A moderate decrease in chamber pressure can result in significant time savings during primary drying.

2. Since optimal heating during the primary drying stage requires high initial heating and a continual decrease in heating as the dried layer grows, volumetric heating is well suited to freeze-drying.

### 8.2.2 Analytical Study

1. Decreasing chamber pressure does result in an increased drying rate when volumetric heating is used.

2. Decreasing chamber pressure to increase drying rate is most effective in the typical freeze-drying pressure range of 1 Torr to 0.01 Torr.

## 8.3 Overall Conclusions

It is evident that incorporating microwave energy into the pharmaceutical freeze-drying process has the potential to reduce the overall processing cost by reducing the processing time. The most significant advantage to volumetric heating is the ability to decrease chamber pressure without a detrimental effect on heating. Other advantages are the ability to heat the dried layer during primary drying and improved control of heating. The benefit of heating the dried layer during primary drying is that secondary drying will start at a

lower residual moisture content, thereby significantly reducing the secondary drying time. Improved control of heating results from the heating rate being reduced as the volume of ice is reduced and also power can be quickly adjusted allowing for an optimized power schedule.

# Chapter 9

# Recommendations

## 9.1 Experimental Apparatus

Several improvements are recommended for the experimental microwave freeze-drying apparatus. The improvements can extend the usefulness of the apparatus and improve the quality of the data.

1. Replace the purge valve with a precision leak valve. The valve currently being used to control the chamber pressure is not capable of the fine adjustments required when controlling the chamber pressure.

2. Replace the electronic balance with a simple mechanism utilizing a cantilevered beam and a strain gauge. The current electronic balance was not designed to operate under low pressure and thus the measurement may not be reliable, especially when going though significant pressure changes.

3. Include the ability to freeze samples after they are placed into the chamber. This would remove the errors caused by frost accumulating on the vial after it is frozen, but before it placed in the chamber and the pressure lowered. This may be possible by cooling dry nitrogen gas with liquid nitrogen and then passing it through the drying chamber to freeze the sample.

## 9.2 Future Research

The following list enumerates items that are recommended for further study.

1. A model incorporating mass transport equations derived from the dusty gas model was presented. However, a solution to this model has not yet been completed. Completion of this solution will allow a more detailed study of the relationship among pressure, temperature and drying rates under a volumetric heating mode.

2. Another area of work that would benefit this project is related to the modeling described in the previous paragraph. Use of the dusty gas model to describe mass transport in freeze-drying should be verified. Also experiments to measure the mass transport coefficients are needed to complete application of the model to the specific materials being used. This information is essential if the model is to accurately predict drying rates.

3. A study of secondary drying would also be beneficial to this project. Secondary drying can have a significant influence on the total drying time and final product quality. Development of a methodology for measuring the appropriate sorption parameters for modeling of secondary drying is also recommended.

4. Modeling of the microwave heating is recommended to improve the accuracy of model by predicting the amount of power dissipated in the sample. This work would also require measurement of dielectric properties of the materials involved.

# Bibliography

Adams, G. D. J., 1991, "Freeze-Drying of Biological Materials," *Drying Technology*, Vol. 9, No. 4, pp. 891–925.

Ang, T. K., Ford, J. D., and Pei, D. C. T., 1977a, "Microwave Freeze-Drying of Food: A Theoretical Investigation," *International Journal of Heat and Mass Transfer*, Vol. 20, No. 5, pp. 517–526.

Ang, T. K., Pei, D. C. T., and Ford, J. D., 1977b, "Microwave Freeze-Drying of Food: An Experimental Investigation," *Chemical Engineering Science*, Vol. 32, pp. 1477–1489.

Arsem, H. B. and Ma, Y. H., 1985, "Aerosol Formation During the Microwave Freeze Dehydration of Beef," *Biotechnology Progress*, Vol. 1, No. 2, pp. 104–110.

Arsem, H. B. and Ma, Y. H., 1990, "Simulation of a Combined Microwave and Radiant Freeze Dryer," *Drying Technology*, Vol. 8, No. 5, pp. 993–1016.

Bruttini, R., Rovero, G., and Baldi, G., 1991, "Experimentation and Modelling of Pharmaceutical Lyophilization Using a Pilot Plant," *The Chemical Engineering Journal*, Vol. 45, pp. B67–B77.

Chang, T. N. and Ma, Y. H., 1985, "Application of Optimal Control Strategy to Hybrid Microwave and Radiant Heat Freeze Drying System," in: *Drying '85*, eds. T. Ryozo and A. S. Mujumdar, Hemisphere Publishing Corp., pp. 249–253.

Connelly, J. P. and Welch, J. V., 1993, "Monitor Lyophilization with Mass Spectrometer Gas Analysis," *Journal of Parenteral Science and Technology*, Vol. 47, No. 2, pp. 70–75.

Copson, D. A., 1958, "Microwave Sublimation of Foods," *Food Technology*, Vol. 12, No. 6, pp. 270–272.

Copson, D. A. and Decareau, R. V., 1957, "Microwave Energy in Freeze-Drying Procedures," *Food Research*, Vol. 22, No. 4, pp. 402–403.

Dolan, J. P., 1994, "Microwave Freeze-Drying of Aqueous Solutions," M.S. Thesis, Viginia Polytechnic Institute and State University.

Dyer, D. F. and Sunderland, J. E., 1968, "Heat and Mass Transfer Mechanisms in Sublimation Dehydration," *Journal of Heat Transfer*, Vol. 90, No. 4, pp. 379–384.

Evans, R. B., Watson, G. M., and Mason, E. A., 1961, "Gaseous Diffusion in Porous Media at Uniform Pressure," *Journal of Chemical Physics*, Vol. 35, No. 6, pp. 2076–2083.

Evans, R. B., Watson, G. M., and Mason, E. A., 1962, "Gaseous Diffusion in Porous Media II," *Journal of Chemical Physics*, Vol. 36, No. 7, pp. 1894–1902.

Franks, F., 1982, *Water: A Comprehensive Treatise*, Vol. 7, Chap. Properties of Aqueous Solutions at Subzero Temperatures, Plenum Press, New York, pp. 215–334.

Franks, F., 1989, "Improved Freeze-Drying: An Analysis of the Basic Scientific Principles," *Process Biochemistry*, Vol. 24, No. 1, Supplement: ProBioTech, iii-vii.

Franks, F., Hatley, R. H. M., and Mathias, S. F., 1991, "Materials Science and the Production of Shelf-Stable Biologicals," *Pharmaceutical Technology International*, Vol. 3, pp. 24–34.

Gould, J. W. and Kenyon, E. M., 1971, "Gas Discharge and Electric Field Strength in Microwave Freeze-Drying," *Journal of Microwave Power*, Vol. 6, No. 2, pp. 151–167.

Gunn, R. D. and King, C. J., 1969, "Mass Transport in Porous Materials under Combined Gradients of Composition and Pressure," *AIChE Journal*, Vol. 15, No. 4, pp. 507–514.

Hatley, R. H. M. and Franks, F., 1991, "Applications of DSC in the Development of Improved Freeze-Drying Processes for Labile Biologicals," *Journal of Thermal Analysis*, Vol. 37, pp. 1905–1914.

Hill, J. E. and Sunderland, J. E., 1970, "Sublimation-Dehydration in the Continuum, Transition and Free-Molecular Flow Regimes," *International Journal of Heat and Mass Transfer*, Vol. 14, pp. 625–638.

Hogg, R. V. and Ledolter, J., 1992, *Applied Statistics for Engineers and Physical Scientists*, 2nd edn., Macmillan Publishing Company, New York.

Hoover, M. W., Markantonatos, A., and Parker, W. N., 1966a, "Engineering Aspects of Using UHF Dielectric Heating to Accelerate the Freeze-Drying of Foods," *Food Technology*, Vol. 20, No. 6, pp. 107–110.

Hoover, M. W., Markantonatos, A., and Parker, W. N., 1966b, "UHF Dielectric Heating in Experimental Acceleration of Freeze-Drying of Foods," *Food Technology*, Vol. 20, No. 6, pp. 103–107.

Jennings, T. A., 1986, "Effect of Pressure on the Sublimation Rate of Ice," *Journal of Parenteral Science and Technology*, Vol. 4, No. 3, pp. 95–97.

Keenan, J. H., Keys, F. G., Hill, P. G., and Moore, J. G., 1978, *Steam Tables*, Wiley, New York.

Liapis, A. I., 1980, "Rates for Freeze Drying," in: *Drying '80*, ed. A. S. Mujumdar, Vol. 2, Chap. Section IV: Drying of Foodstuffs and Grains, Hemisphere Publishing Corp, pp. 224–228.

Liapis, A. I. and Bruttini, R., 1994, "A Theory for the Primary and Secondary Drying Stages of the Freeze-Drying of Pharmaceutical Crystalline and Amorphous Solutes: A Comparison Between Experimental Data and Theory," *Seperation Technology*, Vol. 4, pp. 144–155.

Liapis, A. I. and Bruttini, R., 1995, "Freeze-Drying of Pharmaceutical Crystalline and Amorphous Solutes in Vials: Dynamic Multi-Dimensional Models of the Primary and Secondary Drying Stages and Qualitative Features of the Moving Interface," *Drying Technology*, Vol. 13, No. 1, pp. 43–72.

Liapis, A. I. and Litchfield, R. J., 1979, "Optimal Control of a Freeze Dryer-I," *Chemical Engineering Science*, Vol. 34, No. 7, pp. 975–981.

Liapis, A. I. and Marchello, J. M., 1983, "Freeze Drying of a Frozen Liquid in a Phial," *Drying Technology*, Vol. 2, No. 2, pp. 203–217.

Litchfield, R. J., Farhadpour, F. A., and Liapis, A. I., 1981, "Cyclical Pressure Freeze Drying," *Chemical Engineering Science*, Vol. 36, No. 7, pp. 1233–1238.

Livesey, R. G. and Rowe, T. W. G., 1987, "A Discussion of the Effect of Chamber Pressure on Heat and Mass Transfer in Freeze-Drying," *Journal of Parenteral Science and Technology*, Vol. 41, No. 5, pp. 169–171.

Luxtron Corp., 1992, *The Operator's Guide: Model 790 Fluoroptic Thermometer*, Luxtron Corporation, Santa Clara, CA 955051-0903.

Ma, Y. H. and Peltre, P., 1973, "Mathematical Simulation of a Freeze Drying Process Using Microwave Energy," in: *Food Preservation*, Vol. 69 of *AIChE Symposium Series*, pp. 47–54.

Ma, Y. H. and Peltre, P., 1975a, "Freeze Dehydration by Microwave Energy: Part I. Theoretical Investigation," *AIChE Journal*, Vol. 21, No. 2, pp. 335–344.

Ma, Y. H. and Peltre, P., 1975b, "Freeze Dehydration by Microwave Energy: Part II. Experimental Investigation," *AIChE Journal*, Vol. 21, No. 2, pp. 344–350.

MacKenzie, A. P., 1977, "The Physico-Chemical Basis for the Freeze-Drying Process," in: *Development of Biological Standards*, Vol. 36, International Symposium on Freeze-Drying of Biological Products, Washington, D.C. 1976, pp. 51–67.

MacKenzie, A. P., 1985, "A Current Understanding of the Freeze-Drying of Representative Aqueous Solutions," in: *Fundamentals and Applications of Freeze-Drying to Biological Materials, Drugs and Foodstufffs*, Science and Technology of Refridgeration, International Institute of Refridgeration, pp. 21–34.

Mason, E. A. and Malinauskas, A. P., 1983, *Gas Transport in Porous Media: The Dusty-Gas Model*, Chemical Engineering Monographs, Elsevier Science Publishers B.V., Amsterdam.

Mason, E. A., Malinauskas, A. P., and III, R. B. E., 1967, "Flow and Diffusion of Gases in Porous Media," *Journal of Chemical Physics*, Vol. 46, No. 8, pp. 3199–3216.

Mellor, J. D., 1978, *Fundamentals of Freeze-Drying*, Acedemic Press, London.

Metaxas, A. C. and Meredith, R. J., 1983, *Industrial Microwave Heating*, Peter Peregrinus Ltd., London, UK.

Millman, M. J., Liapis, A. I., and Marchello, J. M., 1985, "An Analysis of the Lyophilization Process Using a Sorption-Sublimation Model and Various Operational Policies," *AIChE Journal*, Vol. 31, No. 10, pp. 1594–1604.

Nail, S. L., 1980, "The Effect of Pressure on Heat Transfer in the Freeze-Drying of Parenteral Solutions," *Journal of the Parenteral Drug Association*, Vol. 34, No. 5, pp. 358–368.

Nozad, I., Carbonell, R. G., and Whitaker, S., 1985, "Heat Conduction in Multiphase Systems – I: Theory and Experiment for Two-Phase Systems," *Chemical Engineering Science*, Vol. 40, No. 5, pp. 843–855.

Patankar, S. V., 1980, *Numerical Heat Transfer and Fluid Flow*, Series in Computational Methods in Mechanics and Thermal Sciences, Hemisphere Publishing Corp., New York.

Pikal, M. J., 1985, "Use of Laboratory Data in Freeze Drying Process Design: Heat and Mass Transfer Coefficients and the Computer Simulation of Freeze Drying," *Journal of Parenteral Science and Technology*, Vol. 39, No. 3, pp. 115–138.

Pikal, M. J., Roy, M. L., and Shah, S., 1984, "Heat and Mass Transfer in Vial Freeze-Drying of Phamaceuticals: Role of the Vial," *Journal of Pharmaceutical Sciences*, Vol. 73, No. 9, pp. 1224–1237.

Pikal, M. J. and Shah, S., 1990, "The Collapse Temperature in Freeze Drying: Dependence on Measurement Methodology and Rate of Water Removal from the Glassy Phase," *International Journal of Pharmaceutics*, Vol. 62, pp. 165–186.

Pikal, M. J., Shah, S., Roy, M. L., and Putman, R., 1990, "The Secondary Drying Stage of Freeze Drying: Drying Kinetics as a Function of Temperature and Chamber Pressure," *International Journal of Pharmaceutics*, Vol. 60, pp. 203–217.

Pikal, M. J., Shah, S., Senior, D., and Lang, J. E., 1983, "Physical Chemistry of Freeze-Drying: Measurement of Sublimation Rates for Frozen Aqeuous Solutions by a Microbalance Technique," *Journal of Pharmaceutical Sciences*, Vol. 72, No. 6, pp. 635–650.

Roy, M. L. and Pikal, M. J., 1989, "Process Control in Freeze Drying: Determination of the End Point of Sublimation Drying by an Electronic Moisture Sensor," *Journal of Parenteral Science and Technology*, Vol. 43, No. 2, pp. 60–66.

Sadikoglu, H. and Liapis, A. I., 1997, "Mathematical Modelling of the Primary and Secondary Drying Stages of Bulk Solution Freeze-Drying in Trays: Parameter Estimation and Model Discrimination by Comparison of Theoretical Results with Experimental Data," *Drying Technology*, Vol. 15, No. 3&4, pp. 791–810.

Sandall, O. C., King, C. J., and Wilke, C. R., 1967, "The Relationship Between Transport Properties and Rates of Freeze-Drying of Poultry Meat," *AIChE Journal*, Vol. 13, pp. 428–438.

Shackelford, J. F., 1988, *Materials Science for Engineers*, Macmillan Publishing Company, New York.

Snowman, J. W., 1993, "Formulation and Cycle Development for Lyophilization: First Steps," *Pharmaceutical Engineering*, Vol. 13, pp. 26–34.

Sperling, L. H., 1992, *Introduction to Physical Polymer Science*, 2nd edn., John Wiley & Sons, Inc., New York.

Sunderland, J. E., 1982, "An Economic Study of Microwave Freeze-Drying," *Food Technology*, Vol. 36, No. 2, pp. 50–52,54–56.

Wolff, E. and Gibert, H., 1989, "Vacuum Freeze-Drying Kinetics and Modelling of a Liquid in a Vial," *Chemical Engineering and Processing*, Vol. 25, pp. 153–158.

# Appendix A

# Experimental Equipment

## A.1 Data acquisition equipment

1. AT-MIO-16F-5 (data acquisition board)

   This board is a multifunction analog, digital and timing I/O board for the PC. The next generation of this model is the AT-MIO-16E-2. Some features are:

   - 5 $\mu$sec, 12-bit, sampling ADC
   - 16 single-ended or 8 differential channels
   - a maximum rate of at least 200 ksamples/sec
   - programmable gains of 0.5, 1, 2, 5, 10, 50 and 100
   - a 256 word A/D FIFO buffer to obtain the highest possible data acquisition rate
   - internal or external A/D timing
   - two double-buffered, multiplying, 12-bit DAC's
   - unipolar and bipolar voltage output
   - an on board DAC reference voltage of 10 V
   - internal time and external signal update capability for wave form generation
   - on board I/O hardware auto calibration circuitry
   - eight digital I/O lines able to sink up to 24 mA of current
   - three independent 16-bit counter/times for frequency counting, event counting and pulse output applications

- timer-generated interrupts
- high-performance RTSI bus interface
- four triggers for system-level timing
- full PS I/O channel DMA capability with both analog input and analog output
- two analog output channels
- eight TTL-compatible digital I/O lines
- three 16-bit counter/timers

2. SCXI-1000 Signal Conditioning Extensions for Instruments Chassis

   The SCXI-1000 is a four slot SCXI chassis that houses the SCXI modules. The SCXI chassis supplies a low-noise environment for signal conditioning. The SCXI supplies power and control circuitry for the modules.

3. SCXI-1100 32 Channel Multiplexer Amplifier

   This is a module that fits into the SCXI chassis. Some features are:

   - multiplexes and amplifies 32 differential channels
   - applications: thermocouples, 4 to 20 mA current sources, millivolt sources, volt sources
   - jumper-selectable filtering: 4 Hz or 10 kHz
   - automatic zeroing
   - scanning rates to 250 kHz

4. SCXI-1300 Terminal block

   The SCXI-1300 is a general-purpose terminal block with an on board temperature sensor for measuring the reference junction temperature when using thermocouples.

5. SCXI-1340 Cable assembly

   The SCXI-1340 is a 1 meter ribbon cable assembly for connecting a plug-in board to a SCXI system. This cable includes a mounting bracket for reliable connection to the SCXI chassis and a 50-pin male breakout connecter for direct access to the I/O pins of the plug-in board. The SCXI-1340 uses a 50-pin flat ribbon cable.

6. SCXI-1343 Rear screw terminal adapter

   The SCXI-1343 is a universal adapter to adapt custom wiring to the SCXI-1100. Screw terminals are provided for the analog output connections, and solder pads are provided for the rest of the signals.

7. CB-50 I/O Connector block with 1 meter type NB1 cable

   Termination accessory with 50 screw terminals. Used to make connections directly to the board.

## A.2 Microwave equipment

1. Cylindrical, tunable, single-mode or controlled multimode microwave applicator (1)

   Wavemat Inc.

   Model CMPR-150

   Specs: N(F) connection

2. Microwave Power Generator (1)

   Opthos Instruments Inc.

   Model MPG-4M

   Specs: 100 Watt max output, 2.45 GHz, N(F) connection

3. 3-port coax tee circulator (1)

   Microwave Associates, Inc.

   Model MA-HC7238

   Specs: 2.5 - 3.5 GHz, 20 dB, 200 W avg., insertion loss: 0.3 dB, N(M/F/F) connection

4. Coaxial Directional Coupler (2)

   Narda Microwave Corp.

   Model 22611

   Specs: 20 - 4.0 GHz, 30 dB, N(M/F/F) connection

5. Coaxial Directional Coupler (2)

   Narda Microwave Corp.

   Model 3000-30

   Specs: 255 - 460 MHz, 30 dB, N(F) connection

6. Variable Line Attenuator (1)

   Antenna & Radome Research Assoc., Inc.

   Model 4426-15D

   Specs: 0 - 15 dB, 2 - 4 GHz, 10 W, multi-turn shaft, N(F/F) connection

7. Dummy load (2)

   Narda Microwave Corp.

   Model 369NF

   Specs: 0.7 - 12.4 GHz, 15 W avg., 10 kW peak, N(F) connection

8. Power sensors (2)

   Hewlett Packard

   Model 8481A

   Specs: 10 MHz to 18 GHz, -30 dBm to +20 dBm (1 $\mu$W to 100 mW), N(M) connection

9. Power meters (2)

   Hewlett Packard

   Model 435B

   Specs: 100 kHz to 26.5 GHz, 3 $\mu$W to 100 mW range

10. Coaxial cable (2) specs: 2 feet

11. Coax adapters (4) specs: Type N(M) connection

## A.3 Vacuum equipment

1. Fisher maxima vacuum pump (1)

   Manufactured by Leybold Vacuum Products Inc.

   Model D16A

   This pump features gas ballast and anti-suck back valve.

   - displacement: 400 L/min (14.1 cfm)
   - ultimate partial pressure: $3\times10^{-4}$ Torr
   - motor: 1 horse power
   - speed: 1725 rpm

- weight: 85 lb

2. Pirani Vacuum gauges (2)
   Edwards High Vacuum International
   Model PRM10K
   - Pressure range: 150 Torr to 0.001 Torr
   - Filament operating temperature: 130°C
   - Maximum internal pressure: 2 atm
   - Overall length: 105 mm
   - Weight: 240 gm
3. Pressure controller (1)
   Edwards High Vacuum International
   Model 1101 Pirani
   - Pressure range: 1000 to $10^{-4}$ Torr
   - Display: LCD
   - Recorder output: 0 to 10V d.c.
   - Relays: Four independent relays

## A.4 Miscellaneous Items

1. Mettler electronic balance
2. 5 ml Wheaton serum vials
3. Cotton thread (used to suspend vials)
4. 1 liter liquid nitrogen dewar
5. 5 liter liquid nitrogen dewar
6. Styrofoam cups for handling small amounts of liquid nitrogen

# Appendix B

# Experimental Procedures

There are several different conditions under which experiments are run: with microwave power, without microwave power, with an air leak (controlled pressure), without an air leak (minimum pressure) or some combination of these. Other process variables are the amount of microwave power used, the time intervals for microwave power and the duration of the experiment (to control the final moisture content).

The following sections provide the information required for startup and shutdown of the microwave freeze-drying experiments. A section giving information on what to expect and what to do during the experiments is also provided.

## B.1 Startup of the microwave freeze-drying experiments

The results of microwave freeze-drying experiments can be difficult to reproduce if the starting conditions are not very similar among experiments. The following steps are very detailed and should be followed carefully. Also, some steps after the freezing of the sample need to be done relatively quickly to avoid excessive accumulation of frost on the vial or unusually high starting temperatures.

1. Turn on pressure controller. The controller and pressure sensors require 10 to 15 minutes to warm up.

2. Turn on microwave power generator and power meters. The microwave power generator requires about 10 minutes to warm up.

3. Confirm that the microwave cavity shunt plate position is at 138mm.

4. Make sure that the vial is clean and dry. Place the vial on the electronic balance. Make sure that the thread that is attached to the vial is also on the plate of the electronic balance. (The vial is suspended from a hook on the bottom of the scale by a cotton thread that is tied around the neck of the vial.)

5. Prepare the log book and record the weight of the empty vial. The log book contains the following information:

   (a) date

   (b) purpose of the experiment

   (c) vial weight

   (d) sample weight

   (e) experiment start time

   (f) initial power setting

   (g) final weight of the sample

   (h) experiment end time

   (i) notes on changes (tuning, power, temperature, pressure, etc.) made during the experiment and on what happened (especially things that are out of the ordinary)

6. Turn on the data acquisition computer. Start Lab Windows (change the current directory to C:\LW and enter lw at the prompt). Go to FILE, then LOAD, then the directory JIMDAQ, and select the program named vetdata.c.

7. Attach the vapor trap. Be sure that there is enough vacuum grease on the joint.

8. Add liquid nitrogen to the dewar (about one quarter full).

9. Place the dewar on the floor next to the vapor trap. Do not place the vapor trap into the dewar until the vacuum system has been closed up and the pump has been turned on to avoid build up of frost inside the vapor trap.

10. Check pressure gauge calibration and adjust if necessary. To check the gauge calibration, press c on the pressure controller and check that the millivolt reading is zero.

11. Close the main valve and start the vacuum pump. The pump should have at least 10 to 15 minutes to warm up.
12. Make sure that the leak valve is closed.
13. Get the solution from the refrigerator.
14. Dip eye dropper in the alcohol. Shake off excess alcohol.
15. Tare the electronic balance with the vial still on the balance.
16. Using the eye dropper, place about 2.05 grams of the solution into the vial.
17. Rinse the eye dropper with water.
18. Return solution to the refrigerator.
19. Record the weight of the sample.
20. Place the freezing cup near the top of the microwave cavity.
21. Position by sliding it up into the box for the electronic balance until the probe tip rests in the freezing cup.
22. Add liquid nitrogen to the insulated beaker and place it next to the microwave cavity.
23. Place the sample in the freezing cup.
24. If using a temperature probe, place the probe tip at the bottom center of the vial and hold it steadily.
25. Add liquid nitrogen to the freezing cup from the insulated beaker.
26. When the sample is frozen, lower the sample into the chamber and hang from the hook.
27. Slide the quartz tube up into the upper seal and tighten the clamp below the shelf onto the quartz tube to hold it in place.
28. Tighten the upper seal while holding the quartz tube up into the fitting.
29. Connect the tube fittings below the shelf.

30. Open the main valve.

31. Place the dewar of liquid nitrogen under the vapor trap.

32. Allow the pressure at the P2 (see Fig. 5.5) sensor to reach the $10^{-3}$ Torr range.

33. If this is a controlled pressure experiment, adjust the pressure based on the upper pressure sensor.

34. Start the Luxtron (push the YES button) if using a temperature probe. The temperature should still be lower than -50°C when the pressure on gauge 2 has reached the $10^{-3}$ Torr range.

35. Set the microwave power to the desired level (usually about 14 Watts forward power).

36. Start the data acquisition program (press control-r) when the temperature is between -60°C and -50°C.

37. Record start time, pressures and temperature in the log book.

38. Check the tuning of the microwave cavity.

## B.2 During the experiment

The following list classifies and describes the various types of experiments. Some notes are given for each of the different types of experiments on the expected behavior of the sample temperature and chamber pressure. Also, noted are expected times for primary drying, total time of the experiments and how to detect and avoid foaming of the sample.

**Type 1**: no leak, with microwave power (about 14 Watts forward power)

1. After the experiment is started, the temperature should take about 5 minutes to reach the -20's (°C). The power should be checked every few minutes for the first 30 minutes. The power needs to be checked often during the transition from primary to secondary drying unless it is turned off at the start of this transition.

2. Watch the temperature and pressure readings for anything unusual. Maximum temperatures should not exceed -20°C during primary drying. Maximum pressures are expected to be in the range of 0.08 to 0.14 Torr during primary drying. The reflected power is always about half of the forward power.

3. IMPORTANT: If the pressure goes above the 0.15 Torr there is a risk of foaming. A sudden increase rapid fluctuation of pressure indicates foaming. For, example if the pressure suddenly rises from 0.14 to 0.18 Torr this would indicate foaming. If the temperature goes above -20°C during primary drying there is also a risk of foaming.

4. You can watch the pressure and the temperature to determine if the cavity is tuned properly. Lower than normal pressure and temperature can indicate that the cavity needs tuning. Generally, the tuning of the cavity should follow this schedule:

   (a) $L_s$ = 138mm initially

   (b) $L_s$ = 139mm, after 3 to 5 minutes

   (c) $L_s$ = 140mm, after 5 to 10 minutes

   (d) $L_s$ = 141mm, after 10 to 15 minutes

   (e) $L_s$ = 142mm, maybe after primary drying

5. The temperature should rise to above -30°C in the first 5 to 10 minutes of the experiment. If it doesn't, then the cavity may not be tuned properly.

6. Occasionally note the temperature and pressure in the log book. Also, occasionally try to tune to cavity and note the time and shunt plate position in the log book. Always make note of the time and temperature when an adjustment is made to the power as well as the reason for the adjustment.

7. Primary drying usually lasts for about 1.5 to 2 hours. Around that time the temperature should be increasing and the pressure should be decreasing. Usually, you will want to turn off the power at the end of primary drying. This prevents over heating in the secondary drying stage. By 3 hours the temperature should be about room temperature if microwave power is was turned off.

8. The usual end time for the experiment is after 5 hours to 6 hours. At this point the residual moisture content should be below 2% (moisture fraction). The value of 2% was chosen as a convenient point for comparison of drying times. You can tell when the process is done by looking at the pressure at pressure sensor 1. The pressure should be below $1.0 \times 10^{-2}$ Torr. Also, if there is no temperature sensor being used, the weight will stabilize (the second column on the data acquisition computer).

**Type 2**: no leak, no microwave power

1. After the experiment is started, watch the temperature and pressure readings for anything unusual. Maximum temperatures should be around -27°C during primary drying. Maximum pressures are expected to be in the range of 0.07 to 0.1 Torr during primary drying.

2. The temperature should rise to about -30°C in the first 10 to 15 minutes of the experiment. Occasionally note the temperature and pressure in the log book.

3. Primary drying usually lasts for about 3 hours. Around that time the temperature should be increasing and the pressure should be decreasing. By 4 hours the temperature should be about room temperature.

4. The usual end time for the experiment is after about 7 to 8 hours. At this point the residual moisture content should be below 2% (moisture fraction).

**Type 3**: controlled pressure, no microwave power

1. This type of experiment requires adjusting the leak valve until the desired pressure is obtained on pressure sensor 1.

2. After the experiment is started, watch the temperature and pressure readings for anything unusual. Maximum temperatures are dependent on the pressure, higher pressure causes higher temperatures. The maximum allowable temperature is still around -20°C

3. Primary drying should be between 2 and 3 hours. The end of primary drying will be gradual and the temperature will increase slowly.

4. The pressure can be maintained at the desired setting by occasionally adjusting the leak valve as the pressure starts to drop.

5. The end time for these experiments are between 5 and 7 hours. At this point the residual moisture content should be below 2% (moisture fraction).

**Type 4**: controlled pressure, microwave power

1. This type of experiment requires adjusting the leak valve until the desired pressure is obtained on pressure sensor 1.

2. After the experiment is started, watch the temperature and pressure readings for anything unusual. Maximum temperatures should not exceed -20°C during primary drying. The reflected power is always about half of the forward power.

3. Primary drying should be about 2 to 2.5 hours. About that time the temperature should be increasing. By 3 hours the temperature should be above room temperature if microwave power is still being applied.

4. The pressure can be maintained at the desired setting by occasionally adjusting the leak valve as the pressure starts to drop.

5. The end time for these experiments are between 5 or 6 hours. At this point the residual moisture content should be below 2% (moisture fraction).

## B.3 Shutdown of the microwave freeze-drying experiments

The shutdown procedure is relatively easy, but don't forget to record the pressure reading before cracking open the leak valve.

1. Press the space bar to stop the data acquisition. The data is automatically saved in a file called BHI[month][day].DAT in the directory C:\VETDATA.

2. Record the pressure from both pressure sensors, the temperature and the time.

3. Turn off the microwave power generator and the power meters.

4. Open the leak valve slightly to allow the pressure to rise for a few seconds.

5. Turn off the pump.

6. Turn off the Luxtron (press the YES button).

7. Open the leak valve a little more and wait till the pressure in the chamber reaches atmospheric pressure.

8. Remove the dewar from the vapor trap and pour the liquid nitrogen back into the large 5 liter dewar.

9. Remove the lower part of the vapor trap.

10. Remove the upper seal.
11. Remove the first lower seal.
12. Loosen the clamp and slide the quartz tube down until it is resting on the wood block.
13. Remove the sample by pulling the thread until you can grab the vial.
14. Carefully remove the temperature probe from the sample.
15. Place the sample on the scale and record the weight.
16. Note any unusual features, such as large cracks or signs of collapse.
17. Remove the sample from the vial and rinse out the vial.
18. Copy the data file to the data transfer disk.
19. Copy the data file from the data transfer disk to htlab ($ mread -t a:bhi0115.dat).
20. Run rawbhi using the current data file as input. The output file name should be the same name except with .dat replaced with .out.
21. Record the 2% time if available.
22. Move the .out file to the processed data directory.
23. Run plotbhi on the output file ($ plotbhi bhi0115  note the extension is not used).
24. Send the output to the printer ($ lpr pdata.ps).
25. Put the printed output into the data notebook.

# Appendix C

# Individual Data Plots

These figures show the representative cases that went into the averaged data that was presented in Chapter 6. The pressure data were taken from experiments where temperature is measured and experiments where temperature is not measured, while all of the drying rate data came from experiments that did not include temperature measurements. The low pressure experiments show that the vacuum pump cannot maintain a constant pressure at the lower limit of the pump. The hump in the low pressure curves shows how the sublimation of ice has a significant effect on the chamber pressure under low pressure conditions.

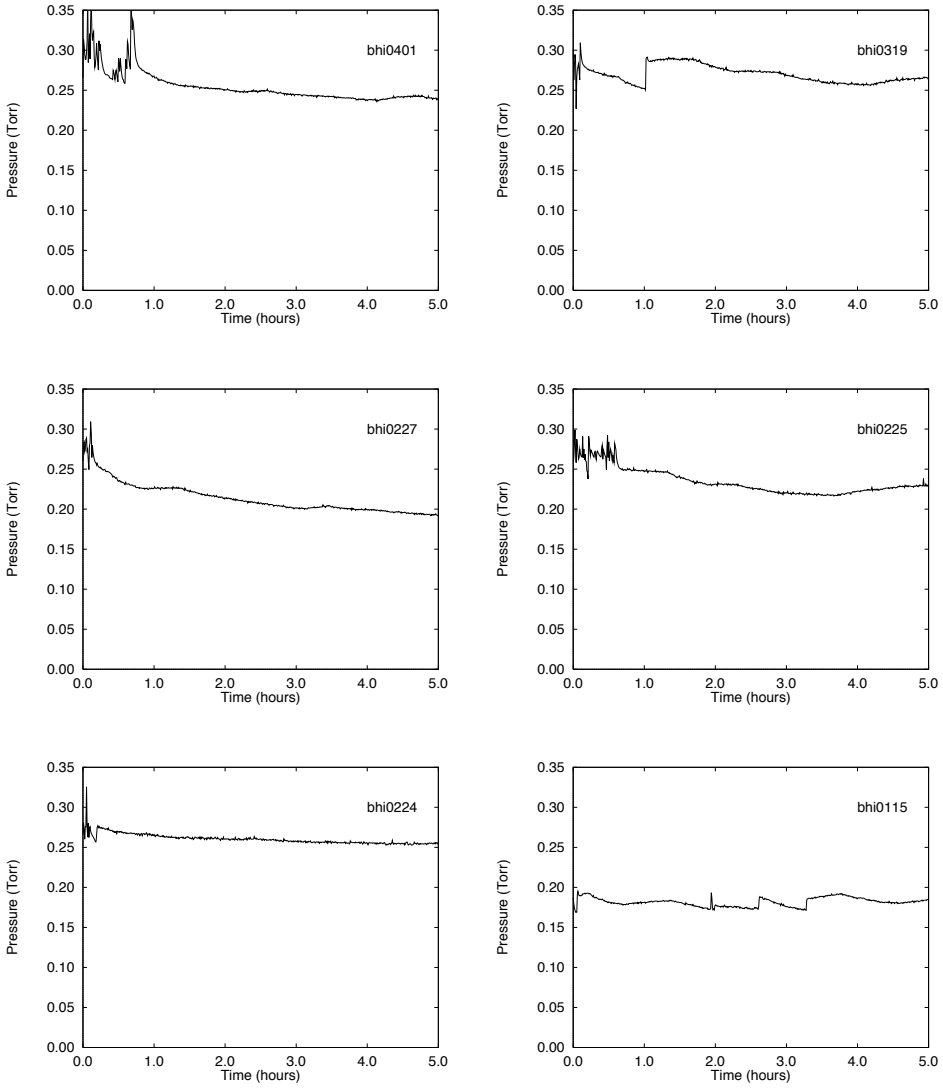


**Figure C.1** The results of high pressure experiments that were averaged for Fig. 6.5

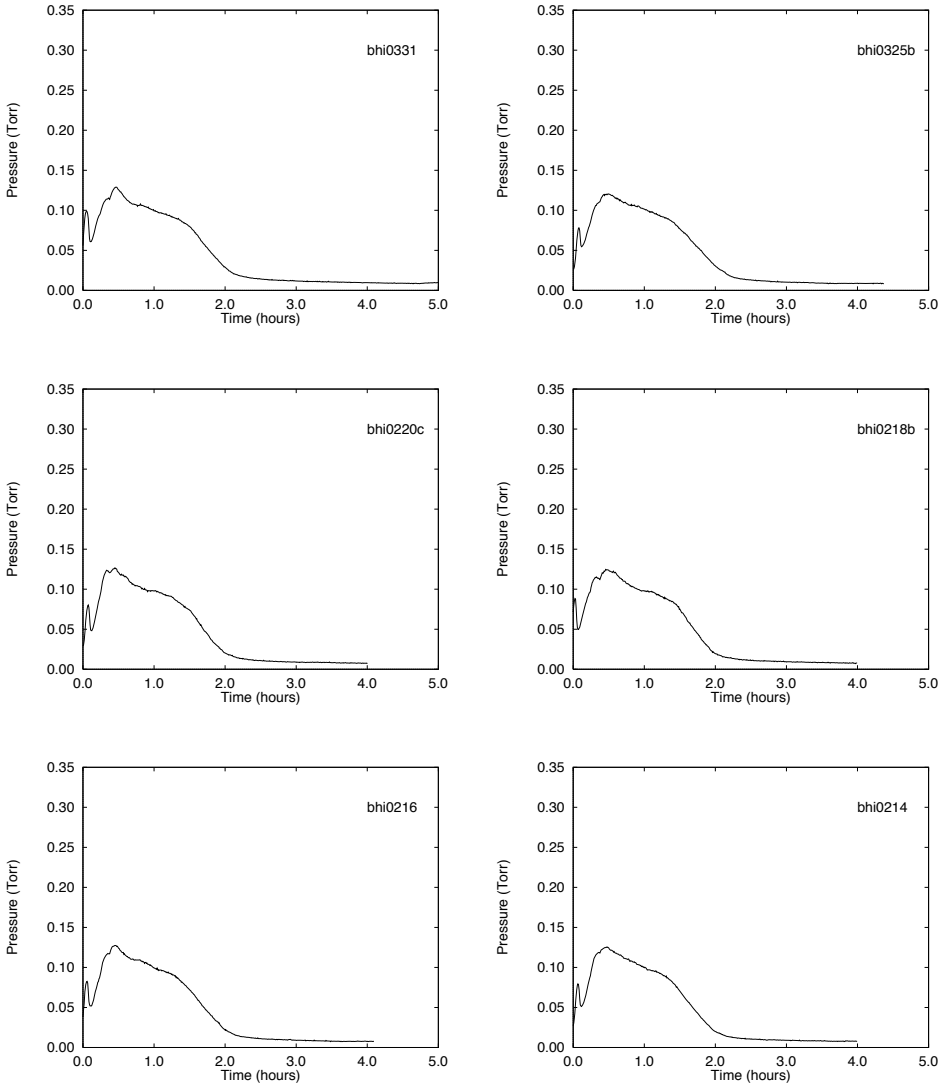


**Figure C.2** The results of low pressure experiments that were averaged for Fig. 6.5

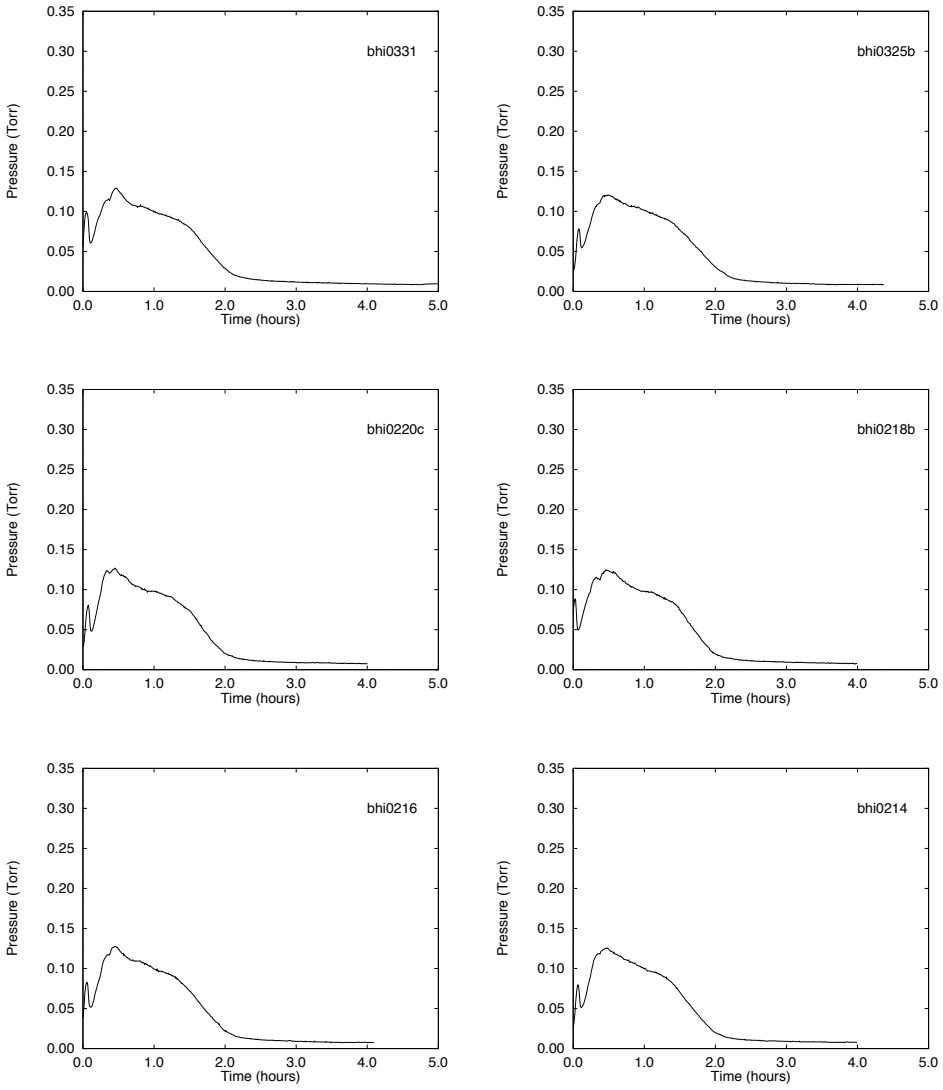


**Figure C.3** Drying rates calculated from the results of low pressure experiments and averaged for Fig. 6.8

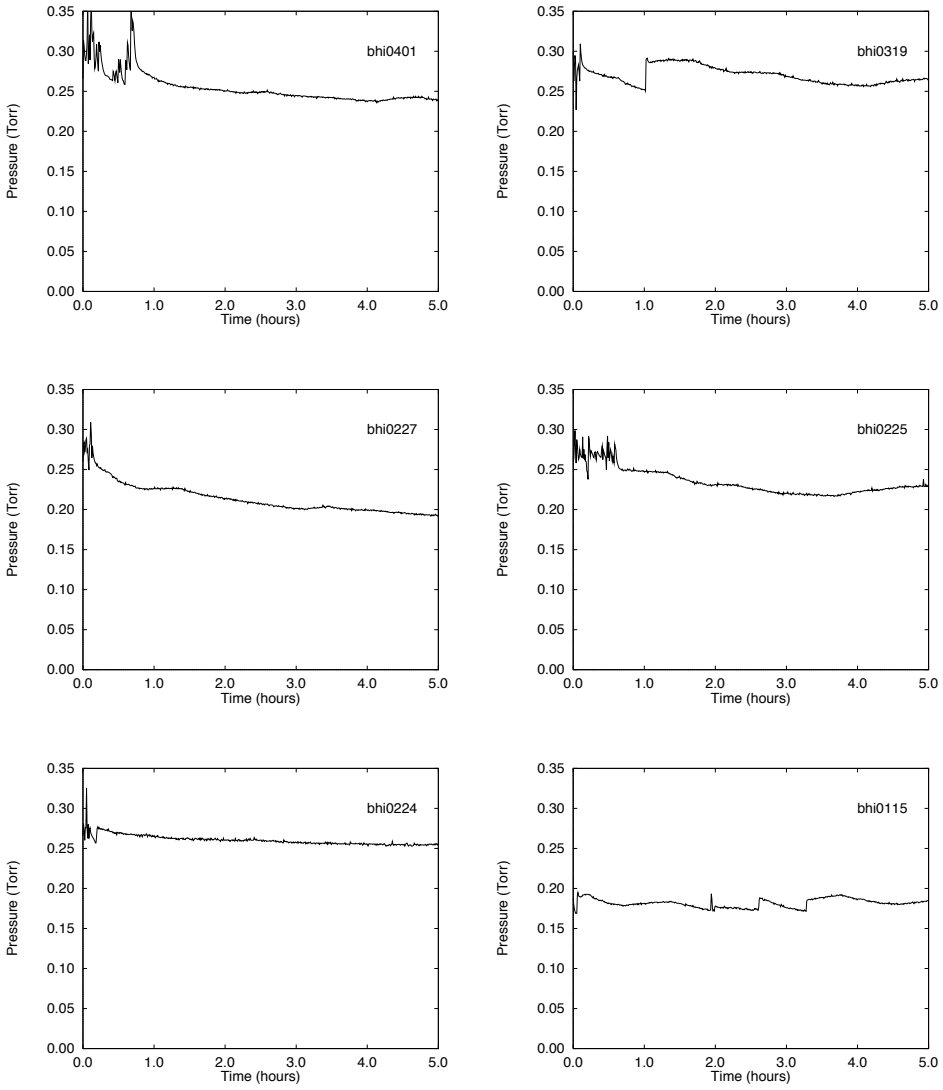


**Figure C.4** Drying rates calculated from the results of high pressure experiments and averaged for Fig. 6.8

# Appendix D

# Data Acquisition and Data Reduction Code

## D.1 Data Acquisition Code

### D.1.1 Main Program: vetdata.c

```
#include "vetdata.h"

/*****************************************************************************

  This program is used to scan multiple channels on the National Instruments
  AT-MIO-16F-5 data acquisition board. Channel 0 should be shorted & grounded.
  This the reading on this channel is the voltage offset to be subtracted from
  the voltage readings.

  The Analog Input defaults, OpenComConfig defaults and some others are
  set in the include file "vetdata.h". The default Analog input mode is
  differential (there are 8 channels, 0-7, in this mode).

  Data is also taken from the Mettler electronic balance through the
  RS-232 output of the balance.  COM port 2 is used. This is the
  parallel port (labeled "LPT1").

  This program was written to record data obtained during microwave
  freeze-drying experiments.

  Output file naming convention: C:\VETDATA\BHI[day][month].DAT
  where [day] is 01 thru 32 corresponding to the day of the month
  and [month] is 01 thru 12 corresponding to the month of the year.

  Multiple runs on the same day will be appended to this file.
  The output file contains six columns:
  1) seconds since midnight
  2) weight loss in grams
  3) temperature probe 1 output in deg C divided by 10
```

```
  4) temperature probe 2 output in deg C divided by 10
  5) pressure controller chan 1 output in volts divided by 2
  6) pressure controller chan 2 output in volts divided by 2

  SOURCE CODE WRITTEN BY: James P. Dolan   7/14/96

*****************************************************************************/

void error_check (char *, int);
int warning (int);

#define     offsetChan      0      /*  Channel used to measure offset       */
#define     gain            1      /*  Gain for the specified chan
                                       Valid settings for AT-MIO-16F-5
                                       -1 (for a gain of 0.5), 1, 2,
                                       5, 10, 20, 50, 100                   */
#define    gainAdjust       1      /*  Gain multiplying factor              */
#define    numChans         4      /*  Number of MIO channels to scan       */
#define    numPts     (2*numChans) /*  TOTAL number of A/D conversions. Must
                                       be an integer multiple of numChans   */
#define    count        numChans   /*  Length of binArray and voltArray     */
#define    DBmode           1      /*  0: Disables double buffering
                                       1: Enables double buffering          */
#define    port             2      /*  Port LPT1 used for RS-232            */


#define    mode1            2      /* 0: open file for reading and writing
                                      1: open file for reading only
                                      2: open file for writing only         */
#define    mode2            1      /* 0: truncate file (delete old contents)
                                      1: write operations append to end of file
                                      2: do not truncate file               */
#define    mode3            1      /* 0: binary   1: ASCII                  */



static int i,
  err,
  flag,
  Month,
  Day,
  file_handle,
  num_source,
  boardCode,
  offset,
  chanVector[numChans],
  gainVector[numChans],
  sampTimebase,
  sampInterval,
  scanTimebase,
  scanInterval,
  buffer[numPts],
  daqStopped,
```

```
  halfReady,
  ptsTfr,
  binArray[numChans];

static double sampleRateDesired,
  scanRateDesired,
  voltArray[numChans],
  time,
  two_hour_time,
  Vreading[16],
  ScaleData;


static char msg[500],
  buf[50],
  file_name[12];

main()
{

  for (i=0; i < numChans; i++) {
    chanVector[i]   = i+1;      /* MIO channels to scan                */
    gainVector[i]   = gain;     /* Array containing gains for each chan */
  }

  sampleRateDesired = 100;       /* A/D conversion rate (pts/sec.)      */
  scanRateDesired   = 30.0;      /* The amount of delay desired
                                    between acquisitions (sec/pt)       */


  cls();

  err = SetDir ("C:\\VETDATA");
  if ( err < 0 ) {
    FmtOut ( "Directory 'C:\VETDATA' not found\n" );
  }
  Scan (DateStr(), "%s>%i-%i", &Month, &Day);
  Fmt (file_name, "%s<BHI%i[w2p0]%i[w2p0].DAT", Month, Day);
  file_handle = OpenFile (file_name, mode1, mode2, mode3);
  FmtOut ("%s\n",DateStr());
/*    FmtFile (file_handle,"%s\n\n",DateStr());  DO NOT WRITE DATE TO FILE */
  FmtOut ("Data written to: %s\n\n",file_name);


/*****************************************************************************

  Init_DA_Brds      required for initializing the data acquisition board
  AI_Config         sets the input mode, range and polarity for the board
                    If you are using default settings, this call is optional.
  AI_Read           used to obtain a binary reading of the voltage offset on
                    the MIO board, it is subtracted from the actual reading
  SCAN_Setup        initializes circuitry for a scanned data acq operation
  DAQ_DB_Config     enables or disables double-buffered data acquisitions
  DAQ_Rate          converts a desired data acquisition rate into the require
```

```
                    time base and interval
  SCAN_Start        initiates a multiple-channel scanned data acq. operation

*****************************************************************************/

  err = Init_DA_Brds (board, &boardCode);
  if (err < 0)
    error_check ("Init_DA_Brds", err);


  err = AI_Configure (board,AIchan,inputMode,inputRange,polarity,driveAIS);
  if (err < 0)
    error_check ("AI_Config", err);


  err = AI_Read (board, offsetChan, gain, &offset);
  if (err < 0)
    error_check ("AI_Read", err);


  err = SCAN_Setup (board, numChans, chanVector, gainVector);
  if (err < 0)
    error_check ("SCAN_Setup", err);


  err = DAQ_DB_Config (board,DBmode);
  if (err < 0)
    error_check ("DAQ_DB_Config", err);


  err = DAQ_Rate (sampleRateDesired, sampleRateUnits, &sampTimebase,
                  &sampInterval);
  if (err < 0)
    error_check ("Samp_DAQ_Rate", err);


  err = DAQ_Rate (scanRateDesired, scanRateUnits, &scanTimebase,
                  &scanInterval);
  if (err < 0)
    error_check ("Scan_DAQ_Rate", err);


  err = SCAN_Start (board,buffer,numPts,sampTimebase,sampInterval,
                    scanTimebase,scanInterval);
  if (err < 0)
    error_check ("SCAN_Start", err);

/*****************************************************************************

  The data acquisition loop acquires data from the double buffer.

  OpenComConfig     Opens COM port and configures defaults
  DAQ_DB_HalfReady  checks whether the next half buffer of data is ready
  DAQ_DB_Transfer   transfers half the data from the buffer being used for
```

```
                    double-buffered data acquisition to another buffer
  DAQ_VScale        converts the binary data into actual measured voltages
  DAQ_Clear         required if DAQ_Check or DAQ_DB_Transfer is not called

*****************************************************************************/
  two_hour_time = Timer() + 7200.00;
  flag = 0;

  OpenComConfig (port,baud_rate,parity,data_bits,stop_bits,iq_size,oq_size,
                 port_addr,int_level);
  if (rs232err > 0)
    error_check ("OpenComConfig", rs232err);

  ComWrt (2,"T\15\12",3);  /* The "T" command tares the balance */
  Delay (1.0);
  ComWrt (2,"T\15\12",3);  /* The "T" command tares the balance */


  while (keyhit() !=1)
    {
      err = DAQ_DB_HalfReady (board, &halfReady, &daqStopped);
      if (err < 0)
        error_check ("DAQ_DB_HalfReady", err);



      if (halfReady == 1){

        ComWrt (port,"SI\15\12",4);
        FlushInQ (port);
        Delay (1.0);
        ComRd (port, buf, 16);
        Scan (buf, "%s>%s[dt#]%f", &ScaleData);

        err = DAQ_DB_Transfer (board, binArray,&ptsTfr,&daqStopped);
        if (err < 0)
          error_check ("DAQ_VScale", err);


        err = DAQ_VScale (board,0,gain,gainAdjust,offset,count,binArray,
                          voltArray);
        if (err < 0)
          error_check ("DAQ_VScale", err);


        time = Timer();
        FmtOut ("%s<%f[w9p2]  %f[w7p3]", time, ScaleData);
        FmtFile (file_handle,"%s<%f[w9p2]  %f[w7p3]", time, ScaleData);
        for (i=0; i < numChans; i++) {
          Vreading[i] = voltArray[i];
          FmtOut ("%s<  %f[w7p3]", Vreading[i]);
          FmtFile (file_handle,"%s<  %f[w7p3]", Vreading[i]);
        }
        FmtOut ("\n");
```

```
        FmtFile (file_handle,"\n");

        if ( (time > two_hour_time) && (flag < 3) )
          {  flag = warning (flag); }
      }

    }
  DAQ_Clear (board);
  CloseCom (1);
  CloseFile (file_handle);
}


/* This function reports an error to the screen using the graphical
   function MessagePopup.                                          *\

void error_check (func, err)
     char func[];
     int err;
{
  Fmt(msg, "%s<Function %s returned error %i", func, err);
  MessagePopup (msg);
  exit(1);
}


/* This function causes the computer to beep when two hours is reached. *\

int warning (int flag)
{
  Beep();
  Beep();
  Beep();
  flag = flag + 1;
  return (flag);
}
```

### D.1.2 Header File: **vetdata.h**

```
/* vetdata.h
   This is the header file for vetdata.c. It contains the configuration
   values  for the data acquisition functions used in vetdata.c.
                                                                    */


#define board       1           /* The MIO board is designated as 1     */


                      /*---------- MIO_Config -------------------------- */
#define dither      0           /* 0: disable   1: enable               */
#define useAMUX     0           /* 0: MIO board chan  1: AMUX chan      */
```

```
                    /*---------- AI_Config defaults ------------------*/
#define AIchan     -1           /* -1: applies to all channels          */
#define inputMode   0           /* 0: Differential
                                   1: Referenced Single-Ended
                                   2: Nonreferenced Single-Ended        */
#define inputRange  20          /* Ignored for the AT-MIO-16F-5         */
#define polarity    0           /* 0: Bipolar (-5 V to +5 V)
                                   1: Unipolar (0 V to +10 V)
                                   If polarity is changed to 1
                                   then call MIO_Calibrate              */
#define driveAIS    0           /* Ignored for the AT-MIO-16F-5         */


                    /*---------- DAQ_Rate defaults --------------------*/
#define sampleRateUnits 0       /* 0: Points/second                     */
#define scanRateUnits   1       /* 1: Seconds/Point                     */


                    /*---------- OpenComConfig defaults --------------*/
#define baud_rate   2400
#define parity      2           /* 0: no parity
                                   1: odd parity
                                   2: even parity                       */
#define data_bits   7           /* either 5, 6, 7 or 8                  */
#define stop_bits   1           /* either 1 or 2                        */
#define iq_size     0           /* 0 selects 512                        */
#define oq_size     0           /* 0 selects 512                        */
#define port_addr   0           /* 0 selects IBM-defined defaults       */
#define int_level   0           /* 0 selects IBM-defined defaults       */
```

### D.1.3 Electronic Balance Testing Code: **scale.c**

```
/*  scale.c - Program for testing the RS-232 data transition on the
              Mettler PM electronic balance.

    AUTHOR: James P. Dolan 7/13/96

    This program basically sets up a port, clears the queues, writes a
    command to the output queue, reads the response from the input queue,
    writes the string that is in the input queue and looks for a number in
    that string.

    The global variable "rs232err" contains the error returned by the most
    recently called RS-232 function. The meaning of these errors are found
    on page 6-35 of the LabWindows Standard Libraries Reference Manual.

    The output of the GetComStat function is a hexadecimal value. View this
    value on variables screen with format set to hexadecimal. The meaning of
    the status code can be found on page 6-19 of the LabWindows Standard
    Libraries Reference Manual.
```

```
*************************************************************************/


#define port_number     2      /* Port 1 is the mouse port (labeled "GAME").
                                  Port 2 is the port labeled "LPT1"         */

static char empty[50],        /* empty char array used to clear buf         */
            buf[50];          /* the buffer in which data is stored         */

static  int i,
            com_status,       /* indicate the status of the COM port        */
            nInBytes,         /* Number of characters in the input queue    */
            nBytesRd,         /* Number of bytes read from the input queue  */
            nWrtBytes;        /* Number of bytes placed in the output queue */

        /*  rs232err             contains the error code if an error condition
                                 occurs during a call to a RS-232 function  */

static double weight;

main()
{
    cls();                              /* clears Std I/O screen */
    Fmt (buf,  "%s",empty);             /* clear buf[50] */
    weight = 0.0;                       /* clear weight */


    FmtOut ("\n  Port Number = %i\n",port_number);


    OpenComConfig (port_number, 2400L, 2, 7, 1, 512, 512, 0, 0);
    FmtOut ("OpenComConfig = %i\n",rs232err);

    com_status = GetComStat (port_number);
    FmtOut ("   Com Status = %i\n",com_status);

    FlushInQ (port_number);
    FmtOut ("     FlushInQ = %i\n",rs232err);

    FlushOutQ (port_number);
    FmtOut ("    FlushOutQ = %i\n",rs232err);



/*-------------- \15 and \12 are CR and LF in OCT format ------------------*/
/*               This function sends a command to the scale.

      ComWrt (port_number, "T\15\12", 3);    */

      nWrtBytes = ComWrt (port_number, "SI\15\12", 4);
      Delay(1.0);
      FmtOut ("\n       ComWrt = %i      Num. bytes placed in the output queue   = %i\n",
                                        rs232err,nWrtBytes);
```

```
/*---------------------------------------------------------------------------*/

    nInBytes = GetInQLen (port_number);
    FmtOut ("    GetInQLen = %i      Num. of characters in the input queue   = %i\n",
                                    rs232err,nInBytes);

    nBytesRd = ComRd (port_number, buf, nInBytes);
    FmtOut ("        ComRd = %i      Num. of bytes read from the input queue = %i\n",
                                     rs232err,nBytesRd);

    com_status = GetComStat (port_number);
    FmtOut ("   Com Status = %i\n",com_status);

    FmtOut ("\n       String contained in the buffer = %s[w16]\n ",buf);

    Scan (buf, "%s>%s[dt#]%f", &weight);
    FmtOut ("      Weight read from the string    = %f\n",weight);


    CloseCom (port_number);

}
```

## D.2 Fortran Code

### D.2.1 Main Program: rawbhi.f

```
      PROGRAM RAWBHI

C     ------------------------------------------------------------------
C
C     This program is used to process raw data from the microwave
C     freeze-drying experiments. The sample is a solution of BHI broth
C     and 20% (w/v) of TREHALOSE. (For every 10ml of BHI broth, 2 grams
C     TREHALOSE is added.)
C
C     The format of the input file is:
C
C     time in seconds  weight  temp1 temp2  pressure1  pressure2
C     since midnight    loss                (controller output)
C
C     time is converted to a relative time in hours
C     weight loss is converted to absolute weight
C     temperatures are voltage readings and are converted to Celsius
C     pressures are also voltage readings and are converted to Torr
C
C     ------------------------------------------------------------------

      REAL        DELTA1,DELTA2,INIWT,ENDWT,DIFF,MWATER,TIME2
      REAL        TIMEIN(5000),TIME(5000),WEIGHT(5000),MF(5000),
     +            WLOSS(5000),TMPIN1(5000),TMPIN2(5000),
     +            TEMP1(5000),TEMP2(5000),W(5000),
     +            X(5000),XPRIME(5000)
```

```
      DOUBLE PRECISION PRES1(5000),PRES2(5000),P1TORR(5000),P2TORR(5000)
      INTEGER     I, NDATA, BREAK, BRKAT, ISIGN, FLAG
      CHARACTER   INFILE*12, OUTFILE*12


C     -------------------- Input parameters ----------------------------
C
C     INFILE          Contains the name of the file containing the raw data.
C
C     OUTFILE         Contains the name of the to which the output is written.
C
C     INIWT           The initial weight of the sample before freezing.
C
C     ENDWT           The final weight given by an independent scale.
C
C     MWATER          The initial total weight of the water in the sample.
C
C     -------------------- RAW DATA. Read from INFILE. ----------------
C
C     TIMEIN          The time in seconds since midnight.
C
C     WLOSS           The weight loss.
C
C     TMPIN1          The Luxtron output set at volts=temp(C)/10.
C
C     TMPIN2          The Luxtron output set at volts=temp(C)/10.
C
C     PRES1           The output of the pressure controller (chan 1).
C
C     PRES2           The output of the pressure controller (chan 2).
C
C
C      -------------------- Calculated Data ----------------------------
C
C
C     NDATA           The number of data points.
C
C     TIME            Contains the time of each data point, in hours,
C                     relative to the start of the experiment.
C
C     WEIGHT          The weight of the sample in grams.
C
C     TEMP1           The temperature, in degrees C, measured by
C                     the the luxtron. (channel 1)
C
C     TEMP2           The temperature, in degrees C, measured by
C                     the the luxtron. (channel 2)
C
C     P1TORR          The pressure reading of sensor 1 in Torr
C
C     P2TORR          The pressure reading of sensor 2 in Torr
C
C     DIFF            The offset between the recorded weight data
C                     and the actual weight of the sample.
```

```
C
C     MF              The calculated moisture fraction.
C
C     W       The calculated wet basis moisture content.
C
C     X               The calculated dry basis moisture content.
C
C     XPRIME          Derivative of X.
C
C     ---------------------------------------------------------------

        WRITE(*,*)'Input file name:'
        READ(*, '(A)')INFILE

        WRITE(*,*)'Output file name:'
        READ(*, '(A)')OUTFILE

        WRITE(*,*)'Enter the initial sample weight:'
        READ(*,*)INIWT

        WRITE(*,*)'Enter the final sample weight:'
        READ(*,*)ENDWT

        WRITE(*,89)INFILE,OUTFILE,INIWT,ENDWT


        OPEN(9,FILE=INFILE)
        OPEN(19,FILE=OUTFILE)

C     ---------- Read data from INFILE to the arrays ------------------

        REWIND(9)

C     ---------- Determine the number of lines in the input file -------

        DO 8 I=1,5000
           READ(9,*,END=9)
 8      CONTINUE
 9      CONTINUE
        WRITE(*,95)I-1


C     ----------- Read in the data -------------------------------------

        REWIND(9)
        DO 10 I=1,5000
           READ(9,*,END=20)TIMEIN(I),WLOSS(I),TMPIN1(I),TMPIN2(I),
     +          PRES1(I),PRES2(I)
 10     CONTINUE
 20     CONTINUE

        NDATA  = I-1
        WRITE(*,91)NDATA
```

```
C     ---------------------------------------------------------------------
C     The following section of code is used to convert seconds since
C     midnight to hours since the start of the experiment. The code handles
C     the case of the experiment crossing over midnight.

        DO 30 I=1,NDATA

           IF((TIMEIN(I).LT.TIMEIN(I-1)).AND.I.NE.1)THEN
              BREAK = 1
              BRKAT = I - 1
              WRITE(*,93)BRKAT,I
              GOTO 40
           ELSE
              BREAK = 0
              BRKAT = NDATA
           ENDIF

 30     CONTINUE
 40     CONTINUE

        DO 50 I=1,BRKAT
           TIME(I) = (TIMEIN(I) - TIMEIN(1))/3600.000
 50     CONTINUE

        IF(BREAK.EQ.1)THEN

           DELTA1  = (86400.000 - TIMEIN(BRKAT))/3600.000
           DELTA2  = TIMEIN(BRKAT+1)/3600.000
           TIME(BRKAT+1) = TIME(I-1) + DELTA1 + DELTA2

           DO 60 I=BRKAT+2,NDATA
              TIME(I) = TIME(I-1) + (TIMEIN(I) - TIMEIN(I-1))/3600.000
 60        CONTINUE

        ENDIF

C     ---------------------------------------------------------------------

        DIFF = ENDWT - WLOSS(NDATA)
        MWATER = 0.808*INIWT

        DO 70 I=1,NDATA

           WEIGHT(I) = WLOSS(I) + DIFF

           TEMP1(I)  = TMPIN1(I)*10.000

           TEMP2(I)  = TMPIN2(I)*10.000

           P1TORR(I) = (-0.006202965D0      + 0.01774566D0*PRES1(I)
     $          + 0.1098143D0*PRES1(I)**2 - 0.0498552D0*PRES1(I)**3
     $          + 0.01855701D0*PRES1(I)**4 - 0.002959556D0*PRES1(I)**5
     $          + 0.0002019377D0*PRES1(I)**6) / 1.333D0
```

```
           P2TORR(I) = (-0.006202965D0      + 0.01774566D0*PRES2(I)
     $          + 0.1098143D0*PRES2(I)**2 - 0.0498552D0*PRES2(I)**3
     $          + 0.01855701D0*PRES2(I)**4 - 0.002959556D0*PRES2(I)**5
     $          + 0.0002019377D0*PRES2(I)**6) / 1.333D0


           MF(I)     = (MWATER - (INIWT-WEIGHT(I))) / MWATER

           W(I)      = MF(I)/(MF(I)+0.2376)

           X(I)      = 4.208*MF(I)

 70     CONTINUE

        CALL PRIME(NDATA,TIME,X,XPRIME)


        DO 80 I=1,NDATA
           WRITE(19,90)TIME(I),WEIGHT(I),TEMP1(I),TEMP2(I),
     +          P1TORR(I),P2TORR(I),MF(I),W(I),X(I),XPRIME(I)
 80     CONTINUE

C     ------------ find the time for MF=0.020 -------------------------

        ISIGN=0
        FLAG=0
        TIME2=0.0
        DO 81 I=1,NDATA

           IF((MF(I)-0.0200).GE.0.000000)THEN
              ISIGN=0
           ELSE
              ISIGN=1
           ENDIF

           IF(ISIGN.EQ.1.AND.FLAG.EQ.0)THEN
              TIME2 = TIME(I-1) + (TIME(I) - TIME(I-1))/2.0
              WRITE(*,92)TIME2,I
              FLAG=1
           ELSEIF(ISIGN.EQ.0.AND.FLAG.EQ.1)THEN
              TIME2 = TIME(I-1) + (TIME(I) - TIME(I-1))/2.0
              WRITE(*,92)TIME2,I
              FLAG=0
           ENDIF

           IF(I.EQ.NDATA.AND.ABS(TIME2-0.0).LT.0.0001)THEN
              WRITE(*,94)MF(NDATA)
           ENDIF

 81     CONTINUE


C     ----------------- FORMAT statements ----------------------------
```

```
 89     FORMAT(1X,/,1X,'Input file name:         ',A,/,
    +       1X,'Output file name:        ',A,/,
    +       1X,'Initial sample weight:   ',F7.3,/,
    +       1X,'Final sample weight:     ',F7.3,/)

 90     FORMAT(1X,F10.4,1X,F8.3,1X,2(F8.2,1X),2(F8.3,1X),4(1X,F8.5))

 91     FORMAT(1x,'Number of data lines processed: ',I5,/)

 92     FORMAT(1X,'2.0% Time: ',F7.4,'   at line',I5,/)

 93     FORMAT(1x,'Midnight crossed between lines',I5,' and',I5)

 94     FORMAT(1X,'Final moisture fraction: ',F7.4)

 95     FORMAT(/,1x,'Total number of data lines in input file:',I6,/)

C     ---------------------------------------------------------------

        CLOSE(9)
        CLOSE(19)

        STOP
        END


C     ---------------------------------------------------------------



      SUBROUTINE PRIME(NDATA,TIME,X,XPRIME)

      REAL  TIME(5000),X(5000),XPRIME(5000),DELTA
      INTEGER  I,NDATA

      DO 10 I=2,NDATA-1
         DELTA     =  TIME(I+1) - TIME(I-1)
         XPRIME(I) = (X(I+1) - X(I-1))/(2.0*DELTA)
 10   CONTINUE

      RETURN
      END
```

### D.2.2 Rate Program: **rate.f**

```
      PROGRAM RATE
C
C This program is used to estimate a slope at each data point for
C the weight curve of the freeze-drying data.
C
C
      REAL       W(5000), R(5000), TIME(5000)
      INTEGER   I, N
      CHARACTER INFILE*12, OUTFILE*14
```

```
      WRITE(*,*)'Input file name:'
      READ(*, '(A)')INFILE

      WRITE(*,*)'Output file name:'
      READ(*, '(A)')OUTFILE

      OPEN(9,FILE=INFILE)
      OPEN(19,FILE=OUTFILE)

C     ---------- Determine the number of lines in the input file -------

      DO 8 I=1,5000
         READ(9,*,END=9)
 8    CONTINUE
 9    CONTINUE


C     ----------- Read in the data -------------------------------------

      REWIND(9)
      DO 10 I=1,5000
         READ(9,*,END=20)TIME(I),W(I)
 10   CONTINUE
 20   CONTINUE

      NDATA  = I-1

C     ---------- Calculate the slope from a central difference --------

      DO I=2,NDATA-1
         R(I) = (W(I+1) - W(I-1))/(TIME(I+1)-TIME(I-1))
      ENDDO

C     ------------- Write out data to a file for plotting --------------

      DO 80 I=2,NDATA-1
         WRITE(19,*)TIME(I),W(I),R(I)
 80   CONTINUE

C      WRITE(*,*)'RATE CALCULATION IS DONE.'
      STOP
      END
```

## D.3 Scripts

### D.3.1 Bourne Shell Script: **plotbhi**

```
#! /bin/bash
#
# This script takes a processed bhi data file
# and plots the results (weight, pressure,
```

```
# temp1 and temp2). The plots are generated
# with gnuplot and placed two on a page with
# latex.
#
#

usemsg=" usage: pdata datafile"

# check if the number of args makes sense
if [ $# -ne 1 ]; then
    echo $usemsg
    exit 1
fi

file1=$1

if [ -f "$file1.out" ]; then
    echo " data file found"
else
    echo " $file1.out does not exist"
    exit 1
fi

#---------- weight ------------------------

# create an eps file of the plot formatted for insertion into
# a LaTeX document

sed "s/#//; 1,2s/set/#set/; 4s/name/weight/; 8s/Temperature (C)/Weight (g)/" \
  /home/dolanjp/bin/pdata.gnu > print.gnu
echo "plot \"$file1.out\" using 1:2 with lines" >> print.gnu
gnuplot print.gnu
rm -f print.gnu


#--------------- pressure 1 and 2 --------------------

# create an eps file of the plot formatted for insertion into
# a LaTeX document

sed "s/#//; 1,2s/set/#set/; 4s/name/pressure/; 8s/Temperature (C)/Pressure (Torr)/" \
  /home/dolanjp/bin/pdata.gnu > print.gnu
echo "plot \"$file1.out\" using 1:5 with lines, \
\"$file1.out\" using 1:6 with lines" >> print.gnu
gnuplot print.gnu
rm -f print.gnu

#---------------------- temperature 1 ---------------

# create an eps file of the plot formatted for insertion into
# a LaTeX document

sed "s/#//; 1,2s/set/#set/; 4s/name/temperature/" \
  /home/dolanjp/bin/pdata.gnu > print.gnu
```

```
echo "plot \"$file1.out\" using 1:3 with lines" >> print.gnu
gnuplot print.gnu
rm -f print.gnu

#------------------------ temperature 2 --------------


# create an eps file of the plot formatted for insertion into
# a LaTeX document

sed "s/#//; 1,2s/set/#set/; 4s/name/temperature2/" \
  /home/dolanjp/bin/pdata.gnu > print.gnu
echo "plot \"$file1.out\" using 1:4 with lines" >> print.gnu
gnuplot print.gnu
rm -f print.gnu

#-------------------------------------------------------


cp /home/dolanjp/bin/pdata.tex ./
/usr/local/bin/teTeX/bin/i686-Linux/latex pdata.tex
/usr/local/bin/teTeX/bin/i686-Linux/dvips pdata
/home/dolanjp/bin/clean
rm -f pressure.eps
rm -f weight.eps
rm -f temperature.eps
rm -f temperature2.eps
rm -f pdata.tex
gv pdata.ps
```

# Appendix E

# Thermal Analysis of BHI/trehalose Materials

For the initial thermal analysis of the BHI/trehalose four sets of measurements were taken. Each set consisted of one TGA and two DSC measurements. The four sets were the following:

1. Dry BHI powder
2. Dry trehalose powder
3. Dry BHI/trehalose mixture from the powder form
4. BHI/trehalose mixture that has been freeze-dried

The TGA measurements were made with a DuPont 2100 V5.1A TGA. The DSC measurements were made with a DuPont 2100 V4.0B DSC. The results of these measurements are plotted on the following pages.

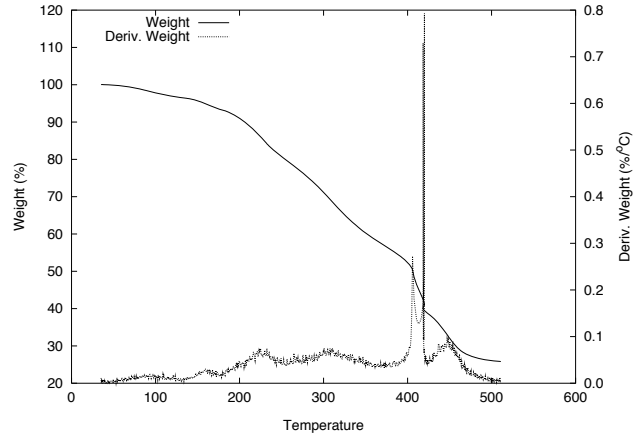


(a) TGA measurement (10°C/min)

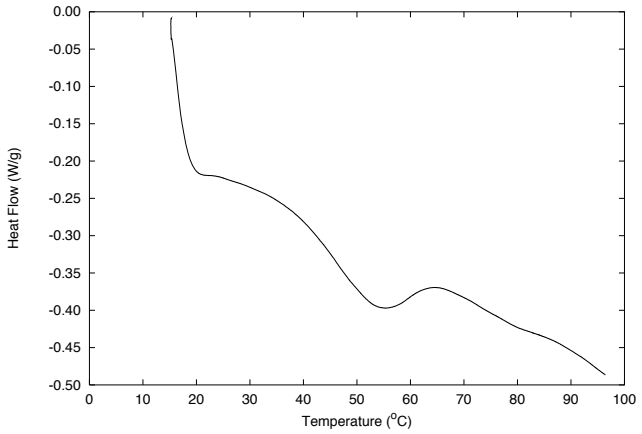


(b) First DSC trace (10°C/min)

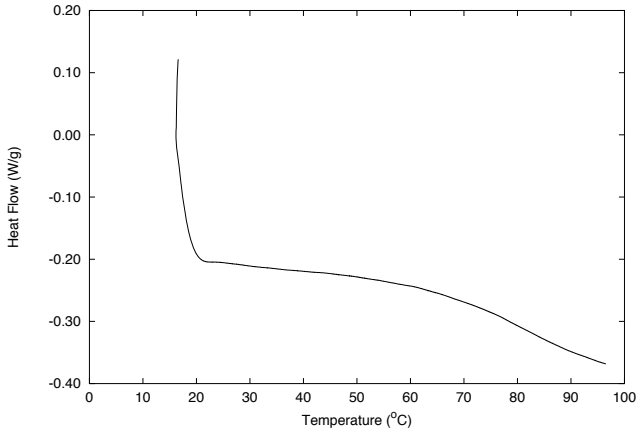


(c) Second DSC trace (10°C/min)

**Figure E.1** Thermal analysis of the dry BHI powder

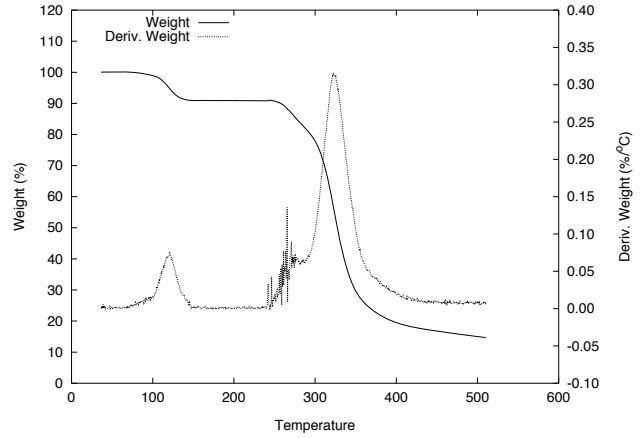


(a) TGA measurement (10°C/min)

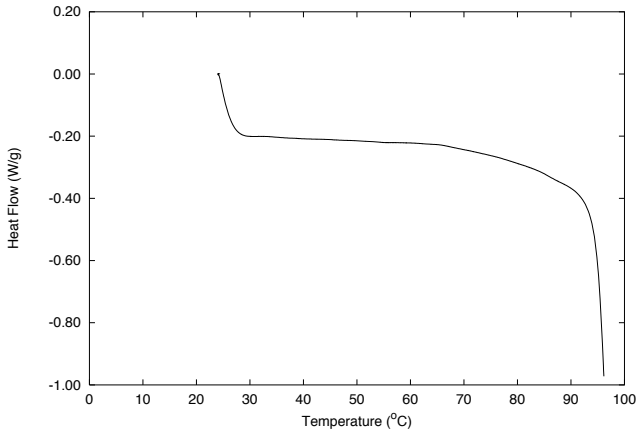


(b) First DSC trace (10°C/min)

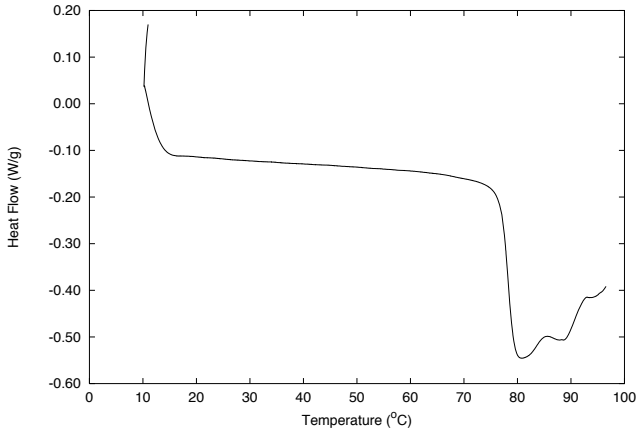


(c) Second DSC trace (10°C/min)

**Figure E.2** Thermal analysis of the dry trehalose powder

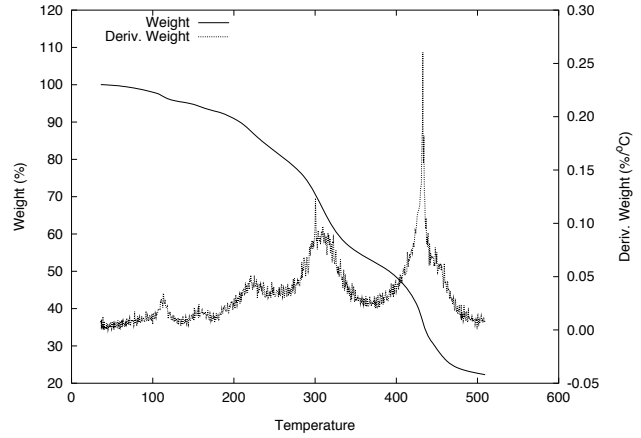


(a) TGA measurement (10°C/min)

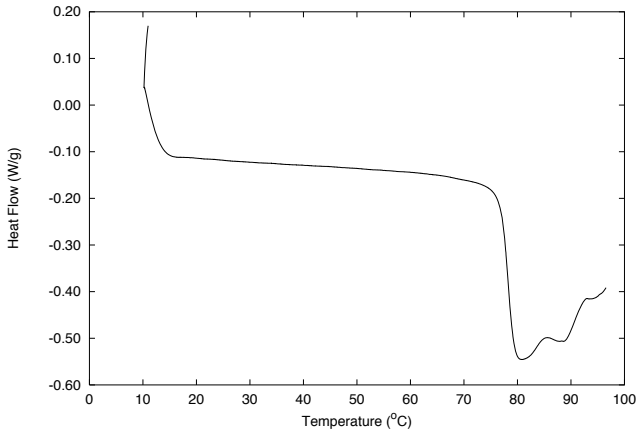


(b) First DSC trace (10°C/min)

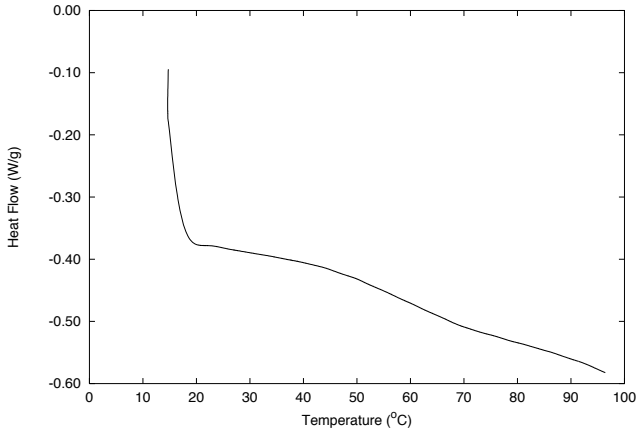


(c) Second DSC trace (10°C/min)

**Figure E.3** Thermal analysis of the mixture of dry BHI powder and dry trehalose powder

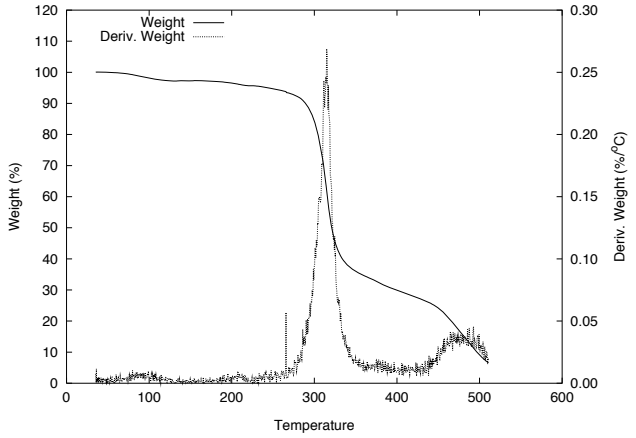


(a) TGA measurement (10°C/min)

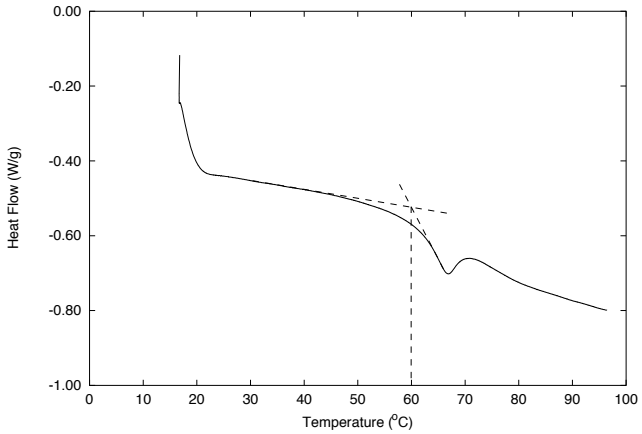


(b) First DSC trace (10°C/min)

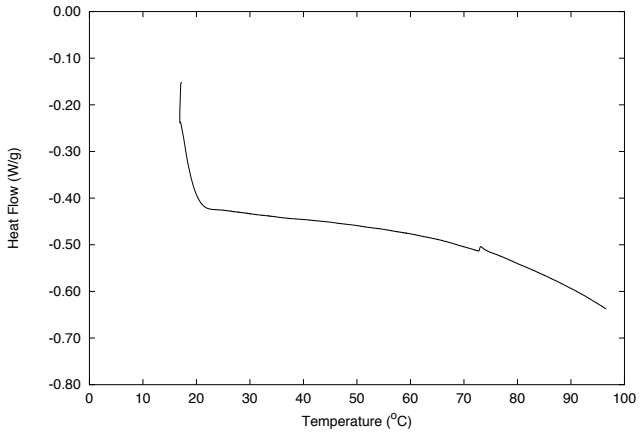


(c) Second DSC trace (10°C/min)

**Figure E.4** Thermal analysis of the freeze-dried mixture of BHI and trehalose with 11% moisture content

# Vita

The author, James P. Dolan, son of Thomas E. Dolan and Sandra J. Dolan, was born on December 5th, 1968 in Teeneck, New Jersey. He obtained his high school diploma from Southing High School in Southington Connecticut in June of 1987. He then went on to attend the University of North Carolina at Charlotte where he earned a Bachelor of Science in Mechanical Engineering. Pursuing his interest in engineering he then moved to Blacksburg, Virginia where he completed the requirements for a Master of Science in Mechanical Engineering during September of 1994 and a Doctor of Philosophy in Mechanical Engineering during September of 1998.

Permanent Address: 1235 Pine Valley Drive
New Bern, North Carolina 28562

This dissertation was typeset with LaTeX $2_\varepsilon$[1] by the author.

[1] LaTeX $2_\varepsilon$ is an extension of LaTeX. LaTeX is a collection of macros for TeX. TeX is a trademark of the American Mathematical Society. The macros used in formatting this dissertation were written by Greg Walker, Department of Mechanical Engineering, Virginia Tech.